UCL Université catholique de Louvain

École polytechnique de Louvain (EPL)

epl

Largely variable inertia power system

Dissertation presented by
Julien PATRIS

for obtaining the Master's degree in
Electro-mechanical Engineering

Supervisor(s)
Prof. Emmanuel DE JAEGER

Reader(s)
Prof. Bruno DEHEZ, Prof. Hervé JEANMART

Academic year 2016-2017

Abstract

With the decline of the limited fossil fuel energy resources as well as the climate change, parts of the traditional generators and loads are being replaced by modern ones connected through power electronics. This technology can work with any type of current shape, thus providing the flexibility needed for the renewable energy sources such wind turbines or photovoltaic panels. However, while traditional synchronous machines naturally support the grid frequency trough the kinetic energy stored in their rotating masses, power converter connected machines do not naturally participate to the grid inertia. Although, the use of renewable has undeniable positive effect, a too strong integration in an unprepared grid can seriously jeopardize its frequency stability.

This master thesis focuses on the study of grid frequency dynamic with an important share of renewable. Grid areas with realistic parameters are performed and analyzed. Later on, a detailed model of a permanent magnet synchronous wind turbine with a a controller emulating its inertia and thus supporting the grid frequency is then proposed. Indeed, with the increasing amount of power module connected through power electronics it is important to find solution so that they can also play a role in the grid frequency stability.

Acknowledgments

Foremost, I would like to express my sincere gratitude to my master thesis advisor, Prof. Emmanuel De Jaeger for advising and guiding me over these few months. I have learned many things thanks to our discussions. This work would not have been possible without his patience, motivation, enthusiasm, availability and scientific expertise.

I would like to thank the other members of my jury, Prof. Hervé Jeanmart and Prof. Bruno Dehez who showed interest in this work and took the time to read this thesis.

I wish to once again thank Prof. De Jeager for his way of teaching and his inspiring courses that motivated me to extend my knowledge in these fields.

I would like also to thank my family and friends for their support during my studies.

Contents

Symbols and Constants

P_{tie} [MW] Tie line power transfer

β [rad] Pitch angle

λ [-] Tip speed ratio

λ [-] Tip speed ratio

ω_n [rad/s] Undamped frequency

ω_0 [rad/s] Nominal angular frequency

Ψ_b [Wb] Permanent magnet flux linkage

σ [-] Speed-droop coefficient

$\widehat{L_d}$ [H] Direct inductance

$\widehat{L_q}$ [H] Quadrature inductance

ζ [–] Damping ratio

c_p [-] Performance coefficient

d [-] Load damping percentage

f_0 [Hz] Nominal frequency

H [s] Inertia constant

J [kgm^2] Moment of inertia

K_I [-] Integral action

K_P [-] Proportional action

L [H] Self inductance

M [H] Mutual inductance

P_e [W] Electric load

P_m [W] Mechanical power

P_{max} [W] Maximal power

T_m [Nm] Mechanical torque

T_P [-] Park Concordia transform

T_P^{-1} [–] Inverse Park Concordia transform

T_{em} [Nm] Electromagnetic torque

T_{em} [Nm] Electromagnetic torque

X_{Tie} [Ω] Tie line inductance

abc [-] Three phases components

dq0 [-] Park Concordia components

$\mathrm{i}_{abc}[A]$ Three phases current

$\mathrm{i}_{dq0}[A]$ Park Concordia current

$\mathrm{L}_{grid}[H]$ Grid side inductance

$\mathrm{R}_{grid}[\Omega]$ Grid side resistance

$\mathrm{V}_{abc}[V]$ Three phases voltages

$\mathrm{V}_{dq0}[V]$ Park Concordia voltages

List of Figures

List of Tables

Introduction

Power grids are characterized by their sinusoidal three phases voltages induced by the rotating synchronous machines. Electric power has been produced this way since the end of the 19th century [15]. For stable operation, the grid voltage frequency is supposed to stay at its nominal value. This has required a standardization of all the components connected to the grid so that they properly run at the fixed nominal frequency imposed by the grid. This way of producing electric power, offering the initial numerous advantages of the alternative machines and voltages, has been adopted and spread world wide.

However, the traditional synchronous power grid has we know it, is facing important challenges and even a profound self-questioning. As a matter of fact, the limited fossil energy supply needed for the traditional turbine to drive the synchronous generator as well as the climate change as forced us to rethink the way we produce and consume power. Therefore, alternative ways to produce power have emerged. Indeed, the research on renewable energy as well as its effective integration to the grid has significantly increased over the last decades.

In this context, the behaviour of the grid and its frequency dynamic has been altered. Indeed, as we will detailed it in this report, the frequency dynamic is directly related to the connected inertia of the synchronous machines. As a matter of fact, the kinetic energy stored in the rotating masses naturally helps to stabilize the grid frequency. Whereas the non-rotating renewable power sources such as photovoltaic panels does not obviously contain any kinetic energy but also rotating renewable power machines such as wind turbines are connected trough power converter isolating their rotor inertia from the grid.

The following report studies the frequency aspect of the grid as well as the modifications brought by the power converter connected sources. In those new grid prospective, a detail model and a proposed way to recover the inertia of a modern wind turbine connected trough power electronics is then considered.

The first chapter present the origin and the behaviour of the grid frequency as well as the different manners to control and adjust it.

The second chapter considered a more detailed frequency analysis and how the increase of renewable integration affects it. An isolated grid is imagined with different turbine types supplying it and working in parallel with renewable connected through power converter. Afterwards, the influence of the frequency deviation has on the inter-grid power exchanges as well as the impact of the possibly high renewable penetration in one area is presented. Along with that, the rules under which the different grid operators of the same interconnected grid must operate are briefly introduce for the European grid. An emphasis was placed on the technical requirements for the different power generating modules.

In the third chapter, the detailed frequency grid data of Belgium of the whole year 2013 was available. Frequency events were spotted and the probabilistic distribution of the frequency as well as its rate of change change is inspect.

Finally the fourth chapter, focuses on the analysis of a modern permanent magnet wind turbine connected to the grid. It described the different components of the wind turbine and how it works and produces electrical power. This part considers the challenges encountered with the modern variable speed wind turbine and proposed a possible detailed model of a wind turbine providing a frequency. The model is implemented numerically and the different results obtained are analyzed.

Chapter 1

Frequency control

1.1 A brief history of the electric frequency

Electric power grid runs at a three-phase sinusoidal voltage set at a frequency of 50 Hz for the majority of the world (Europe, Asia, Africa) and 60 Hz for North America.

Historically, at the end of the 19th century, power grid were using DC current to feed the lightning system of cities and eventually motor loads. Indeed, the first industrial generator was made by the Belgian inventor Zénobe Gramme in 1871 and was meant to produce direct current. Few years later, Thomas Edison played an important role in the development and the spreading of the DC electrical grid with his company, General Electric, which still exists today. This ultimately led to the "electric war" between Edison defending his DC vision of the grid and Nikola Tesla supporting the AC current with the help of George Westinghouse and his company. As we know, AC current finally won this war and established itself as the reference.

As a matter of fact, AC current was technically superior and presented numerous advantages over the DC current. The voltage of the AC could be stepped up or stepped down with a transformer and therefore be carried with less losses and over longer distances. Furthermore, AC generator did not need slip rings and brushes making them simpler, cheaper and more robust.

Until now, AC grid, characterized by its frequency has stayed the main mode of electric power transportation in the world although things have changed and will continue to evolve with the development of power electronics technology.

1.2 Grid frequency

The electric frequency is directly related to the speed of the connected rotating machines by $f_{grid} = N_p \frac{\omega_{rotor}}{2\pi}$. The dynamic of the rotational speed of the machine depends on its moment of inertia, J and the mismatch between the mechanical torque, T_m and the electromagnetic torque, T_{em}. It is described by the equation of motion [8]:

$$J\frac{\mathrm{d}\omega_m}{\mathrm{d}t} = T_m - T_e \tag{1.1}$$

It is also useful to re-express the equation of motion 1.1 in term of the power mismatch:

$$J\frac{\mathrm{d}\omega_m}{\mathrm{d}t} = \frac{P_m}{\omega_m} - \frac{P_e}{\omega_m} \tag{1.2}$$

Where P_m is the mechanical power and P_e is the electrical power.

Assuming that, even during a disturbance, the speed of the synchronous machine stays close to its nominal speed, ω_0. The differential equation 1.2 can be simplified and re-written as:

$$J\frac{\mathrm{d}\omega_m}{\mathrm{d}t} \approx \frac{P_m}{\omega_0} - \frac{P_e}{\omega_0} \tag{1.3}$$

According to equation 1.3, any imbalance between the electric load and the mechanical power delivered will impact the rotational speed of the machine. Indeed, if the electric load increases, the machine tends to decelerate, and conversely if the mechanical power increases the machine tends to accelerate.

This equation can be generalized to a whole grid area with interconnected synchronous machines where P_m would be the total mechanical power provided by all the generators, P_e, the total electric load, ω_0, the nominal angular frequency of the grid and the machines and J, the total moment of inertia of all the connected machines. Therefore, we can obtain the dynamic of the grid frequency:

$$(2\pi)^2 J\frac{df}{dt}f_0 = P_m - P_e \tag{1.4}$$

Load damping effect

If we want to increase the accuracy of the equation 1.4 we have to take into consideration the effect of the load. Indeed, a wide variety of electrical load exists, such as lightning or heating systems for which the electric power is independent of frequency. However, many rotating electrical machines for which operating speed, and thus power consumption, is directly dependent on the grid frequency are present.

Hence, the load damping percentage, d is introduced to model the frequency-dependent characteristic of the grid load. It is defined as the change in percentage of the electric load power due to 1 % of the grid frequency change. This means that the overall damping effect of the grid area, D is obtained as :

$$D = \frac{d\,(Total\ Load)}{0.01\,f_0}\ \left[\frac{MW}{Hz}\right] \tag{1.5}$$

Hence, by taking the load damping effect into account we obtain the relation:

$$(2\pi)^2 J\frac{df}{dt}f_0 = P_m - P_e - D(f - f_0) \tag{1.6}$$

The negative sign of the load damping effect in equation 1.6 represents the favourable reaction it has on the frequency. Indeed, if the power produced P_m increases, frequency will rise and amplify the load damping and therefore reduce the overall value of the right side of the equation. In the same manner, the equivalent counteraction happens in case of a frequency decay.

It physically works the same way as for the generator except that in this case the load damping term encompasses the inertia effect of the rotating loads. Hence, when the frequency rises, the motor loads absorb energy into their rotating masses and as the frequency declines they deliver their stored kinetic energy to the grid.

In parallel to the increase of power produced through power electronics, traditional synchronous and asynchronous motors are increasingly replaced by newer models running with power converter. They come with the advantage to run over a broader regime range with a better efficiency but cancel the positive damping effect that they initially provided.

Matching the power and the load

The power load, P_e varies strongly depending on the time of the day (figure 1.1) and even the day of the week or the season.

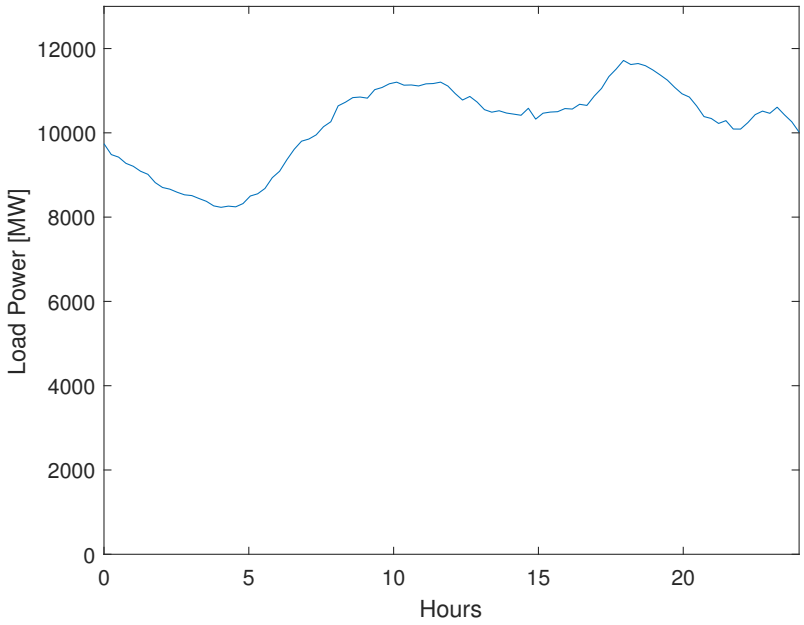

Figure 1.1: Load power variation on the 4th of January 2017 (data from [2])

The challenge is to perpetually tune the power produced and the power consumed to make sure the power mismatch is as little as possible to stay at the nominal frequency f_0.

Factually, it is almost exclusively the power produced that is constantly adjusted to match the load. As we know, we can consume electric power whenever it suits us and power production will adapt to it. Indeed, the power adjustment happens in the production side (automatically and manually) through the different frequency control.

Therefore, the different power generating units must be flexible enough to follow the demand. This is why rather constant power producer like nuclear power plant are accompanied with "peakers" such as thermal or hydroelectric turbine able to broadly modulate their power output.

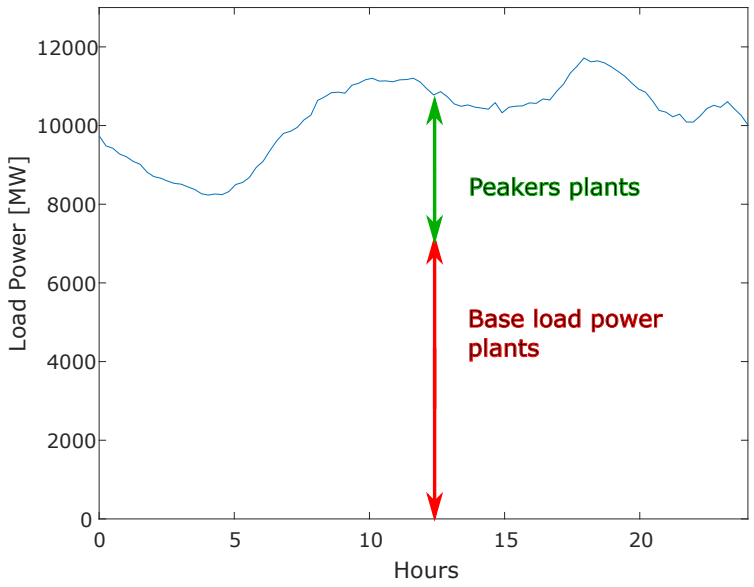

Figure 1.2: Graphical representation of peakers and base load power plants

In addition to this, storage systems are also used to compensate the remaining power difference between the demand and the consumption by stocking/releasing power when the production is superior/inferior to the demand. Among the existing storage solutions, the pumped storage system allows large storage and large power capacity. Unfortunately, this system needs large suitable hilly site with access to water which is likely to either be a wildlife reserve or already used. In Belgium, we can mention Coo-Trois-Ponts hydroelectric power station with an installed capacity of 1 GWh for an annual average energy stored and released of 1600 GWh [4] . Storage systems such as Coo, which was initially build to store the excess power of the Tihange nuclear station, are now needed to support the renewable power generation characterized by a power production, which is not controllable. This means that it does not always produce power when we need it and might produce it when there is no power demand.

However, it should be noted that among the different future vision of the electrical grid, we are also talking about making a more important effort on the power consumption side. In fact, there is already existing legislation aiming to control the power consumption for instance the night rate of electric energy present in countries with important nuclear production such as France or Belgium. Nonetheless, a nuclear power plant cannot be turned-off and on as we would like. Therefore, they constantly produce power even when the load is at its minimum. Thus, the night rate encourages the clients to postpone their operation demanding electrical power to the night or the week-end when the demand is usually low.

This vision of controlling the consumption side is driven by the context of limited fossil fuel energy and the increasing renewable energy integration characterized by its random component. It is even imagined that the client would guarantee to schedule the use of his power devices and also the period he will not use it such as an electric car, for instance, that would be recharging

only when the solar or wind power production is important [10]. However, this would affect our habits in a lot of the ways, as well as how we see and use electric energy.

1.3 Inertia response

As we have seen above, the moment of inertia of the synchronous generators directly influences the dynamic of the grid frequency. In electric power systems, the inertia constant, H is more often used. It is defined by the kinetic energy stored in the machine at its nominal rotating speed over its based power:

$$H = \frac{E_{kinetic}}{S_{base}} = \frac{1/2 J \omega_0^2}{S_{base}} \ [s] \tag{1.7}$$

Thus, we can re-write the equation 1.6 as:

$$\frac{2HS_{base}}{f_0}\frac{\mathrm{d}f}{\mathrm{d}t} = P_m - P_e - D(f - f_0) \tag{1.8}$$

Analysis of the grid frequency can be studied with equation 1.8 where H and S_{base} represent respectively the inertia constant and the nominal power of the whole grid. To simplify the frequency analysis, the block system in the Laplace domain of the linearized frequency equation is often used because it is easier to manipulate and it provides a better physical comprehension of the problem. The linearization is performed around:

$$P_m = P_{m,0} + \Delta P_m$$

$$P_e = P_{e,0} + \Delta P_e$$

$$f = f_0 + \Delta f$$

For which we obtain:

$$\frac{2HS_{base}}{f_0}\frac{\mathrm{d}\Delta f}{\mathrm{d}t} = (P_{m,0} + \Delta P_m) - (P_{e,0} + \Delta P_e) - D\Delta f \tag{1.9}$$

In normal operation we consider that $P_m = P_e$, thus we have:

$$\frac{2HS_{base}}{f_0}\frac{\mathrm{d}\Delta f}{\mathrm{d}t} = \Delta P_m - \Delta P_e - D\Delta f \tag{1.10}$$

This equation is represented in the Laplace domain in block system in the figure 1.3.

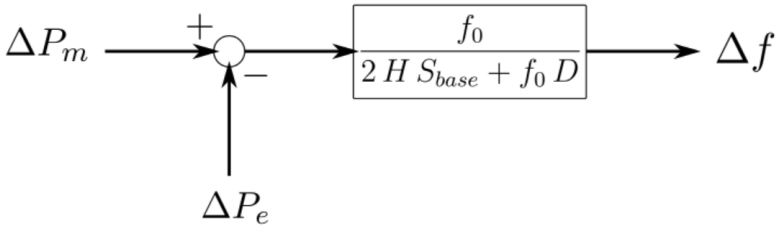

Figure 1.3: Transfer function relating frequency deviation to power disturbance

The figure 1.4 shows the frequency deviation caused by a power disturbance for an area characterized by the parameters in table 1.2.

Parameter	Value
Nominal base power	$S_{base} = 6000\ MVA$
Connected load	$Load = 3000\ MW$
Load damping effect	$f_0 = 50\ Hz$
Generator loss	$\Delta P_e = 80\ MW$
Load damping	$d = 1.5\%$

Table 1.2: Area characteristics

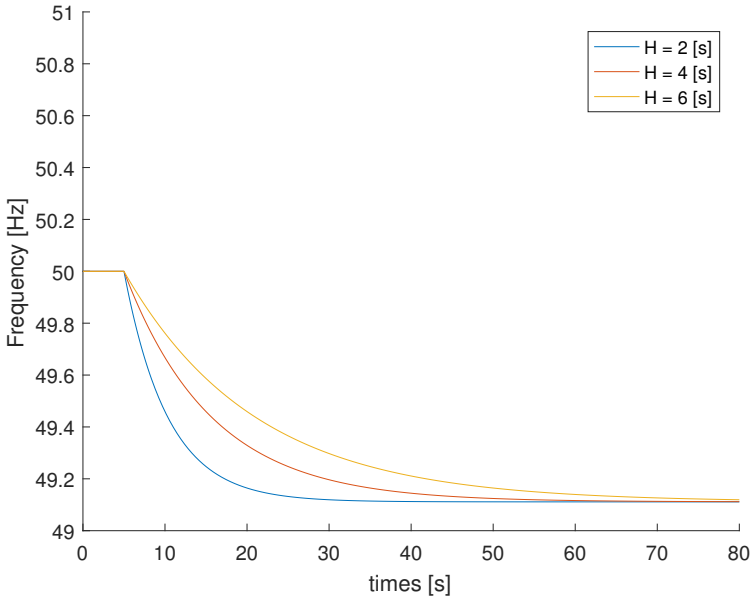

Figure 1.4: Inertia response of a generator loss for different values of inertia

We observe that the lower the inertia, the faster the frequency dynamic, and conversely, the bigger the inertia the slower the frequency dynamic of the grid. Indeed, every synchronous machine directly connected to the grid will slow down by Δf meaning that they will support the grid by injecting into it a total of $\Delta E_{kinetic} = 2\pi^2 J \Delta f$.

1.4 Primary control

Synchronous generators are normally driven by a turbine equipped with a governing system with a speed droop characteristic working as a proportional controller. The value of the proportional action depends on the speed-droop coefficient σ which can be interpreted as the percentage of frequency change needed to cause 100 % change in the power output. Speed-droop definition is illustrated in figure 1.5.

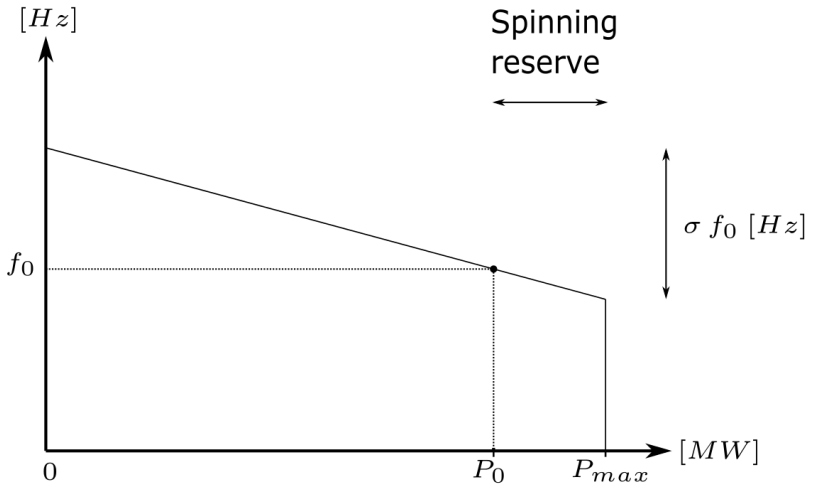

Figure 1.5: Illustration of the speed-droop definition

The proportional action of the controller is thus defined as:

$$\frac{1}{R} = \frac{Pmax}{\sigma\, f_0} \quad \left[\frac{MW}{Hz}\right] \tag{1.11}$$

This allows the synchronous machines to work in parallel by sharing the load proportionally to their power rating. The spinning reserve shown in figure 1.5 is the reserve of power the machine can deliver in case of a frequency drop. Once the machine operates at its maximal power, P_{max}, there is no more power reserve left and the machine cannot participate anymore to the primary control in case of a further frequency decay.

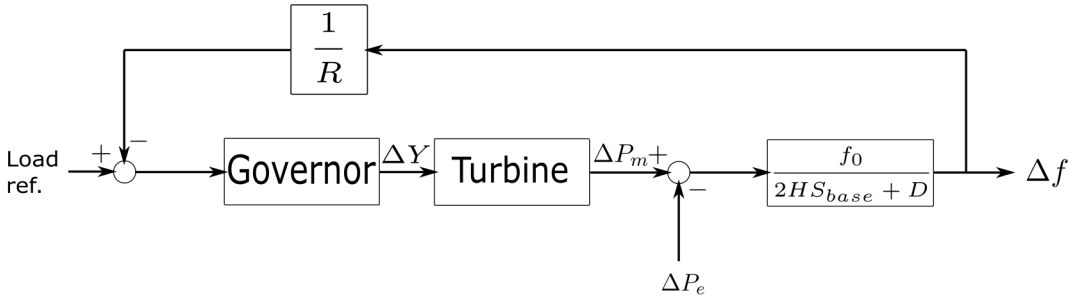

Figure 1.6: Transfer function of a turbine with primary control

The primary response of a reheat steam turbine to a generator loss of 80 MW is performed in figure 1.7. The model of the turbine is given in the Appendix (figure A.2) and the characteristics of the grid in table 1.3.

Parameter	Value
Nominal base power	$S_{base} = 6000\ MVA$
Connected load	$Load = 3000\ MW$
Load damping effect	$f_0 = 50\ Hz$
Generator loss	$\Delta P_e = 80\ MW$
Load damping effect	$d = 1.5\%$
droop	$\sigma = 5\%$

Table 1.3: Area characteristics with primary control

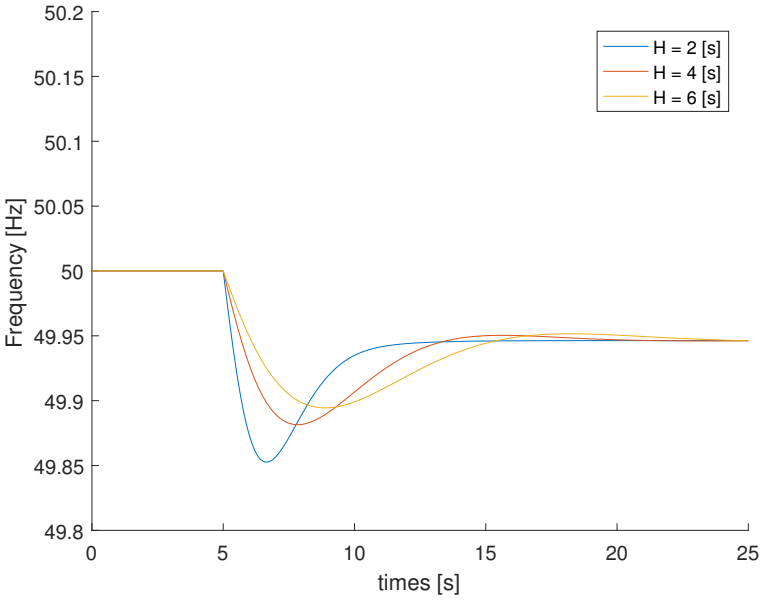

Figure 1.7: Primary control after a generator loss

We observe that after the power event, the frequency is decaying. However, this time, once the primary control has taken over, the rate of change of frequency become positive in order to reach a frequency close to the nominal one. Indeed, the spinning reserve of the power units are used to put on the lack of generation until reaching a new steady state point.

1.5 Secondary control

For the same frequency, the power output of a generating unit can be increased if we move upward the governor speed-droop characteristic curve. This is actually done for the secondary control where the load reference set point is slowly adjusted (figure 1.8) to bring back the frequency at its nominal value.

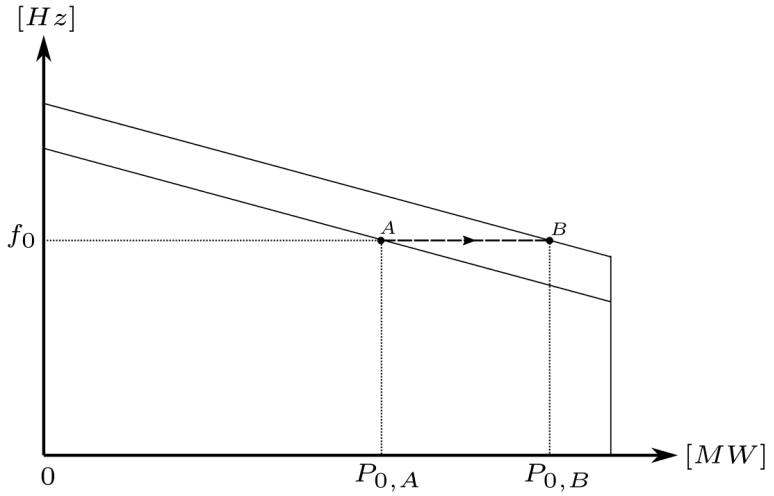

Figure 1.8: Effect on governor characteristic curve when secondary control is initiated

This supplementary control is performed with an integral action (figure 1.9) to correct the steady state frequency error. While primary control is equipped in almost all power generating module, supplementary control is present only on certain strategic units.

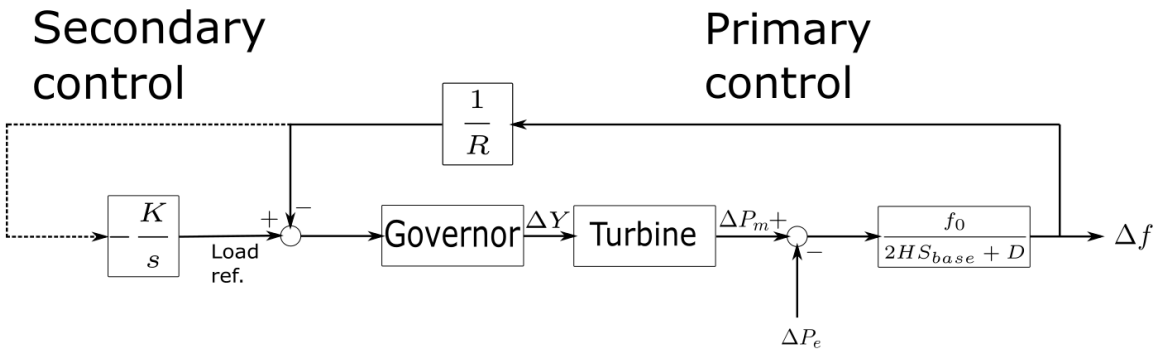

Figure 1.9: Transfer function of a turbine with secondary control.

1.6 The decrease of grid inertia

Normally, the inertia response is provided by traditional synchronous machines directly coupled to the grid. However, with the evolution of power electronics technology and in order to confront the changing energy situation, inverter-connected renewable energy sources have been steadily growing.

This increase of non-traditional power production is irredeemable because of the diminishing fossil fuel resources and energy price hikes as well as the alarming climate change. Nowadays, the main non-traditional renewable power sources are wind turbine and photovoltaic panels which depend respectively on the wind and solar irradiation. These technologies have increased in reliability and efficiency while their cost have reduced.

Besides the positive environmental impact, non-traditional energy sources are connected to the grid through power electronics and they do not participate to the inertia response of the grid as the traditional synchronous generators did. One can thus confidently say that the dynamic of the grid is changing and will be changing even further in the future.

Although the different frequency controls come into play at the same time, it is considered that each control takes place to some extent at different moments because their influences vary completely differently over time (see figure 1.10).

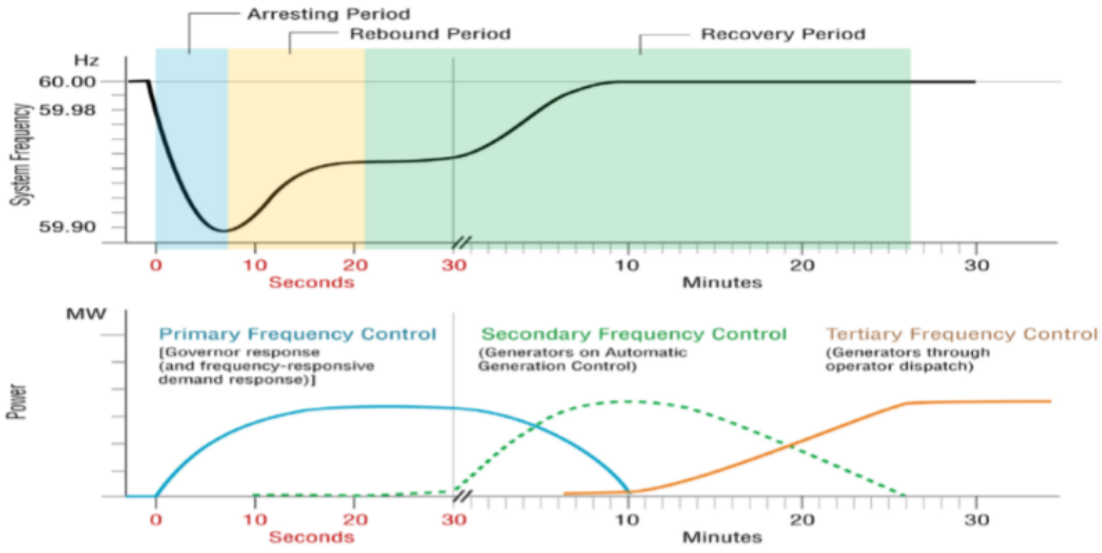

Figure 1.10: The different frequency control over time [12]

This is why, for the rest of this report, the secondary control will be put aside. Indeed, the influence of the latter during the first seconds of a power disturbance is marginal.

Inertia response is considered to be happening during the first seconds after the disturbance. It means that any system able to quickly inject or absorb power during the very first moment after the power imbalance will be playing a role in the inertia response. Among the existing way to compensate the lack of inertia, a fast primary response is one of them it can quickly react t

Chapter 2

Dynamic frequency analysis

2.1 Isolated network

The frequency dynamic of a grid area is directly related to its inertia (equation 1.8), but also depends on the dynamic response of the turbine and their governor. Indeed, just as the frequency starts to decrease, their primary control comes into play. As already explained, it modifies the power output of the power generating module in order to minimize the frequency deviation. Therefore, the faster we can activate it, the better it will help the grid frequency dynamic. For this reason, it can play a similar role than the grid inertia.

In order to compare the influence of different primary control dynamics, three different cases are being studied:

- Case 1: The whole power generation is supplied by hydro turbines characterized by their rather low dynamic response. The model used is available in the Appendix (figure A.4).
- Case 2: The power is now supplied by 50% of hydro turbine and 50% of renewable connected through a power converter working at their maximum power output.
- Case 3: This time, the share of renewable working at MPPT is 75% and only 25% of the power generation is ensured by fast steam turbine. The model used is available in the Appendix (figure A.3).

The 3 different cases share the same parameters gathered in table 2.1.

Parameter	Value
Nominal base power	$S_{base} = 6000\ MVA$
Connected load	$Load = 3000\ MW$
Load damping effect	$f_0 = 50\ Hz$
Generator loss	$\Delta P_e = 80\ MW$
Load damping	$d = 1.5\%$
droop	$\sigma = 5\%$
Inertia constant of hydro turbine	$H_{hydro} = 5\ s$
Inertia constant of steam turbine	$H_{steam} = 5\ s$

Table 2.1: Parameters of the isolated grid

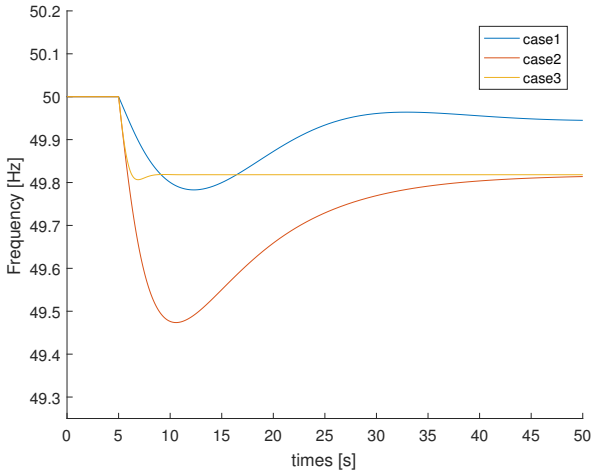

Figure 2.1: Graph of the different frequency control

As we can observe, the maximum peak value of frequency deviation occurs with case 2. It is interesting to notice that the peak value wasn't actually reached for the grid with the higher renewable grid integration. Furthermore, not only the case 3 performed better than case 2 but it also has a peak frequency deviation slightly lower than case 1 which has 100 % of traditionally synchronous machines. Therefore, we can claim that frequency deviation is smaller for really low inertia ($H_{grid} = 1.5\ s$) level but with fast primary control compared to a higher inertia level ($H_{grid} = 6\ s$) but with slow primary response.

Because the primary control can play a significant role in the so called inertia response corresponding to the first moment after the disturbance, we can imagine stable frequency grid dynamic with really low inertia, such as case 1, but with sufficiently fast primary response. Indeed, supporting low inertia grid with fast responding primary control units is one solution for the grid frequency stability.

2.1.1 Actual isolated grid with low inertia in EU

In Europe, Ireland is similar to the simplified case 3. Indeed, the whole island has no AC tie line with other countries which makes it isolated from what is happening outside. However, two HVDC links with Great Britain are present to ensure the power import/export as shown in figure 2.2.

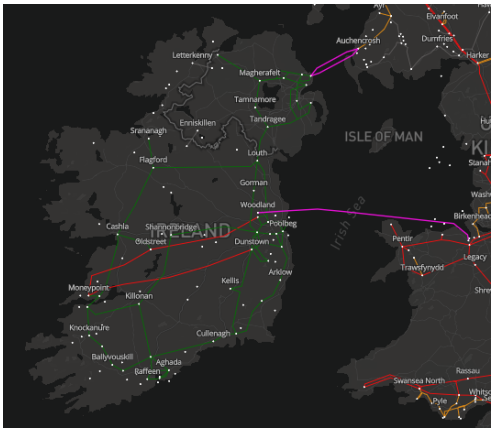

Figure 2.2: Map of the two HVDC line connection of Ireland [3]

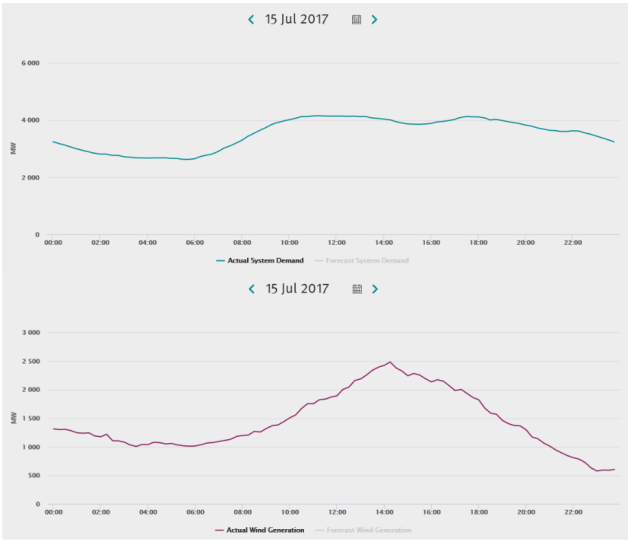

Figure 2.3: Load and wind power generation of the Irish power grid [1]

We can observe on the figure 2.3 that the Saturday 15th of July 2017 at 14:00, wind power generation reaches up to 2 500 MW. This is equivalent to more than two nuclear power units. At the same time the load was about 3950 MW, this means that more than 60 % of the electric power need of Ireland is achieved only with wind power. Consequently, traditional kinetic energy of synchronous machine is considerably reduced. This means that the rate of change of frequency change is much stronger and that the grid operator have to work with a stability closer to the edge. Therefore, Ireland is working in parallel with a solid gas power generation support characterized by their fast primary response to compensate the lack of grid inertia. And, it should further be noted as well that the controllable high-voltage direct current transmission lines play an important role in strengthening the grid frequency stability through synthetic inertia.

2.2 Power transfer

2.2.1 Tie line power transfer

For the study of the frequency and the tie line power exchanges, as long as we are not interested in the area intermachine oscillations, the grid area can be interpreted as one equivalent generating unit represented by a voltage source behind an equivalent reactance (figure 2.4).

Therefore, the power transfer between two areas is simply obtained as:

$$P_{T,12} = \frac{V_1 V_2}{X_T} sin(\delta_1 - \delta_2) \tag{2.1}$$

With $X_T = X_1 + X_{tie} + X_2$

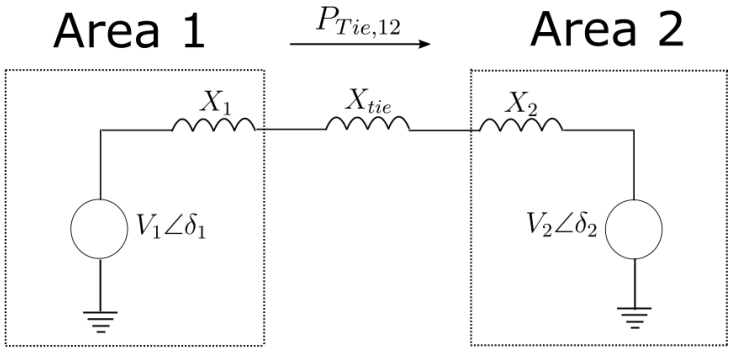

Figure 2.4: Electrical equivalent of two grid areas

Additionally, the equation 2.1 is often linearized as:

$$\Delta P_{tie,12} = \underbrace{\frac{V_1 V_2}{X_{Tie12}} cos(\delta_{1,0} - \delta_{2,0})}_{T_{12}} (\Delta\delta_1 - \Delta\delta_2) \tag{2.2}$$

Indeed, it allows to simply represent the tie line power transfer as if it was an additional load seen by the grid. In figure 2.5, the block diagram of the power exchange between two areas is shown. If the tie line power transfer $P_{tie,12}$ is realized from area 1 to area 2, a negative sign in area 1 is used as if its electric load increases and a positive sign is used for area 2 as if the load decreases. And conversely, if the power is realized from area 2 to area 1.

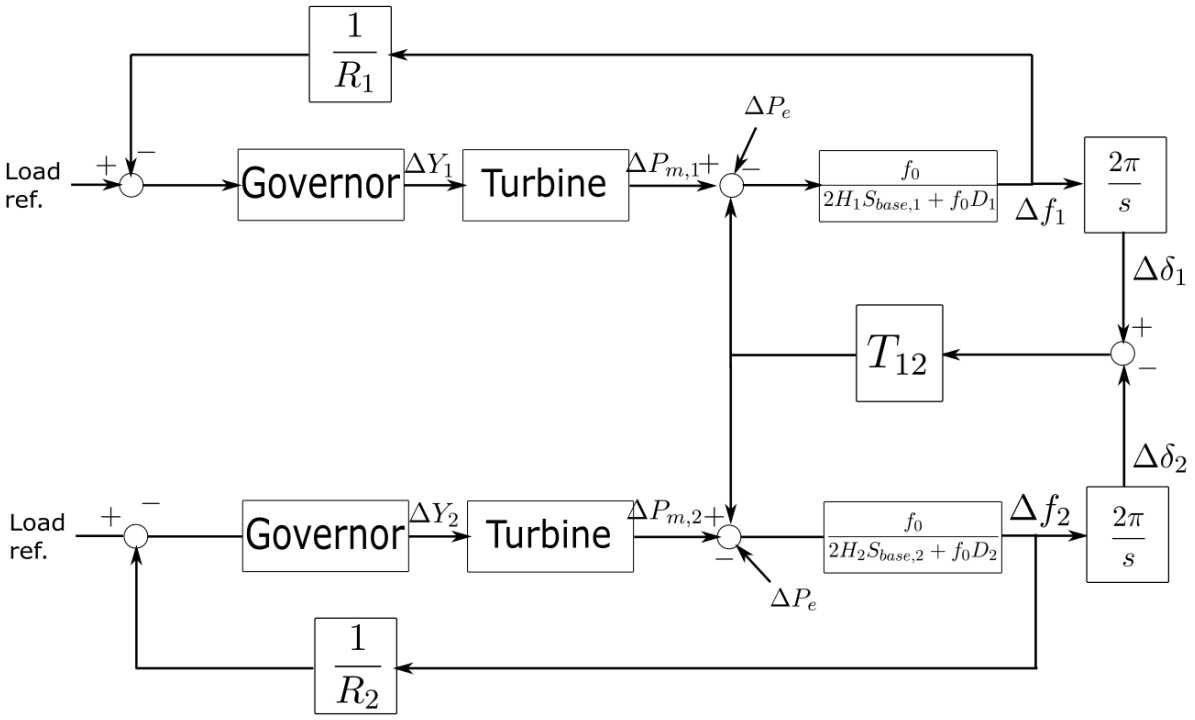

Figure 2.5: Block diagram for tie line power exchange

2.2.2 Three areas power exchange

With the same logic, the power exchanges in a three areas interconnected grid is:

$$P_{tie,12} = \frac{V_1 V_2}{X_{T12}} sin(\delta_1 - \delta_2) \tag{2.3}$$

$$P_{tie,13} = \frac{V_1 V_3}{X_{T13}} sin(\delta_1 - \delta_3) \tag{2.4}$$

$$P_{tie,23} = \frac{V_2 V_3}{X_{T23}} sin(\delta_2 - \delta_3) \tag{2.5}$$

Linearizing about the operating point $\delta_1 = \delta_{1,0}$, $\delta_2 = \delta_{2,0}$ and $\delta_3 = \delta_{3,0}$, we have:

$$\Delta P_{tie,12} = \underbrace{\frac{V_1 V_2}{X_{Tie12}} cos(\delta_{1,0} - \delta_{2,0})}_{T_{12}} (\Delta\delta_1 - \Delta\delta_2) \tag{2.6}$$

$$\Delta P_{tie,13} = \underbrace{\frac{V_1 V_3}{X_{Tie13}} cos(\delta_{1,0} - \delta_{3,0})}_{T_{13}} (\Delta\delta_1 - \Delta\delta_3) \tag{2.7}$$

$$\Delta P_{tie,23} = \underbrace{\frac{V_2 V_3}{X_{Tie23}} cos(\delta_{2,0} - \delta_{3,0})}_{T_{23}} (\Delta\delta_2 - \Delta\delta_3) \tag{2.8}$$

However, it is important to point out that when there is at least more than two interconnected areas, the scheduled interchange power flow does not travel in the tie line as we would have wished. Therefore, if a grid area wishes to import a certain amount from an other area, the power flow will not only go to the tie line connecting those two areas but will also take a parallel path depending on their relative impedance. Indeed the whole interconnected grid must obey to the Kirchhoff circuit law.

2.2.3 Simulation of interconnected three areas

A three areas grid system is imagined to study its dynamic after a power disturbance. Firstly, the different areas will be supplied by standard reheat steam turbines (model in Appendix figure A.2). After that, the case where an important part of the generation is ensured by renewable connected through power electronics is performed.

The actual power flow exchange between the three areas are shown in figure 2.6, where all the tie line inductance X_{Tie} are the same.

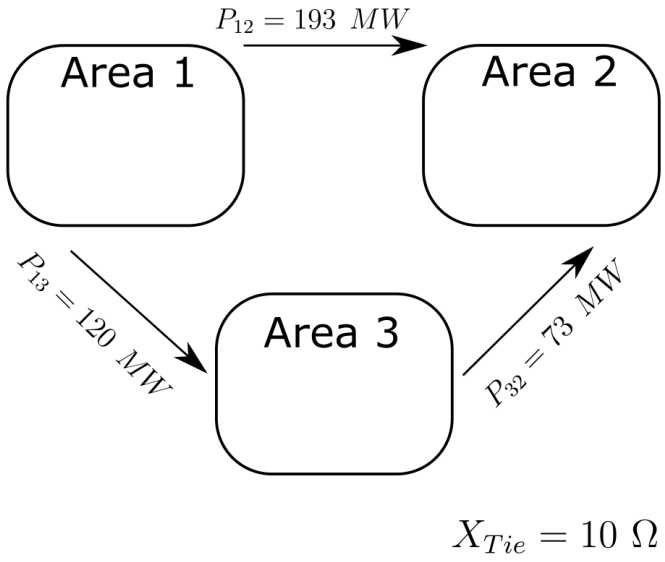

Figure 2.6: Power exchange between three interconnected grid areas

Their different key parameters are shown in the tables 2.2, 2.3 and 2.4 below:

Area 1 parameters	Values
Nominal base power	$S_{base,1} = 13000\ MVA$
Connected load	$Load_1 = 12000\ MW$
Load damping effect	$f_0 = 50\ Hz$
Generator loss	$\Delta P_e = 300\ MW$
Load damping	$d_1 = 1.5\%$
droop	$\sigma_1 = 5\%$
Inertia constant	$H_1 = 5\ s$
Electric equivalent source	$V_1 \angle \delta_1 = 230kV \angle 14.5°$
Equivalent impendance	$X_1 = 20\ \Omega$

Table 2.2: Area 1 parameters

Area 2 parameters	Values
Nominal base power	$S_{base_2} = 9000\ MVA$
Connected load	$Load_2 = 6000\ MW$
Load damping effect	$f_0 = 50\ Hz$
Load damping	$d_2 = 1.5\%$
droop	$\sigma_2 = 5\%$
Inertia constant	$H_2 = 5\ s$
Electric equivalent source	$V_1 \angle \delta_1 = 230kV \angle 4°$
Inertia constant	$H_2 = 5\ s$
Equivalent impendance	$X_2 = 20\ \Omega$

Table 2.3: Area 2 parameters

Area 3 parameters	Values
Nominal base power	$S_{base_3} = 12000\ MVA$
Connected load	$Load_3 = 9000\ MW$
Load damping effect	$f_0 = 50\ Hz$
Load damping	$d_3 = 1.5\%$
droop	$\sigma_3 = 5\%$
Inertia constant	$H_3 = 5\ s$
Electric equivalent source	$V_1 \angle \delta_1 = 230kV \angle 8°$
Equivalent impendance	$X_3 = 20\ \Omega$

Table 2.4: Area 3 parameters

The simulation is performed for the loss of a 300 MW generator in area 1. The corresponding frequency and power changes are shown on figures 2.7, 2.8,2.9 and 2.10.

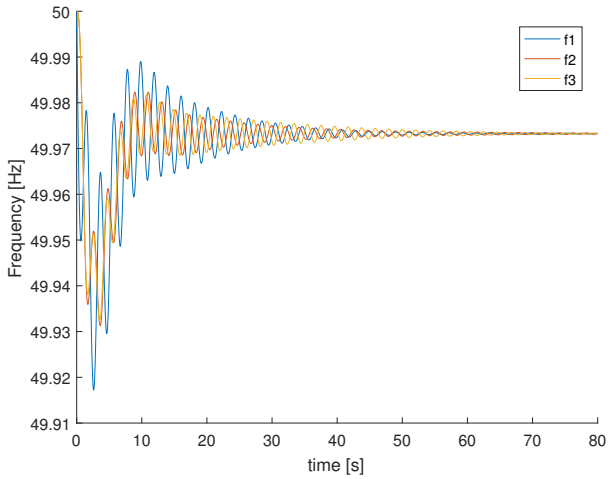

Figure 2.7: Frequency deviation

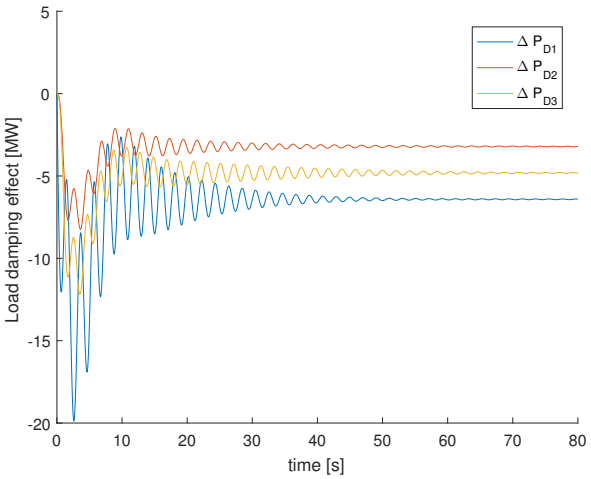

Figure 2.8: Load power change

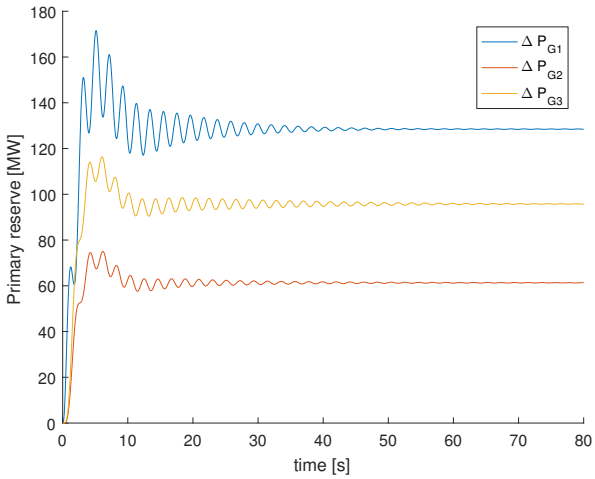

Figure 2.9: Primary response generation

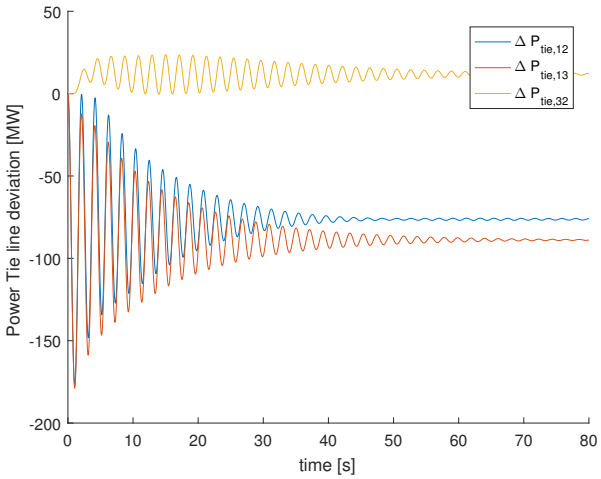

Figure 2.10: Tie line power deviation

We can observe that the whole interconnected grid is reacting to the power disturbance occurred in area 1. The frequency of each area is decaying and oscillating (figure 2.7) with different dynamics depending on their characteristics and inertia. This is until they find a new common frequency for the interconnected grid. Indeed, the load power has decreased slightly thanks to the load damping (figure 2.8) and primary control has responded to the frequency drop by increasing the power generation in each areas up to the balance between the total load and the total generation meaning a steady frequency (figure 2.9).

As it can be obviously seen in the results, the primary control is responding to a power disturbance happening anywhere in the grid. It comes with the advantage of providing a greater stability to the different interconnected areas. However, because a frequency disturbance is perceived by all the grid areas and causes conjointly the primary control reaction of all the areas, it greatly increases the power flow management complexity.

High renewable penetration in one area

The power generation in area 2 is now ensured at 80% by renewable power sources providing no primary control and no inertia due to their different technology. Similarly, an identical sudden loss of 300 MW occurred in area 1.

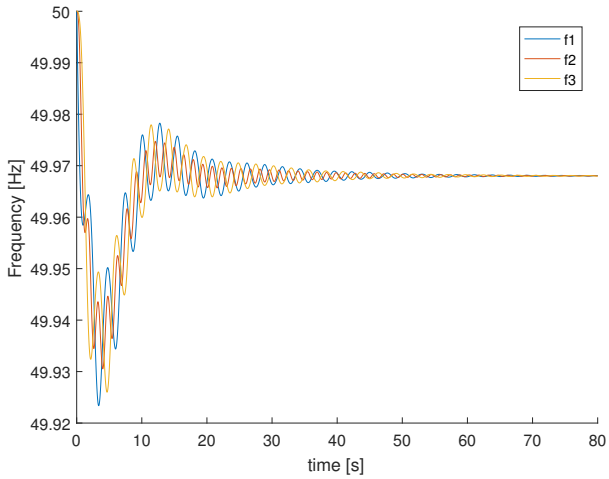

Figure 2.11: Frequency deviation

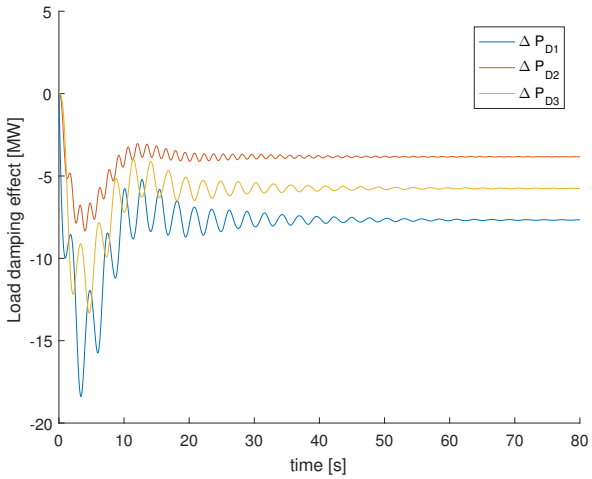

Figure 2.12: Load power change

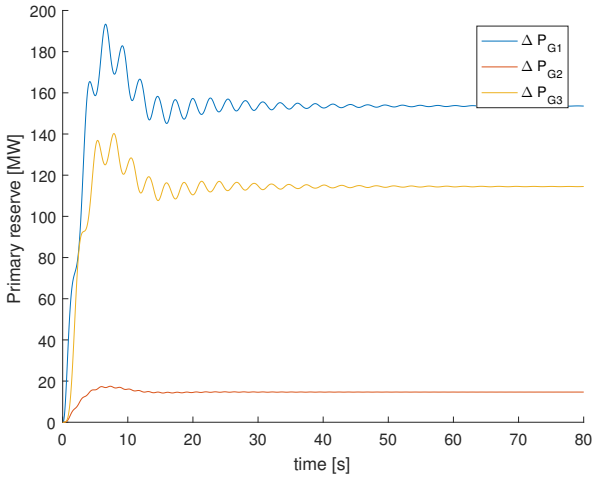

Figure 2.13: Primary response generation

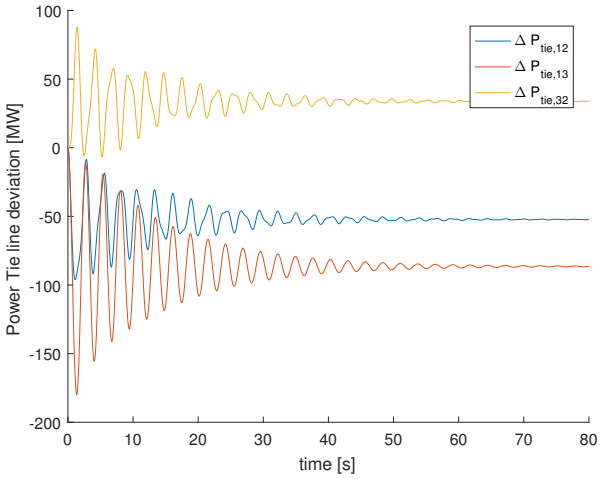

Figure 2.14: Tie line power deviation

The power flow in the tie line connecting area 2 with area 3 has amplified and reaches a power peak three times bigger than before during its transient.

Care must be taken when running interconnected grid with important renewable integration area because its faster and stronger dynamic provokes more important unscheduled and unwanted power flow during the transient and eventually reaches the power capacity limit of the tie lines. Its is to note that the tie line power deviation $\Delta P_{1,2}$ and $\Delta P_{2,3}$ are now almost the same.

Over the time, secondary control of the faulty area will take on and compensate the power disturbance in order to bring the frequency back at its nominal value but also to restore the scheduled power transferred. However, it does take several minutes prior to taking effect. This means that if the transients of the grid are stronger due to an important share of renewable, the planning and the sell of electric energy between the different grid areas are significantly constrained.

2.3 European interconnected grid

Because the member states of the European Union (EU) are interconnected, a harmonized way to manage the grid has been developed throughout the years.

After World War II, with the limited resources remaining and driven by the Marshall Plan, the powerful idea of interconnecting the countries emerged. Gradually European countries became more and more interconnected until forming today the biggest power grid in the world. Indeed, the latter is composed of 34 countries delivering more than half billion clients for a production capacity higher than one million MW.

This enormous grid ensures a great reliability and effectiveness of the use of energy but also comes with a greater complexity. This forces the different members of the grid to coordinate and standardize their operations.

2.3.1 ENTSOE

To even better harmonized the European power grid operated by 41 different transmission operators (TSO), the European Network Transmission System Operators for Electricity (ENTSOE) was created in 2009.

Among its many objectives, ENTSOE mainly aims to a further liberalization of the electricity market with a deeper integration of the renewable and a closer coordination between the different TSO members. As explained before, integrating more renewable power sources into the grid decreases the grid inertia and stability. TSO will have to work with more sensitive dynamic and therefore will have to update their network code.

ENTSOE is currently working and developing new technical documents on which all TSO members have already agreed. Consequently, those new European grid code will be entered into force the EU and each member state will have to integrate them into their national grid code. The laws will ask a better coordination between the transmission, the generators and distributors of electric energy. Indeed with the liberalization of energy market and decentralization of production, the new rules will impact and concern everyone as far as the small local producer who will be obligated to align.

2.3.2 Technical document regularizing the power generating module

Among the technical document on frequency regulation published by ENTSOE, we can find those concerning the power producers and thus directly influencing the frequency stability.

In order to appropriately legislate the power producers, power generating modules are classified into 4 different categories A,B,C and D from the less to the more powerful as followed:

Synchronous areas	Limit for maximum capacity threshold from which a power-generating module is of type B	Limit for maximum capacity threshold from which a power-generating module is of type C	Limit for maximum capacity threshold from which a power-generating module is of type D
Continental Europe	1 MW	50 MW	75 MW

Table 2.5: Limits for thresholds for type B, C and D power-generating modules [5]

The legislation applies differently depending in which category the generating module falls into. The more important the power producer, the stricter is the rule to be authorized in the power grid. Therefore, system operators are allowed to refuse the connexion of power generating module if it does not comply with the new regulation.

To sum up roughly, generator A, is limited at automated response and minimal system operator control, while generator B has wider range of automated dynamic response to maximize the dynamic generation to system event. Generator C requires to provide a stable and highly controllable real time dynamic response aiming to provide ancillary service.

And the requirement for generator D is specific to high voltage connected power generation with an impact on control and operation on the entire system as it should ensure stable operation of the interconnected grid system and allowing of ancillary service from generation Europe wide [5].

An important quantity of grid code, is published in the ENTSOE website or in the Official Journal of the European Union concerning many aspects of the grid such the voltage quality, the reactive power control capability, the fault-ride trough capability, frequency containment etc.

As regard of the frequency stability, plenty of rules and exceptions exist. Among them, we can for instance see that all types of generators shall be capable of staying connected at a specific range of frequency and operating during a minimum time in the table 2.6.

Synchronous area	Frequency range	Time period for operation
Continental Europe	47,5 Hz-48,5 Hz	To be specified by each TSO, but not less than 30 minutes
	48,5 Hz-49,0 Hz	To be specified by each TSO, but not less than the period for 47,5 Hz-48,5 Hz
	49,0 Hz-51,0 Hz	Unlimited
	51,0 Hz-51,5 Hz	30 minutes
Ireland	47,5 Hz-48,5 Hz	90 minutes
	48,5 Hz-49,0 Hz	To be specified by each TSO, but not less than 90 minutes
	49,0 Hz-51,0 Hz	Unlimited
	51,0 Hz-51,5 Hz	90 minutes

Table 2.6: Range of frequency deviation under which a power generating module has to be capable of operating for a minimum time period

Indeed, it is important that the connected power generating devices are able to run at a minimum frequency range to avoid snowball effect in case of important frequency deviation event.

One can notice different requirements for Ireland for instance. As a matter fact, its grid characteristics are significantly different from the rest of EU thus it required customized rules. In fact, the different TSO have some margin of freedom to apply the legislation depending on their grid standard.

For instance, the different TSO freely specify the admissible maximum power reduction of a power generating module type A facing a frequency decay. However, it should be included within the boundaries of figure 2.15.

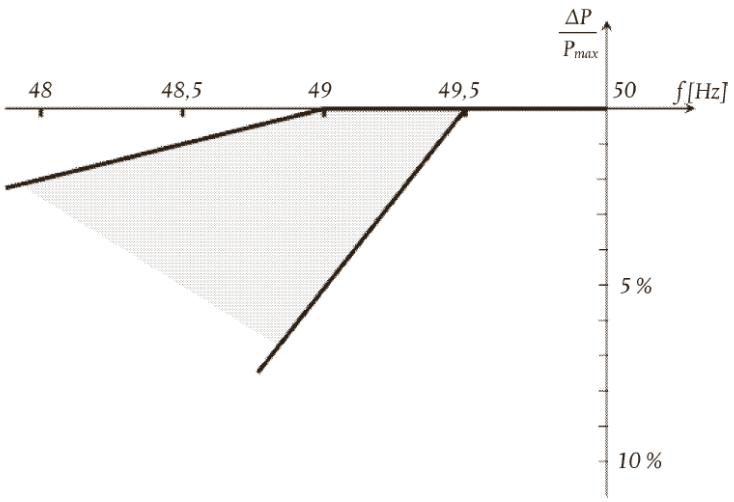

Figure 2.15: Maximum power capability reduction with falling frequency [5]

For superior types of power generating module it should of course satisfy the boundaries condition of figure 2.15 but also be able of rising its power output to participate in the grid primary control. Similarly, the range of the minimum primary action required is given by ENTSOE and the specific TSO will wisely select one satisfying the condition for its own grid. As we go to superior types of generator, the flexibility allowed by the common grid code declines and the TSO must align more firmly.

Chapter 3

Analysis of frequency data throughout a year

For this report, an important data file of the grid frequency in Belgium was available. It was measured throughout the whole year of 2013, from the 1st of January until the 31th of December. The frequency is given approximately every half second therefore about 6 4281 600 of frequency values are accessible. Thus, with this vast amount of detailed data, we can expect to observe interesting grid frequency phenomena.

However, the inertia effect is limited considering that Belgium is among the biggest interconnected power grid in the world. Additionally, information about the grid power disturbances and the type of unit connected would be needed to evaluate precisely the impact of inertia response.

In parallel of the frequency data, we calculated an approximation of the rate of frequency change throughout the whole year, which is simply obtained with the difference of two measured frequency over the time step:

$$\frac{df}{dt} \approx \frac{\Delta f}{\Delta t} = \frac{f_{i+1} - f_i}{\Delta t} \tag{3.1}$$

This value is relevant and is directly related to the inertia of the grid and also the mismatch between the power produced and the load (equation 1.2).

3.1 How it is measured

As already explained, two frequency measurements are available for every second. In fact, the measuring tool detects when the voltage crosses zero, therefore it can count a voltage period. With a precise GPS watch, it measures the time needed for 25 periods. Obviously in our 50 Hz grid, it will be really close to 0.5 s. Therefore it does not identify the instantaneous frequency but rather a mean frequency value each 25 periods detected. One way to obtain the instantaneous frequency value would be to directly measure the speed on a synchronous power generator because they are directly inducing the voltage frequency of the grid.

There will not have the same number of data from one day to an other, because the 25 periods measurements will not take exactly half a second each time. This would be the case only if the frequency was exactly 50 Hz and never fluctuating.

3.1.1 Quality problem and glitch

Unfortunately, a non negligible number of data are false. Indeed, unrealistic frequency and rate of frequency change are present. As a matter of fact, the measuring device is not glitch-free and is also subject to voltage quality problems present in the place where the data was taken. The voltage measured is not a perfectly balanced three phases sinusoidal signals and a cross-zero can be detected where it should not. Therefore, a filtering program to treat the raw data is mandatory. Some example of obvious erroneous data are shown in figures 3.1,3.2 and 3.3.

	1 date	2 Secondes1	3 Delta_t1	4 frequency	5 Delta_f_Delta_t
50924	'01-Jan-2013 07:05:18'	2.5518e+04	0.5000	50.0133	1.8310e-04
50925	'01-Jan-2013 07:05:19'	2.5519e+04	0.5000	50.0134	9.9181e-05
50926	'01-Jan-2013 07:05:19'	2.5519e+04	0.5000	50.0144	0.0020
50927	'01-Jan-2013 07:05:20'	2.5520e+04	0.5000	50.0146	3.9672e-04
50928	'01-Jan-2013 07:05:20'	2.5520e+04	0.5000	50.0145	-3.8146e-05
50929	'01-Jan-2013 07:05:21'	2.5521e+04	0.5000	50.0142	-6.0271e-04
50930	'01-Jan-2013 07:05:21'	2.5521e+04	0.5000	50.0142	-1.4496e-04
50931	'01-Jan-2013 07:05:22'	2.5522e+04	0.5000	50.0142	0
50932	'01-Jan-2013 07:05:22'	2.5522e+04	0.5000	50.0142	0
50933	'01-Jan-2013 07:05:22'	2.5522e+04	0	50.0142	NaN
50934	'01-Jan-2013 07:05:22'	2.5522e+04	0	50.0142	NaN
50935	'01-Jan-2013 07:05:22'	2.5522e+04	0	50.0142	NaN
50936	'01-Jan-2013 07:05:24'	2.5524e+04	2.0000	50.0142	-7.6293e-06
50937	'01-Jan-2013 07:05:25'	2.5525e+04	0.5000	50.0144	4.1960e-04
50938	'01-Jan-2013 07:05:25'	2.5525e+04	0.5000	50.0149	9.6892e-04

Figure 3.1: Glitch with the time step measurement

	1 Sjanvier	2 Secondesjanvier	3 Delta_tjanvier	4 frequencyjanvier	5 Delta_f_Delta_tjanvier
2499851	'15-Jan-2013 11:24:18'	1.2507e+06	0.5000	49.9887	2.1362e-04
2499852	'15-Jan-2013 11:24:18'	1.2507e+06	0.5000	49.9889	3.2806e-04
2499853	'15-Jan-2013 11:24:19'	1.2507e+06	0.5000	49.9893	8.3159e-04
2499854	'15-Jan-2013 11:24:19'	1.2507e+06	0.5000	49.9905	0.0024
2499855	'15-Jan-2013 11:24:20'	1.2507e+06	0.5000	49.9906	1.6021e-04
2499856	'15-Jan-2013 11:24:20'	1.2507e+06	0.5000	49.9906	0
2499857	'15-Jan-2013 11:24:21'	1.2507e+06	0.5000	49.9906	0
2499858	'15-Jan-2013 11:24:21'	1.2507e+06	0.5000	49.9906	0
2499859	'15-Jan-2013 11:24:22'	1.2507e+06	0.5000	49.9906	0
2499860	'15-Jan-2013 11:24:22'	1.2507e+06	0.5000	49.9906	0
2499861	'15-Jan-2013 11:24:23'	1.2507e+06	0.5000	49.9906	0
2499862	'15-Jan-2013 11:24:23'	1.2507e+06	0.5000	49.9906	0
2499863	'15-Jan-2013 11:24:24'	1.2507e+06	0.4063	52.6284	6.4928
2499864	'15-Jan-2013 11:24:24'	1.2507e+06	0.5938	49.9923	-4.4396
2499865	'15-Jan-2013 11:24:25'	1.2507e+06	0.5000	49.9927	7.5528e-04

Figure 3.2: Values of frequency are stuck then suddenly increase

	Sjanvier	Secondesjanvier	Delta_tjanvier	frequencyjanvier	Delta_f_Delta_tjanvier
863346	'05-Jan-20...	4.3198e+05	0.5000	50.0684	0.0015
863347	'05-Jan-20...	4.3199e+05	0.5000	50.0686	5.0353e-04
863348	'05-Jan-20...	4.3199e+05	0.5000	50.0688	2.6702e-04
863349	'05-Jan-20...	4.3199e+05	0.5000	50.0689	3.5095e-04
863350	'05-Jan-20...	4.3199e+05	0.5000	50.0687	-5.0353e-04
863351	'05-Jan-20...	4.3199e+05	0.5000	50.0683	-8.0870e-04
863352	'05-Jan-20...	4.3199e+05	0.5000	50.0691	0.0017
863353	'05-Jan-20...	4.3199e+05	0.5000	50.0692	1.2207e-04
863354	'05-Jan-20...	4.3199e+05	0.5000	50.0687	-0.0011
863355	'05-Jan-20...	4.3199e+05	0.5000	50.0686	-1.1444e-04
863356	'05-Jan-20...	4.3199e+05	0.5000	1.4567e-38	-100.1357
863357	'06-Jan-20...	4.3200e+05	0.5000	50.0682	2.3651e-04
863358	'06-Jan-20...	4.3200e+05	0.5000	50.0678	-8.1633e-04

Figure 3.3: Evident issue with the frequency measurement

3.1.2 Filtering

In consequence, suspect data are filtered with a matlab program. However, the conditions the data must fulfill to be saved for the analysis must not be to strong otherwise we could lose interesting frequency events. It is chosen to delete the data when frequency is over 51 Hz and under 49 Hz as well as when the calculated rate of frequency change is higher than $|50\ mHz|$. Sometimes the frequency values and the corresponding time step doesn't change and stays the exact same (fifteen digit after the decimal) for a while, which is really suspicious and therefore deleted. Finally some improbable data are also manually deleted.

3.2 Visualization of the frequency data

A plot of the filtered frequency data and its corresponding rate of frequency change is performed when the frequency level was low between 21:02:00 and 21:03:30 the 10th of September (figure 3.4 and 3.5).

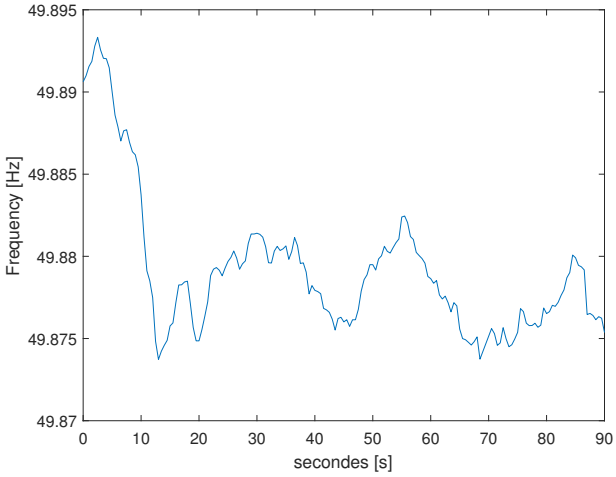

Figure 3.4: Frequency measured the 10th of September from 21:02:00 to 21:03:30

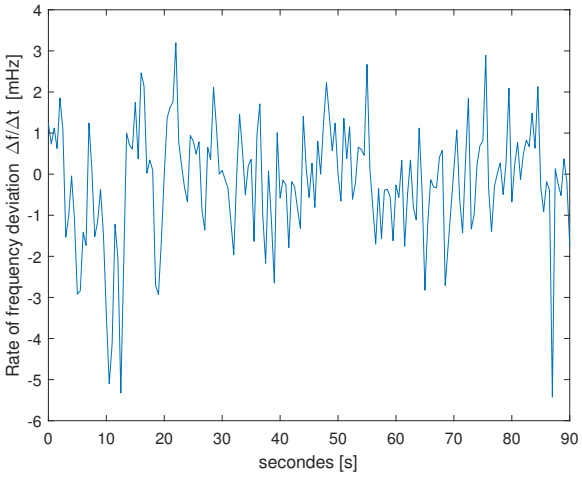

Figure 3.5: Calculated rate of frequency change from 21:02:00 to 21:03:30

We can clearly observe the dynamic of the grid frequency varying with time. In figure 3.4, the frequency is 0.1 Hz under its nominal value but it is still an acceptable level. Secondary control will then have to come into play to bring back the frequency at 50 Hz.

An interesting frequency dynamic was spotted the 24th of October at 10:55:00 shown in figure 3.6 and 3.7.

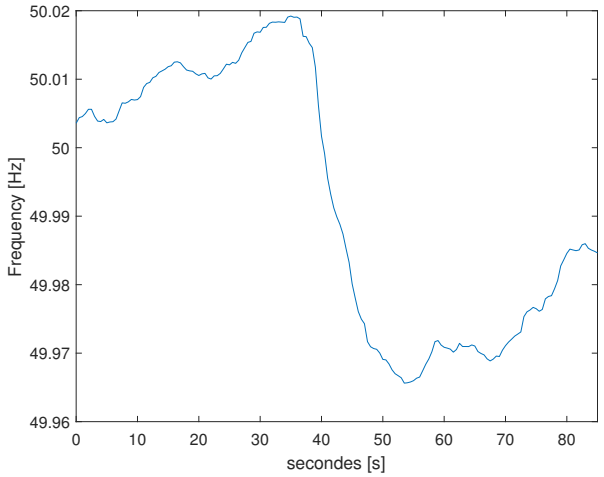

Figure 3.6: Frequency measured in October from 10:54:30 to 10:55:55

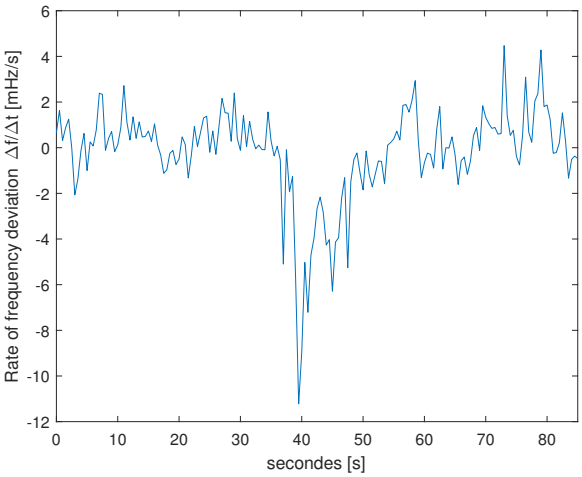

Figure 3.7: Calculated rate of frequency change from 10:54:30 to 10:55:55

This is a typical frequency response when generation has suddenly decreased compared to the load. Thus, we can conclude that either a generator might have been disconnected from the grid or really a sudden important load popped up. As frequency starts to decay, the inertial response, including some fast primary control, will try to reduce the rate of frequency change. We observe that the frequency drop happens in less than 15 seconds which is the time where the

inertia followed by the primary control comes into play. The rate of frequency change $\Delta f/\Delta t$ reaches -10 mHz/s which is an important value for the Belgium grid but not critical at all and the strong interconnected EU can easily manage it.

An histogram is used to graphically represent the distribution of the data. The entire range of values is divided into 100 intervals. The y axis represents the normalized number of time the data falls in the interval. This graphical representation is shown for the the whole filtered data of January in figure 3.8 and 3.9.

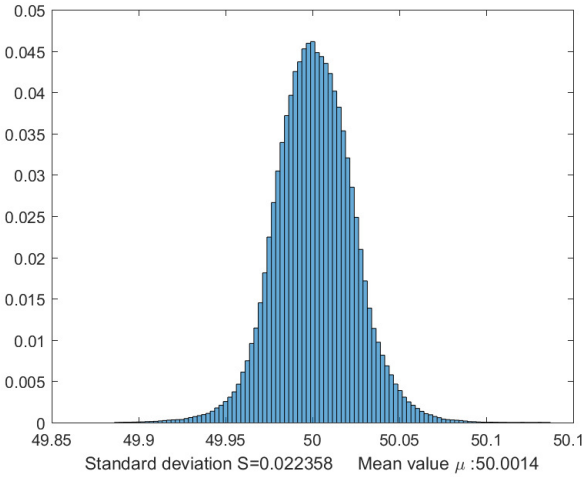

Figure 3.8: Histogram of the frequency in January

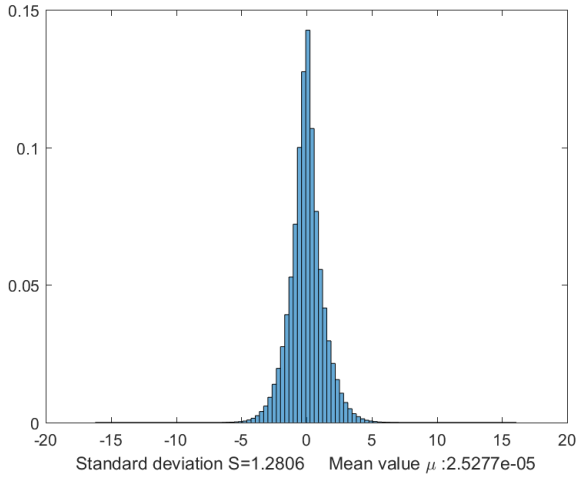

Figure 3.9: Histogram of the rate of frequency deviation in January

For the January grid frequency, we can observe an excellent normal distribution tightly centered at 50 Hz which is what is expected for a strong grid. The mean value of the data is 50.0014 with a standard deviation of 0.022358 with some rare event happening under 49.9 Hz and over 50.1 Hz.

As for the histogram of the calculated rate of frequency deviation in mHz/s, we detect a normal distribution centered at zero with occasional events exceeding $|15\ mHz/s|$. We can notice that slight negative rate frequency of change are more likely to happen by comparing the bar just to the left and just to the right of the middle one.

Finally, one can compare the distribution of each month with the figures in the Appendix.

3.3 Table of the maximum values

A table gathering all he important frequency event for the year 2013 is shown in 3.1.

	f_{max}	Time event	f_{min}	Time event	$\frac{\Delta f_{max}}{\Delta t}$	Time event	$\frac{\Delta f_{min}}{\Delta t}$	Time event
January	50.1367	18.01.13 06/01/00	0.0161	10/01/13 00:00:55	49.8864	11/01/13 20:01:18	-0.0162	02/01/13 22:58:34

February	50.1190	14/02/13 06:00:56	0.0216	28/02/13 08:08:53	49.8732	28/02/13 20:02:30	-0.0287	28/02/13 08:08:55
March	50.1153	03/03/13 18:02:56	0.0239	15/03/13 10:14:00	49.8793	14/03/13 20:01:13	-0.0215	15/03/13 10:13:43
April	50.1458	15/04/13 21:57:37	0.0118	14/04/13 17:00:15	49.8593	23/04/13 00:02:05	-0.0210	27/04/13 08:05:06
May	50.1200	27/05/13 06:01:06	0.0200	24/05/13 23:18:39	49.8810	01/05/13 00:01:35	-0.0239	25/05/13 01:15:34
June	50.1058	13/06/13 07:01:03	0.0268	01/06/13 03:27:20	49.8721	16/06/13 23:02:58	-0.0291	05/06/13 19:48:48
July	50.1006	25/07/13 07:00:42	0.0279	10/07/13 13:27:47	49.8901	10/07/13 00:02:14	-0.0329	31/07/13 16:52:48
August	50.1053	29/08/13 07:00:45	0.0172	17/08/13 22:49:17	49.8872	31/08/13 00:02:04	-0.0363	14/08/13 15:46:26
September	50.1159	09/09/13 21:56:12	0.0219	01/09/13 06:22:44	49.8737	10/09/13 21:02:13	-0.0447	19/09/13 10:17:47
October	50.1172	17/10/13 06:00:51	0.0479	24/10/13 11:06:23	49.8638	28/10/13 17:43:08	-0.0415	24/10/13 11:06:23
November	50.1221	08/11/13 06:01:48	0.0229	30/11/13 00:13:41	49.8835	22/11/13 00:02:30	-0.0429	07/11/13 11:51:56
December	50.1080	17/12/13 06:00:39	0.0326	24/12/13 02:12:34	49.8887	10/12/13 00:02:23	-0.0327	24/12/13 14:40:37

Table 3.1: Table of the important frequency events for each month

We can observe that the different frequency deviation values Δf are comparable with each other, indeed the maximum frequency deviation slightly exceed 0.1 Hz each month. The maximum frequency reached during the whole year 2013 is 50.1458 Hz and the minimum value is 49.8593 Hz. We can say that Europe and thus Belgium did not face any important power outages capable of jeopardizing his grid frequency during the year 2013.

The maximum rate of frequency change $\Delta f/\Delta t$ can more than triple from one month to an other. Although, the frequency is each time quickly corrected as demonstrated by the maximum frequency deviation values. Those more important varying maximum rates of frequency change might be happening because the overall inertia of Belgium and Europe is fluctuating depending on the renewable integration and the total load. Indeed, during sunny and windy week-end day, the share in renewable can be much more important thus increasing the rate of of frequency change.

As matter of fact, only in Belgium the installed power capacity of the wind turbines is about 2.3 GW and the peak power capacity of all combined photovoltaics panels reach 3 GWp (although those ones were installed after 2013 pushed by the state subventions) which means that the grid can reach quite strong renewable integration during favorable conditions. However as the grid is supported by the strong interconnected European grid, the rate of frequency deviation are limited.

Actually the frequency data of Ireland for instance would have been more relevant for the low inertia impact analysis since it has a strong wind power integration and is not connected to others countries with AC tie lines.

Chapter 4

Wind turbine analysis

Windmills have been used for thousands of years for grinding grain and pumping water. The use of windmill (or wind turbine) to directly produce electricity dates back to the end of the 19th century. Afterwards, the technology of wind turbine developed slowly until the 1973 crisis when the sudden increase of oil price greatly encouraged the research as well as the development of government-funded programs. In addition to the increase of oil prices, the global warming caused by the combustion of fossil fuel has also stimulated the development of wind turbine. Furthermore, the improvement of the performance has grown in parallel with the development of power converter which enabled the wind turbine to work in variable speed. The overall power produced in our grid has considerably increased during the last decades as shown in figure 4.1 for EU.

Today, wind turbine are a part of our landscape. They are generally not alone but gathered on a same favorable windy site to form a wind park which may include over a hundred units. The more advanced modern wind turbine are capable to produce up to 10 MW! In this chapter, a detailed control of 1.5 MW synchronous permanent magnet wind turbine is performed as well as a technique to recover its inertia.

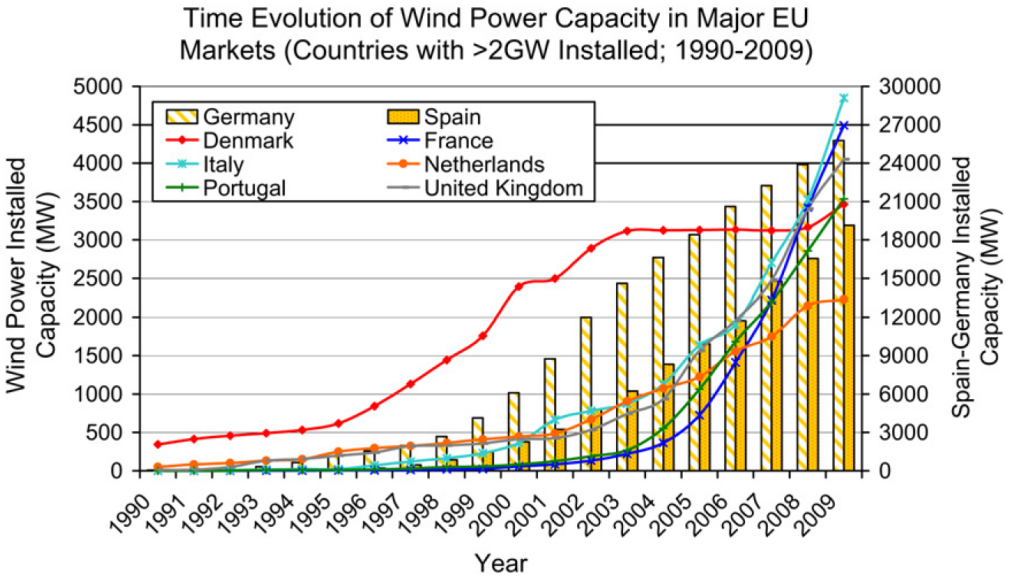

Figure 4.1: Time evolution of wind power capacity in the major EU countries [11]

4.1 Wind resource

The power delivered by the wind depends on the surface of the wind turbine, the density of the air and the speed of the wind:

$$P_{wind} = \frac{1}{2}\rho\,\pi\,R^2\,v_{wind}^3 \quad [W]$$

It is proven by Betz' law that we can theoretically capture at most $\frac{16}{27}$ of this kinetic wind power. Indeed, to put it simple, it is not physically possible for a wind turbine to slow down the mass air flow down to zero. After passing through the wind turbine, the air has still enough kinetic energy to leave. The performance coefficient c_p expressing the power capture over the kinetic power of the wind depends on the tip speed ratio $\lambda = \omega_{rotor}\,R/v_{wind}$ and the pitch angle β of the rotor blades. A generic equation of c_p for a three rotor blades wind turbine is given by [7]:

$$c_p(\lambda,\beta) = c_1\left(c_2(\frac{1}{\lambda+0.08\beta} - \frac{0.035}{\beta^3+1}) - c_3\beta - c_4\right)e^{-c_5(\frac{1}{\lambda+0.08\beta}-\frac{0.035}{\beta^3+1})} + c_6\lambda$$

The coefficient c_1 to c_6 are: $c_1 = 0.5176$, $c_2 = 116$, $c_3 = 0.4$, $c_4 = 5$ and $c_5 = 21$, $c_6 = 0.0068$. Therefore the total power capture by the wind turbine is:

$$P_{turbine} = c_p(\lambda,\beta)\,P_{wind} \tag{4.1}$$

This performance coefficient according to the tip speed ratio for different pitch angle is illustrated in figure 4.2:

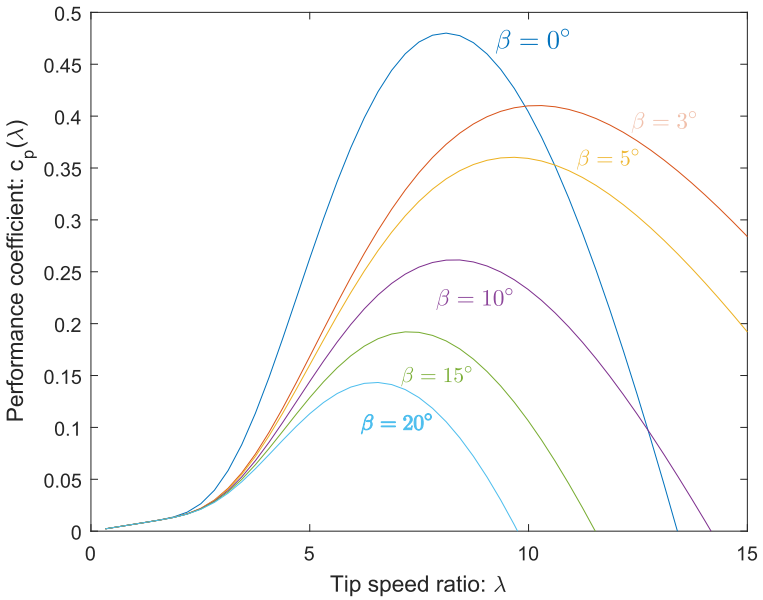

Figure 4.2: Performance coefficient c_p according to the tip speed ratio λ for different pitch angles β

We observe that best performance curve c_p is obtain when the pitch angle is 0°. Indeed it allows the maximum lift force on the rotor blade.

The mechanical output power of an ideal wind turbine of a radius $R = 33\,[m]$ as a function of the rotor speed for different speeds is illustrated in figure 4.3.

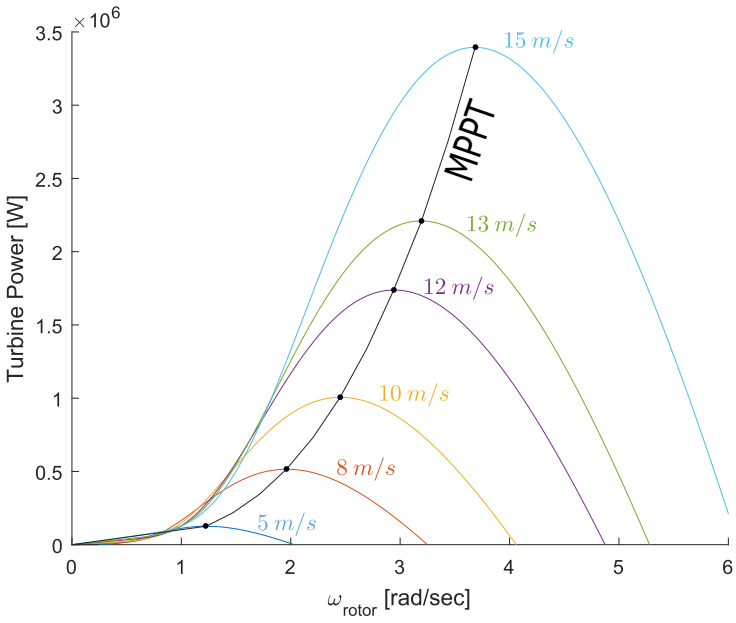

Figure 4.3: Mechanical power of a 33 [m] radius wind turbine according to the speed rotation for different wind

We clearly see the optimal rotor speed to reach for each different wind speed. In order to control the rotor speed, modern wind turbine are equipped with power electronics and controller to modulate the frequency of the applied stator voltages.

Above a wind speed of about 15 [m/s] the wind turbine will reach its maximum power and will continue to deliver it even at greater wind speed by decreasing its performance coefficient thanks to the pitch control of the blades. Eventually when the wind reaches the cut-out speed and becomes dangerously strong, shut down of the wind turbine is initiated.

Reaching the MPPT for each different wind speed through the speed controller greatly improves the efficiency of the machine but comes with the drawback of isolating the rotor inertia from the grid. Indeed, when traditional synchronous machine coupled to the grid frequency naturally deliver their inertia when the frequency drops, the modern generators obey only to the speed dictated by the controller and therefore do not naturally participate to the inertia response.

In this chapter we will design and simulate the different component of a modern permanent magnet synchronous wind turbine connected to the grid and a strategy to recover its inertia.

4.2 Control of a synchronous permanent magnet wind turbine

Synchronous permanent magnet wind turbine are part of the modern variable speed machine. They cannot obviously be directly connected to the grid because the stator voltage frequency is changing depending on the wind speed. Therefore, the machine needs a back to back power converter chain to be connected with the electrical grid.

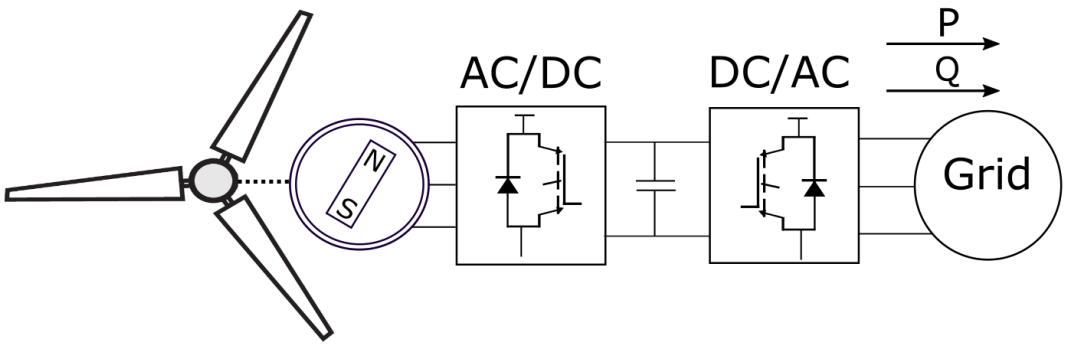

Figure 4.4: Synchronous permanent magnet wind turbine with fully rated converter

For important machines this frequency can be quite low. Indeed, the bigger the radius of the rotor blade, the slower it has to rotate to reach the MPPT. However, because the permanent magnet wind turbine is fed with a power converter running regardless of the grid frequency, the machine can run without a gear box which is a technical difference compared to the doubly-fed electric wind turbine.

4.3 Concordia Park Transformation

Before detailing the control of the PMSG turbine, we will introduce the Concordia Park transformation which is a powerful mathematical tool in electrical engineering. Concordia Park transformation is used to reduce the time varying tree-phases equations to a virtual bi-phases system varying at desired rotational speed. In electrotechnical domain, it allows the reduction of the complexity of the electric equations.

4.3.1 Concordia Transformation

The first transfomation, named after Mr Concordia, is given by:

$$T = \sqrt{\frac{2}{3}} \begin{bmatrix} \frac{1}{\sqrt{2}} & 1 & 0 \\ \frac{1}{\sqrt{2}} & \frac{1}{2} & \frac{\sqrt{3}}{2} \\ \frac{1}{\sqrt{3}} & -\frac{1}{2} & \frac{\sqrt{3}}{2} \end{bmatrix} \tag{4.2}$$

This transformation allows to reduce the three electric phasors a, b, c into the components α, β and 0. The last one is called the homopolar and is equal to zero if the system is balanced and physically doesn't exist if there is no electrical connection to the ground. It is equivalent to a projection of the three electric phasors into the two orthogonal axes α and β as shown in figure 4.5.

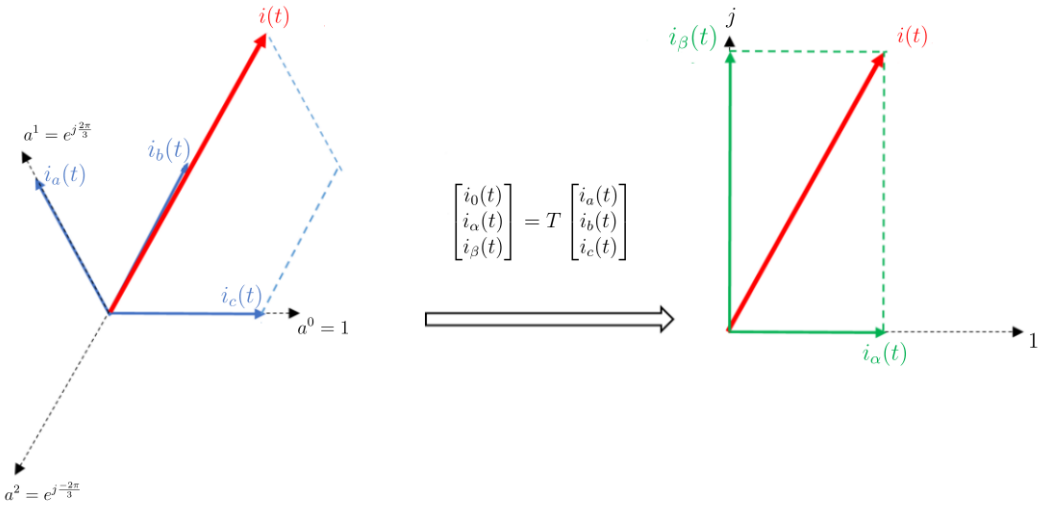

Figure 4.5: Graphical representation of the Concordia transform

The inverse transformation is simply obtain by inverting the matrix T:

$$\begin{bmatrix} i_a(t) \\ i_b(t) \\ i_c(t)) \end{bmatrix} = T^{-1} \begin{bmatrix} i_0(t) \\ i_\alpha(t) \\ i_\beta(t)) \end{bmatrix} \tag{4.3}$$

It is interesting to notice that $T^{'}T^{-1} = I$ which means that the transformation conserves the scalar product and the norm of the vectors. Thus, the power is preserved after the transformation.

4.3.2 Park Transformation

This transformation is given by:

$$P = \begin{bmatrix} 1 & 0 & 0 \\ 0 & cos(\theta(t)) & -sin(\theta(t)) \\ 0 & sin(\theta(t)) & cos(\theta(t)) \end{bmatrix} \tag{4.4}$$

It is equivalent to expressing our phasors α and β in a rotating frame at a desired speed angle $\theta(t)$.

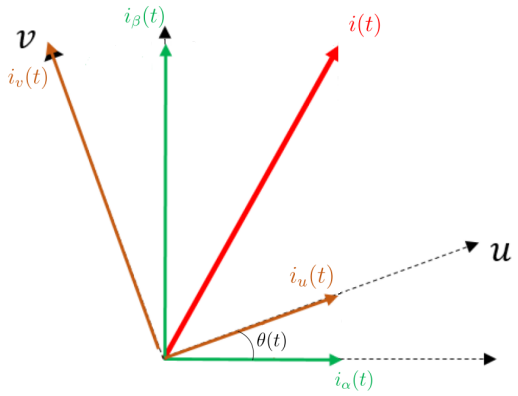

Figure 4.6: Graphical representation of the Park transform

Again $P^{'}P^{-1} = I$ and the power is conserved.

4.4 Vector control technique and Pulse Width Modulation

The vector control, is a modern control technique to command the dq components of a three-phase circuit. It also allows to control the torque or the speed of a three phase AC machine. For the PMSG it is done by adjusting the stator voltages feeding the machine depending on the measured current. This control strategy works in the Park Concordia frame turning with the rotor ($\theta(t) = \theta_{rotor}(t)$).

A fast computing unit is needed to calculate the inverse Park Concordia transform of the measured current in real time to directly work in the dq frame; and also to compute the Park Concordia transformation to directly transform the desired v_d and v_q voltages into the real three phases world.

Feeding the three stator phases with the desired voltage is done through power electronics. The pulse width modulation is usually used for this application. It benefits from a great flexibility and is able to modulate any kind of needed signal. Indeed, it consists of a controllable power semiconductor device acting like switches that can be turn on or off as desired.

For modern wind turbine application, Insulated Gate Bipolar Transistor (IGBT) is usually used. It can transfer great power with high efficiency with a frequency range that lies between 1 kHz to 100 kHz.

According to the Fourier analysis, the square shape modulated signal by the IGBT is the sum of sine wave consisting of a fundamental component at the desired frequency and the undesirable harmonics at higher frequency which can be eventually eliminated with a low pass filter.

For our model, we use the IGBT-diode three phases power converter available model in SimPowerSystem. The pulse width modulation is done by comparing the reference signal with triangle shape carrier at an higher frequency. This approach is shown for one branch of the three phase power converter in figure 4.7.

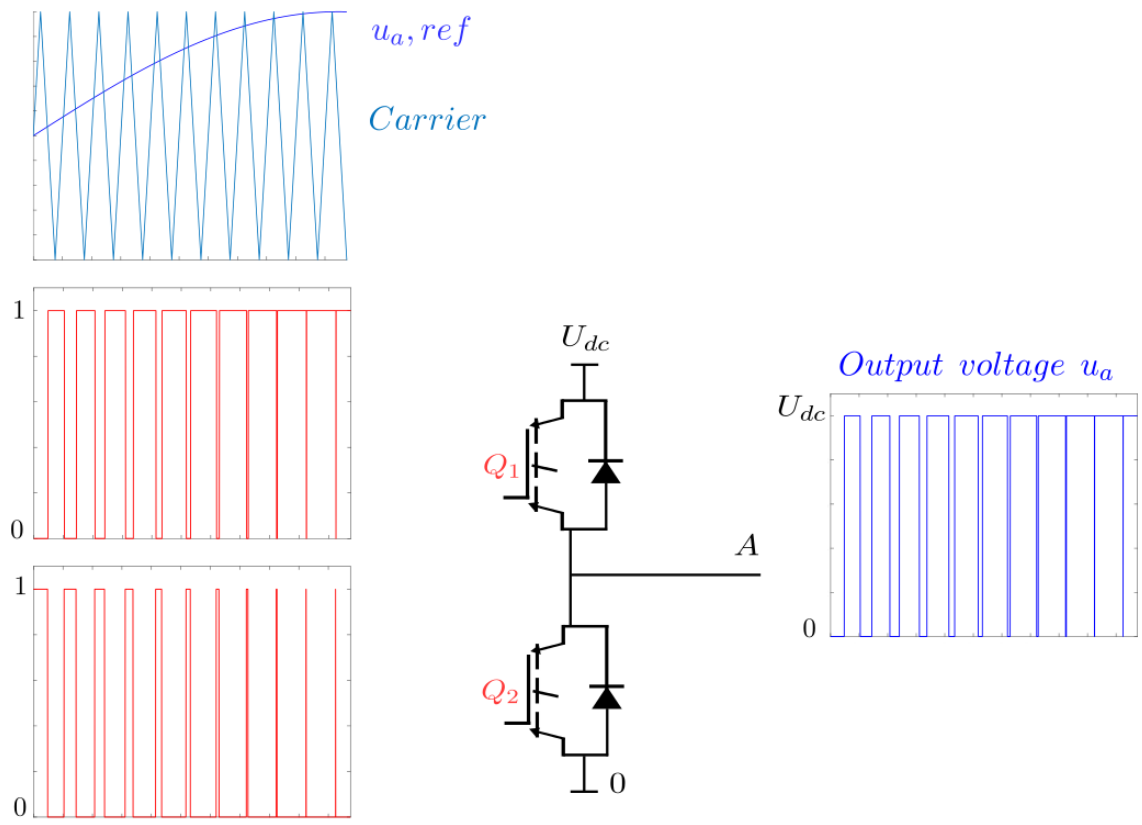

Figure 4.7: Pulse Width modulation of one branch of a power converter

Visually the output voltage obtained may not look like the reference voltage. But in reality the fundamental component is really close to it while the harmonic content is small.

4.5 Constitutive equations of a PMSG

In order to design a controller PMSG wind turbine, we need to first detail the equations of the machine. The generator is composed of a stator with a three phase armature winding and a rotor with a permanent magnet inducing a flux linkage Ψ_b. Damper winding are not used in the model, indeed because the machine is aimed to be controlled by power electronics, the supplied frequency will be constantly adapted to the rotation speed of the machine making the damper useless. We neglect the saturation of the magnetic circuit and we suppose that the change in the inductance of the stator winding according to the rotor position is sinusoidal and does not contain higher harmonic.

The stator circuits equation are given by:

$$v_A(t) = R_A(t) + \frac{\mathrm{d}\psi_A(t)}{\mathrm{d}t} \tag{4.5}$$

$$v_B(t) = R_B(t) + \frac{\mathrm{d}\psi_B(t)}{\mathrm{d}t} \tag{4.6}$$

$$v_B(t) = R_B(t) + \frac{\mathrm{d}\psi_B(t)}{\mathrm{d}t} \tag{4.7}$$

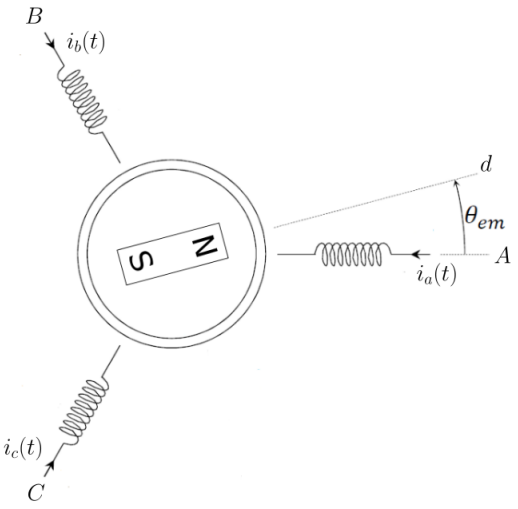

Figure 4.8: PMSG circuit representation

The flux linkages of the machine can be calculated with :

$$\begin{bmatrix}\psi_A(t)\\ \psi_B(t)\\ \psi_C(t)\end{bmatrix} = \underbrace{\begin{bmatrix}L_{AA}(\theta(t)) & M_{AB}(\theta(t)) & M_{AC}(\theta(t))\\ M_{BA}(\theta(t)) & L_{BB}(\theta(t)) & M_{BC}(\theta(t))\\ M_{CA}(\theta(t)) & M_{CB}(\theta(t)) & L_{CC}(\theta(t))\end{bmatrix}}_{L_{SS}(\theta(t))} \begin{bmatrix}i_A(t)\\ i_B(t)\\ i_C(t)\end{bmatrix} + \begin{bmatrix}cos(\theta(t))\\ cos(\theta(t)-2\pi/3)\\ cos(\theta(t)-4\pi/4)\end{bmatrix} \Psi_b \qquad (4.8)$$

Where L and M are the self and mutual inductance respectively and Ψ_b is the permanent magnet flux linkage.

The self inductance $L(\theta(t))$ of each stator phase winding reaches a maximum value when the rotor is aligned with the stator phase axis because in this condition the reluctance is minimum. The rotor is parallel with each stator phase axis twice each complete rotation, thus we can express the stator self inductance as:

$$L_{AA}(\theta(t)) = L_S + L_{S2}\, cos(2\theta(t))$$

$$L_{BB}(\theta(t)) = L_S + L_{S2}\, cos(2(\theta(t) - 2\pi/3))$$

$$L_{CC}(\theta(t)) = L_S + L_{S2}\, cos(2(\theta(t) - 4\pi/3))$$

The mutual inductance $M(\theta(t))$ will reach its maximum when the rotor is aligned midway between stator phase axis:

$$M_{AB}(\theta(t)) = M_{BA}(\theta(t)) = M_S + L_{S2}\, cos(2(\theta(t) - 4\pi/3))$$

$$M_{BC}(\theta(t)) = M_{CB}(\theta(t)) = M_S + L_{S2}\, cos(2\theta(t))$$

$$M_{CA}(\theta(t)) = M_{AC}(\theta(t)) = M_S + L_{S2}\, cos(2(\theta(t) - 2\pi/3))$$

The machine circuit equation with the self and mutual inductance terms varying with time are complex to manipulate and solve. With the help of the previously described Park Concordia transformation, they can be considerably simplify.

By restarting with the complete stator circuit equations (4.5, 4.6, 4.5 and 4.8):

$$\begin{bmatrix} v_A(t) \\ v_B(t) \\ v_C(t) \end{bmatrix} = \boldsymbol{R_S} \begin{bmatrix} i_A(t) \\ i_B(t) \\ i_C(t) \end{bmatrix} + \frac{\mathrm{d}}{\mathrm{d}t} \left(\boldsymbol{L_{ss}(\theta(t))} \begin{bmatrix} i_A(t) \\ i_B(t) \\ i_C(t) \end{bmatrix} + \begin{bmatrix} cos(\theta(t)) \\ cos(\theta(t) - 2\pi/3) \\ cos(\theta(t) - 4\pi/4) \end{bmatrix} \Psi_b \right) \tag{4.9}$$

We can now use the Park Concordia transform for the current and the voltage:

$$\boldsymbol{T_P} \begin{bmatrix} v_0(t) \\ v_d(t) \\ v_q(t) \end{bmatrix} = \boldsymbol{R_S T_P} \begin{bmatrix} i_0(t) \\ i_d(t) \\ i_q(t) \end{bmatrix} + \frac{\mathrm{d}}{\mathrm{d}t} \left(\boldsymbol{L_{ss}(\theta(t)) T_p} \begin{bmatrix} i_0(t) \\ i_d(t) \\ i_q(t) \end{bmatrix} + \begin{bmatrix} cos(\theta(t)) \\ cos(\theta(t) - 2\pi/3) \\ cos(\theta(t) - 4\pi/4) \end{bmatrix} \Psi_b \right) \tag{4.10}$$

By multiplying the left side and the right side of expression 4.10 by the inverse Park Concordia transform T_P^{-1}, we obtain:

$$\begin{bmatrix} v_0(t) \\ v_d(t) \\ v_q(t) \end{bmatrix} = \boldsymbol{R_S} \begin{bmatrix} i_0(t) \\ i_d(t) \\ i_q(t) \end{bmatrix} + \boldsymbol{T_P}^{-1} \frac{\mathrm{d}}{\mathrm{d}t} \left(\boldsymbol{L_{ss}(\theta(t)) T_p} \begin{bmatrix} i_0(t) \\ i_d(t) \\ i_q(t) \end{bmatrix} + \begin{bmatrix} cos(\theta(t)) \\ cos(\theta(t) - 2\pi/3) \\ cos(\theta(t) - 4\pi/4) \end{bmatrix} \Psi_b \right) \tag{4.11}$$

Finally by doing the math, the system simplifies for the phase axis-d and the quadrature axis-q to:

$$v_d = R_S i_d + \underbrace{(L_S - M_S + \frac{3}{2} L_{S2})}_{L_d} \frac{\mathrm{d}i_d}{\mathrm{d}t} - \omega_{em} \underbrace{(L_S - M_S - \frac{3}{2} L_{S2})}_{L_q} i_q \tag{4.12}$$

$$v_q = R_S i_q + \underbrace{(L_S - M_S - \frac{3}{2} L_{S2})}_{L_q} \frac{\mathrm{d}i_q}{\mathrm{d}t} + \omega_{em} \underbrace{(L_S - M_S + \frac{3}{2} L_{S2})}_{L_d} i_d + \omega_{em} \underbrace{\sqrt{\frac{3}{2}} \Psi_b}_{K_T} \tag{4.13}$$

Equations 4.12 and 4.13 describing the machine are simpler to use and interpret. They also lead to a clear physical picture of the problem (figure 4.9).

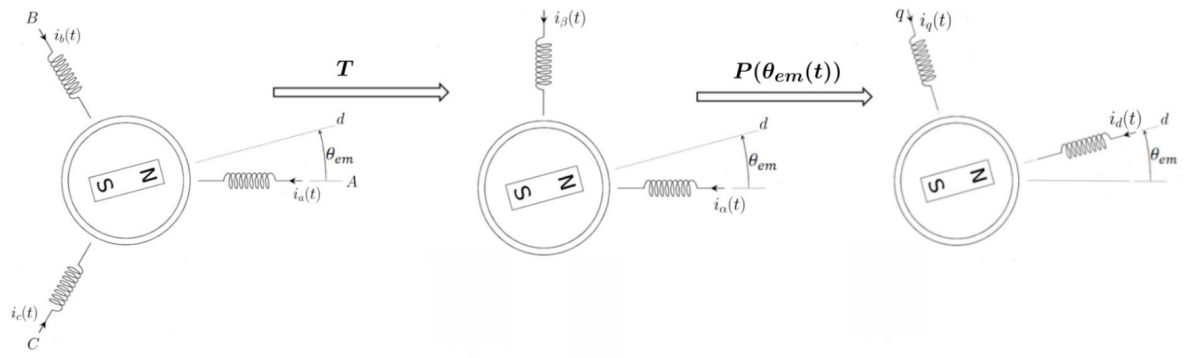

Figure 4.9: Park Concordia transform on the permanent synchronous machine

Computation of the electromagnetic T_{em} torque in the Park Concordia frame

The instantaneous three phase power of the stator is

$$P_{stator} = v_A(t)i_A(t) + v_B(t)i_B(t) + v_C(t)i_C(t) \tag{4.14}$$

Reformulating it in terms of $dq0$ component, we have

$$P_{stator} = v_d(t)i_d(t) + v_q(t)i_q(t) + v_0(t)i_0(t) \tag{4.15}$$

Under balanced condition, $v_0(t) = i_0(t) = 0$, the expression of instantaneous power is given by:

$$P_{stator} = v_d(t)i_d(t) + v_q(t)i_q(t) \tag{4.16}$$

Using the instantaneous power of the stator 4.16 with the dq components of the stator voltages 4.12 and 4.13 and rearranging, we have

$$P_{stator} = \underbrace{R_S(i_d^2 + i_q^2)}_{P_{joule\ Stator}} + \underbrace{L_d\frac{\mathrm{d}i_d}{\mathrm{d}t}i_d + L_q\frac{\mathrm{d}i_q}{\mathrm{d}t}i_q}_{\frac{dW_{mag\ Stator}}{dt}} + \underbrace{\omega_{em}i_di_q(L_d - L_q) + \omega_{em}K_Ti_q}_{P_{Stator\to Rotor}} \tag{4.17}$$

We can finally obtain the expression for the electromagnetic torque by dividing the power transferred across the machine air-gap by the mechanical rotor speed ($\omega_m = \omega_{em}/N_p$), and we have:

$$T_{em} = \frac{P_{Stator\to Rotor}}{\omega_m} = \underbrace{N_p(L_d - L_q)i_di_q}_{Reluctance\ Torque} + \underbrace{N_pK_Ti_q}_{Synchronising\ Torque} \tag{4.18}$$

4.6 Electromagnetic torque control

The electromagnetic torque we want to be able to control for the maximum power point tracking depends on the value of the i_d and i_q current component as shown in the equation 4.18. The first one induces the reluctance torque while the second one induces the synchronizing and reluctance torques at the same time. Synchronizing torque is due to the interaction of the magnetic field between the stator and the rotor while the reluctance torque is due to the asymmetry of the rotor. The best strategy to control the electromagnetic torque would be to use both components by correctly adjusting the currents i_d and i_q at the same time. This is done by finding the optimal value of the current components that minimize redsi c'est l'optimal value qui minimise alors "minimizes". Si c'est les current component alors "minimize". the joule losses $R(i_d^2 + i_q^2)$ for each desired torque. The computation of the points minimizing the joule losses is graphically represented in the figure 4.10 below for a rotor with a phase inductance $L_d = 0.5$ $[mH]$ and a quadrature inductance $L_q = 0.3$ $[mH]$.

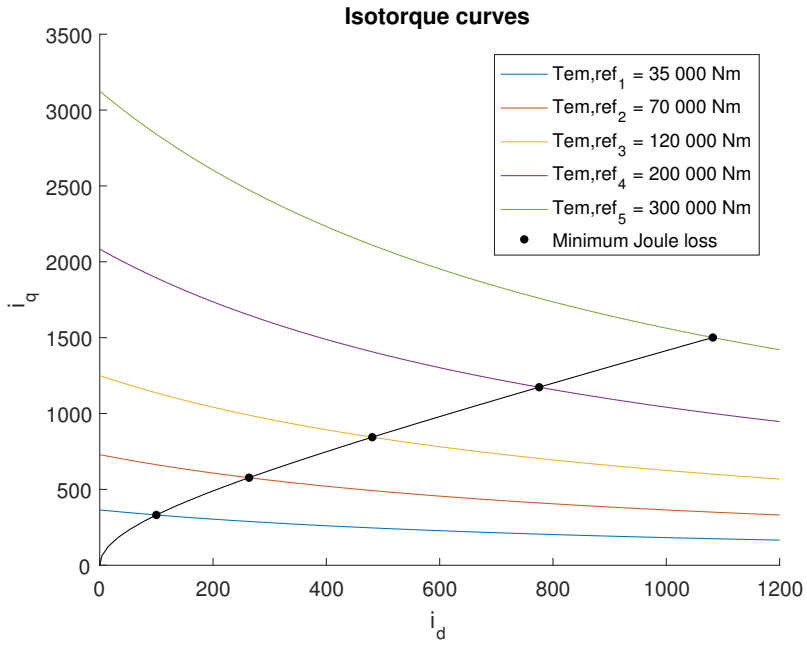

Figure 4.10: Graphical representation of the isotorque curves with the minimum joule losses points

Consequently, we are capable of computing the lookup tables (figure 4.11 and 4.12) for our controller to obtain the optimal current components for each every desired torques.

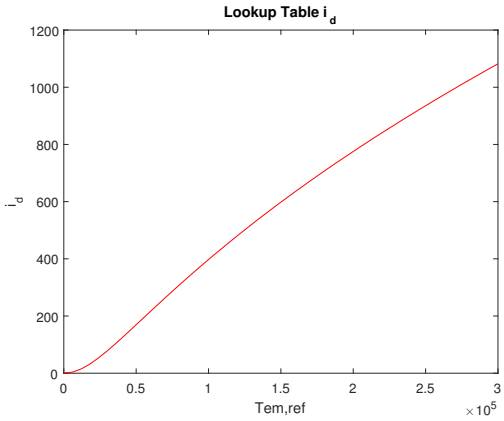

Figure 4.11: Lookup table for the i_d current

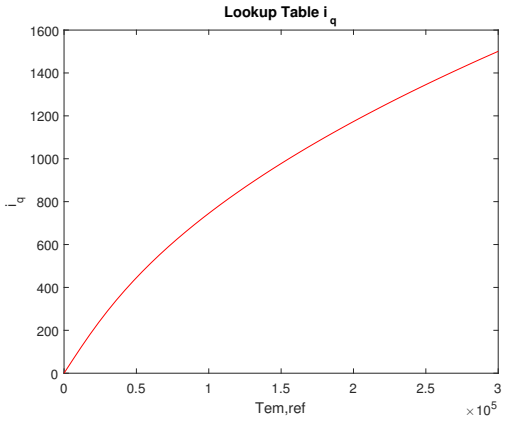

Figure 4.12: Lookup table for the i_q current

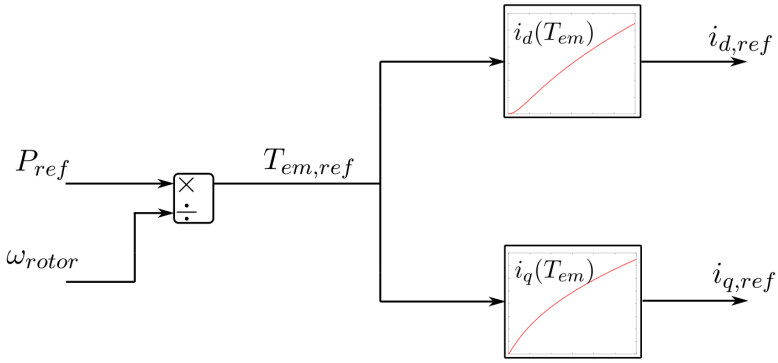

Figure 4.13: Obtained reference currents according to the reference torque

Mechanical equation

The speed of mechanical turbine coupled with the PMSG we want to control using the electromagnetic torque is described by the mechanical equation of motion:

$$T_{em} - T_{mech} = J \frac{\mathrm{d}\omega_m}{\mathrm{d}t} + K_v \, \omega_m \tag{4.19}$$

Where K_v is the viscous friction coefficient, J is the combined moment of inertia of the generator and the rotor blades, and T_{mech} is the mechanical torque applied to the machine. In our case this would be the total torque induced by the wind to the rotor blades previously calculated with the help of the Betz performance coefficient in equation 4.1.

PMSG model parameters

Below, in table 4.1, are the different parameters we will be using for our model of the PMSG.

Parameter	Value
Pair of poles	$N_P = 48$

Stator resistance	$R_s = 6\ m\Omega$
d-axis inductance	$L_d = 0.5\ mH$
q-axis inductance	$L_q = 0.3\ mH$
Permanent magnet flux linkage	$\Psi_b = 2\ Wb$
Total moment of inertia	$J = 35000\ kg\,m^2$
Viscous friction coefficient	$K_v = 0.01$

Table 4.1: PMSG model parameters [14]

4.7 Block diagram representation

We will now represent the equations 4.12, 4.12 and 4.18, 4.19 in a block system in Laplace domain. It enables us to clearly see the physical problem of the PMSG and the interactions between the different components (figure 4.14 and 4.15). Also, it allows to be easily implemented in graphical block diagram software for dynamic system such as *Simulink*. Thus, for any stator voltage we feed to this PMSG block system we can easily compute and observe the corresponding stator currents, rotor speed and electromagnetic torque.

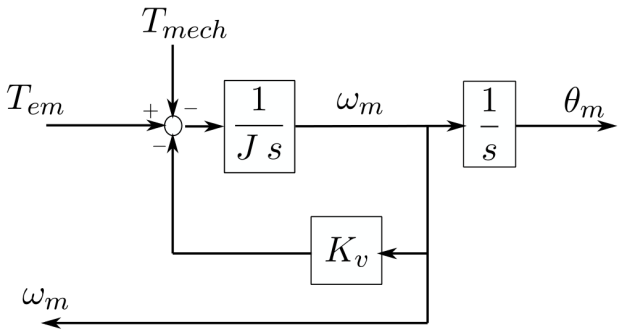

Figure 4.14: Block diagram of the mechanical equation of motion (equation 4.19)

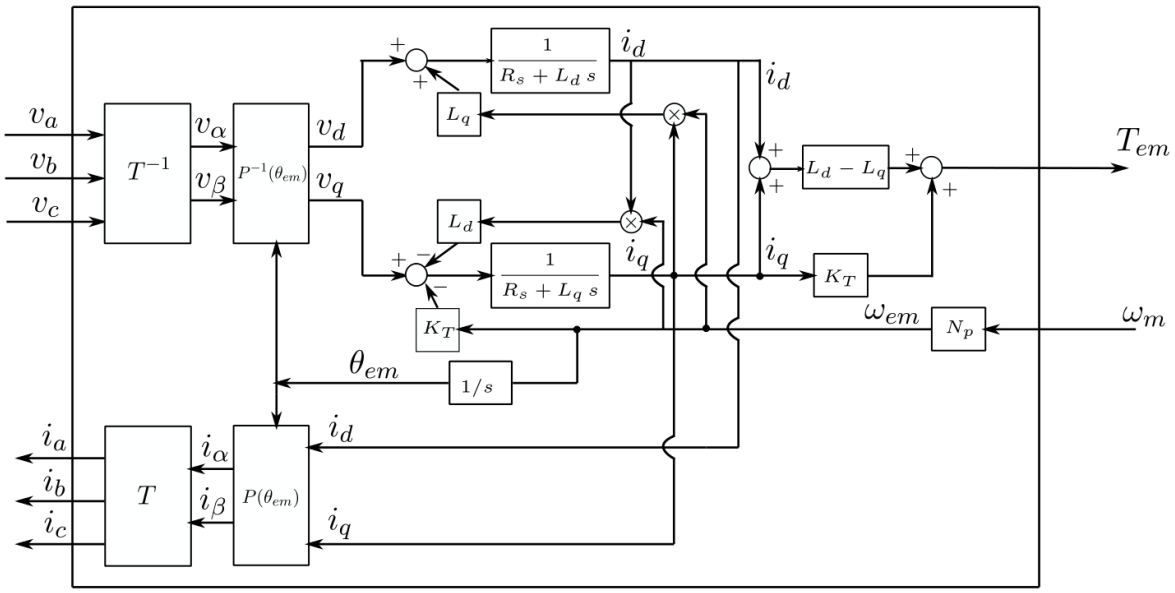

Figure 4.15: Block diagram of the PMSG (equations 4.12, 4.12 and 4.18)

As already explained, the controller will directly manage the stator current in the dq frame. Therefore, it is equipped with a a unit calculating the Park Concordia transform and its inverse in real time with a precise measurement of the rotor position (figure 4.16). This last one can be given by a Hall sensor for instance [6].

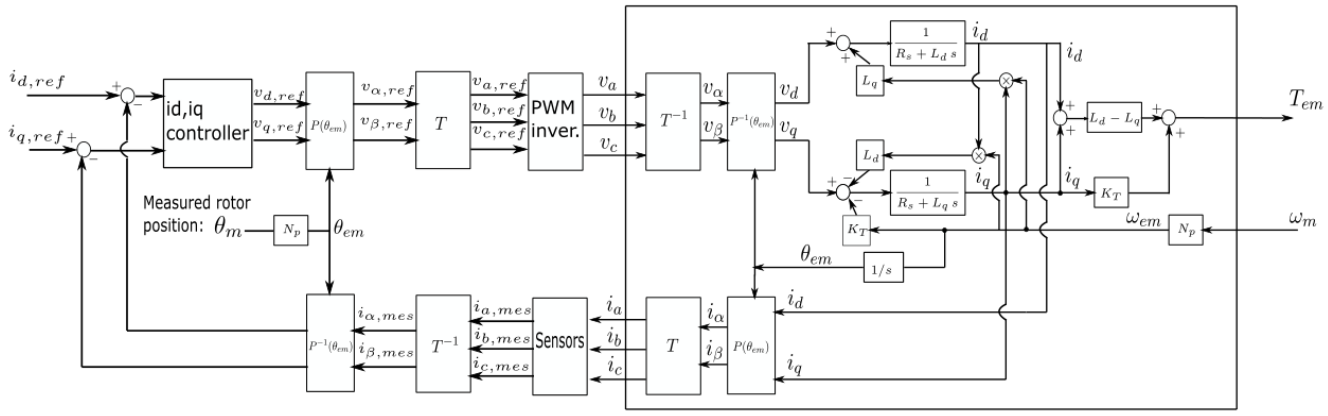

Figure 4.16: Control of the i_d and i_q current of the PMSG

Controlling the i_d, i_q currents with a multi-input, multi-outup controller is a highly complex process in automatic control. Fortunately, it is possible to compensate the dq coupling terms which allows to control the currents dq independently with two single input single output current controllers. The decoupling compensation procedure is shown in figure 4.17. The power electronics converter and the sensor are represented by a gain G_u and G_i respectively and the Park Concordia transformation and its inverse are considered perfectly calculated so they can be simplified.

The compensation of the dq coupling terms are shown in blue and red. To be performed, the measured current and speed are needed. In practice the reference currents are often directly used for the compensation. Additionally, we observe that the compensation also requires a

precise estimation of the direct and quadrature inductance ($\widehat{L_d}$,$\widehat{L_q}$). Therefore, the "physical controller" needs those precise machine inductance estimations to accurately perform the control. Finally to reach a better precision, a compensation of the electromotive force is done on the q axis.

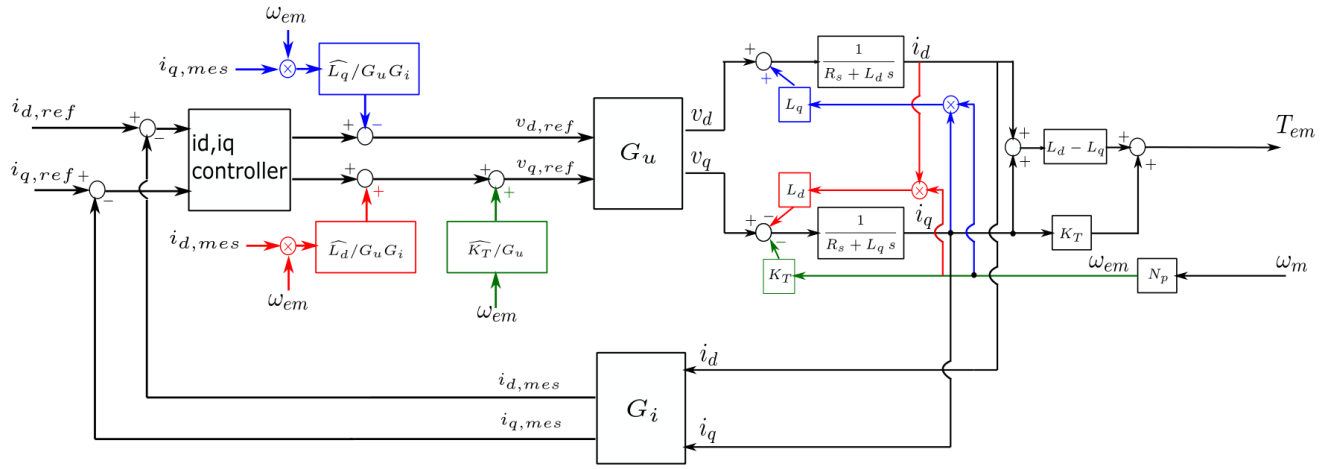

Figure 4.17: Compensation of the dq coupling terms of the PMSG

Making the assumption that the estimation of all the parameters are perfectly done, the block system for the control of the permanent magnet synchronous machine is greatly simplified and the current dq are completely decoupled (figure 4.18).

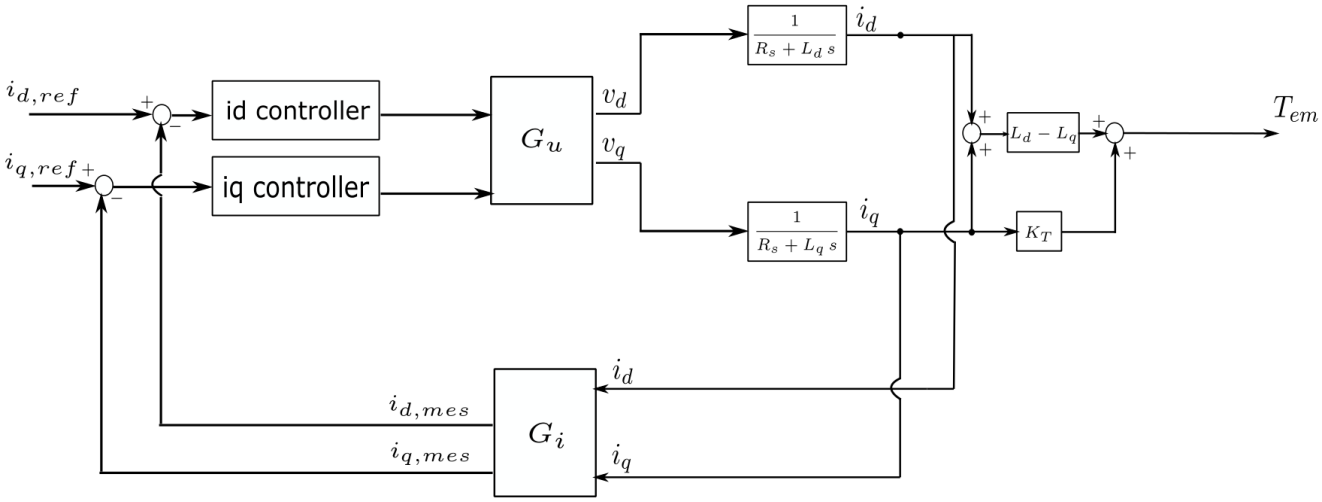

Figure 4.18: Simplified block system of the PMSG control

PMSG controller model parameters

The dq axes inductance of the generator are considered to be perfectly known and the gain representing the power converter and sensors is unitary.

d-axis inductance estimation	$\widehat{L_d} = 0.5\ mH$
q-axis inductance estimation	$\widehat{L_q} = 0.3\ mH$

Power converter gain	$G_u = 1$
Sensor gain	$G_i = 1$

Table 4.2: PMSG controller model parameters

4.8 Tuning of the rotor side controller

The control of the current can be done with a proportional and integral action, K_P and K_I respectively. This control method is shown for the d and q axes in the figures 4.19 and 4.20 below.

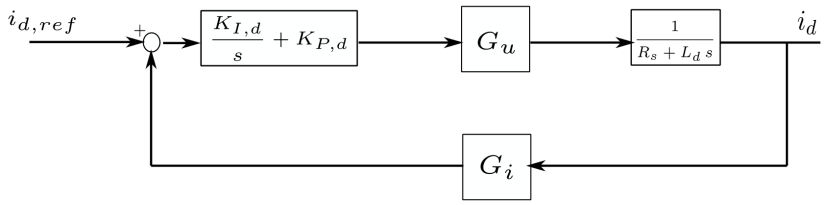

Figure 4.19: PI control of the i_d stator current

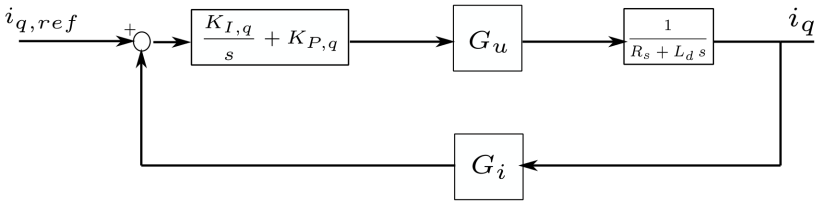

Figure 4.20: PI control of the i_q stator current

The work consists of correctly tuning the parameters K_I and K_P in order to have a fast and stable control.

d axe control

The transfer function of the i_d current loop is:

$$T(s) = \frac{i_d(s)}{i_{d,ref}(s)} = \frac{G_u(K_P + K_I/s)\frac{1}{R_s + L_d\, s}}{1 + G_u(K_p + K_I/s)\frac{1}{R_s + L_d\, s}} \tag{4.20}$$

The trick is to compare it to the standard form of second order transfer function [17] given by:

$$T(s) = \frac{T(0)\,\omega_n^2}{s^2 + 2\zeta\omega_n s + \omega_n^2} \tag{4.21}$$

Where ζ is the damping ratio and ω_n is the undamped frequency. Thus, with some algebraic manipulations of equation 4.20 we can re-write it as:

$$T(s) = \frac{G_u/L_d(K_P + K_I/s)}{s^2 + s(\frac{G_i\,G_u\,K_P + R_s}{L_d}) + \frac{G_i\,G_u\,K_I}{L_d}} \tag{4.22}$$

And confront it with the standard transfer function 4.21, to find that:

$$2\zeta\omega_n = \frac{G_i G_u K_{P,d} + R_s}{L_d} \qquad\qquad \omega_n^2 = \frac{G_i G_u K_{I,d}}{L_d} \tag{4.23}$$

It is known that the time constant response of the standard second order system is obtained by:

$$\tau = \frac{1}{\zeta\omega_n}\ [s] \tag{4.24}$$

Therefore, the values of the proportional and integral actions should be chosen in order to have a sufficiently fast current control loop. At least faster than the natural dynamic response of the i_d current which is characterized by the time constant:

$$\tau_{i_d} = \frac{L_d}{R_s}\ [s] \tag{4.25}$$

Finally by setting:

$$\zeta = 1 \qquad\qquad \tau_{controller} = \frac{\tau_{i_d}}{100} \tag{4.26}$$

We can reach a critically damped and stable control system with a fast current control. Thus, we can find the correct tuning for the PI controller:

$$K_{I,d} = \frac{(100R_s)^2}{L_d G_i G_u} \qquad\qquad K_{P,d} = \frac{199R_s}{G_i G_u} \tag{4.27}$$

q axe control

By comparing figure 4.19 with 4.20, we see that it is the exact same problem. Thus, the correct value for the proportional and integral actions are directly obtained as:

$$K_{I,q} = \frac{(100R_s)^2}{L_q G_i G_u} \qquad\qquad K_{P,q} = \frac{199R_s}{G_i G_u} \tag{4.28}$$

4.9 Grid side

Once we are able to control the speed of the wind turbine, we still have to transmit and to convert the power produced to the grid. It is done through a DC/AC power converter placed behind reactive inductance.

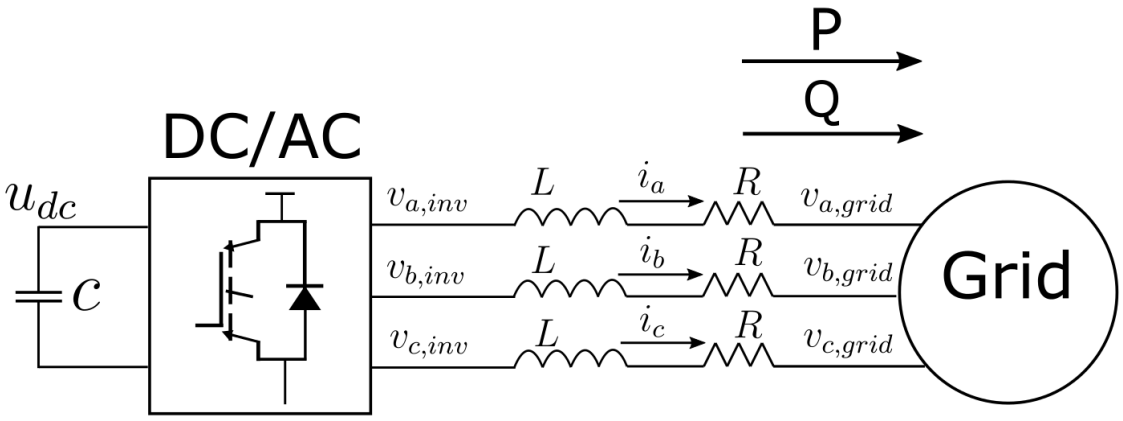

Figure 4.21: Grid side of the power converter chain

The electric equations describing the grid side in figure 4.21 of our system are given by:

$$\begin{bmatrix} v_{a,inverter}(t) \\ v_{b,inverter}(t) \\ v_{c,inverter}(t) \end{bmatrix} - \begin{bmatrix} v_{a,grid}(t) \\ v_{b,grid}(t) \\ v_{c,grid}(t) \end{bmatrix} = \boldsymbol{R} \begin{bmatrix} i_a(t) \\ i_b(t) \\ i_c(t) \end{bmatrix} + \boldsymbol{L} \frac{\mathrm{d}}{\mathrm{d}t} \begin{bmatrix} i_a(t) \\ i_b(t) \\ i_c(t) \end{bmatrix} \tag{4.29}$$

By using the Park Concordina transform, we obtain:

$$\boldsymbol{T_P} \begin{bmatrix} v_{0,inverter}(t) \\ v_{d,inverter}(t) \\ v_{q,inverter}(t) \end{bmatrix} = \boldsymbol{R}\boldsymbol{T_P} \begin{bmatrix} i_0(t) \\ i_d(t) \\ i_q(t) \end{bmatrix} + \boldsymbol{L} \frac{\mathrm{d}}{\mathrm{d}t} \left(\boldsymbol{T_P} \begin{bmatrix} i_0(t) \\ i_d(t) \\ i_q(t) \end{bmatrix} \right) + \boldsymbol{T_P} \begin{bmatrix} v_{0,grid}(t) \\ v_{d,grid}(t) \\ v_{q,grid}(t) \end{bmatrix}$$

Now, by multiplying by the inverse transform and simplifying:

$$\begin{bmatrix} v_{0,inverter}(t) \\ v_{d,inverter}(t) \\ v_{q,inverter}(t) \end{bmatrix} = \boldsymbol{R} \begin{bmatrix} i_0(t) \\ i_d(t) \\ i_q(t) \end{bmatrix} + \boldsymbol{T_P^{-1}} \boldsymbol{L} \frac{\mathrm{d}}{\mathrm{d}t} \left(\boldsymbol{T_P} \begin{bmatrix} i_0(t) \\ i_d(t) \\ i_q(t) \end{bmatrix} \right) + \begin{bmatrix} v_{0,grid}(t) \\ v_{d,grid}(t) \\ v_{q,grid}(t) \end{bmatrix} \tag{4.30}$$

Which lead to the dq components:

$$v_{d,inverter} = Ri_d - \omega_{grid} L i_q + L \frac{di_d}{dt} + v_{grid} \tag{4.31}$$

$$v_{q,inverter} = Ri_q + \omega_{grid} L i_d + L \frac{di_q}{dt} + v_{grid} \tag{4.32}$$

We observe that equations 4.31 and 4.31 are very similar to the *dq* equations 4.12 and 4.13 obtained for the rotor side.

And finally, the active and reactive power expressed in the *dq* coordinates are

$$P = v_{d,grid} i_d + v_{q,grid} i_q \tag{4.33}$$

$$Q = v_{q,grid} i_d - v_{d,grid} i_q \tag{4.34}$$

Grid side model parameters

Parameter	Value
Grid side resistance	$R_{grid} = 0.66\ m\Omega$
Grid side inductance	$L_{grid} = 0.22\ mH$

Table 4.3: Grid side model parameters

4.9.1 Grid side block diagram

As we did for the rotor side, we will represent the equations describing the grid side in a block system Laplace domain.

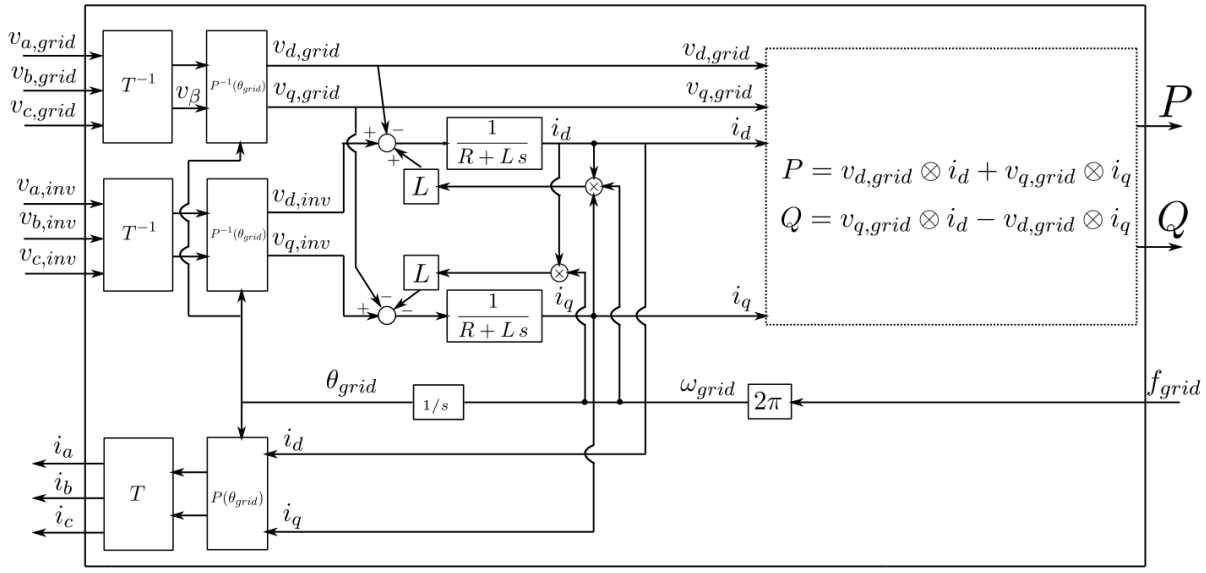

Figure 4.22: Block diagram of the grid side (equations 4.31, 4.32 and 4.33, 4.34)

The grid side controller will also manage the currents it is injecting to the grid directly in the *dq* Park Concordia frame. To perform the Park Concordia transform and its inverse, it needs to measure frequency with a phase-locked loop.

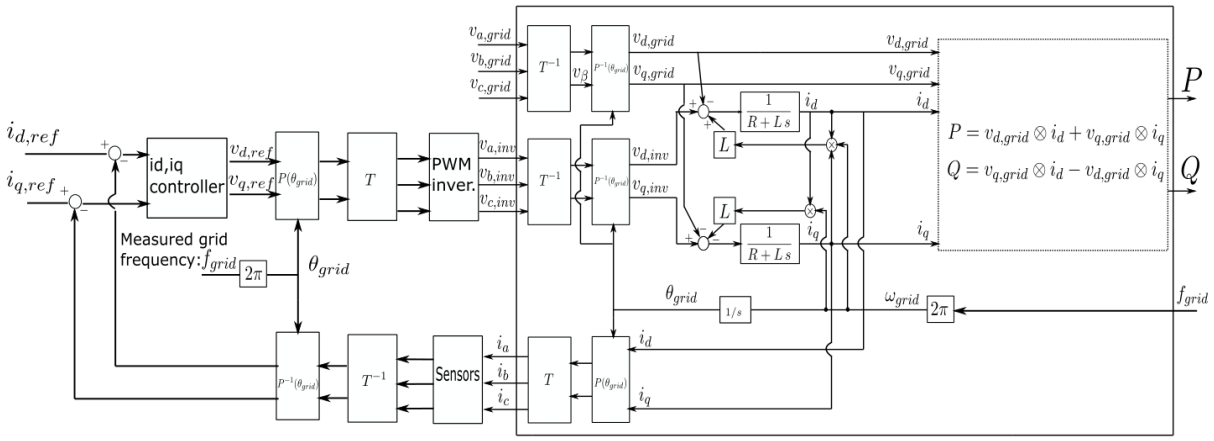

Figure 4.23: Control of the i_d and i_q current of the grid side

Again the currents i_d and i_q we want to control can be decoupled from each other (figure 4.24) after simplifying the block system by considering that Park Concordia transformation and its inverse are perfectly performed (for which we have to assumed that the grid frequency is perfectly measured) and by representing the power converter and sensors by a simple gain.

The compensation of the dq coupling terms are shown in blue and red. It required a precise value of the grid side reactive inductance which is generally more easily obtained than the preceding estimation for the PMSG on the phase and quadrature inductance. Additionally, a compensation of the dq grid voltage is also done to reach better performances.

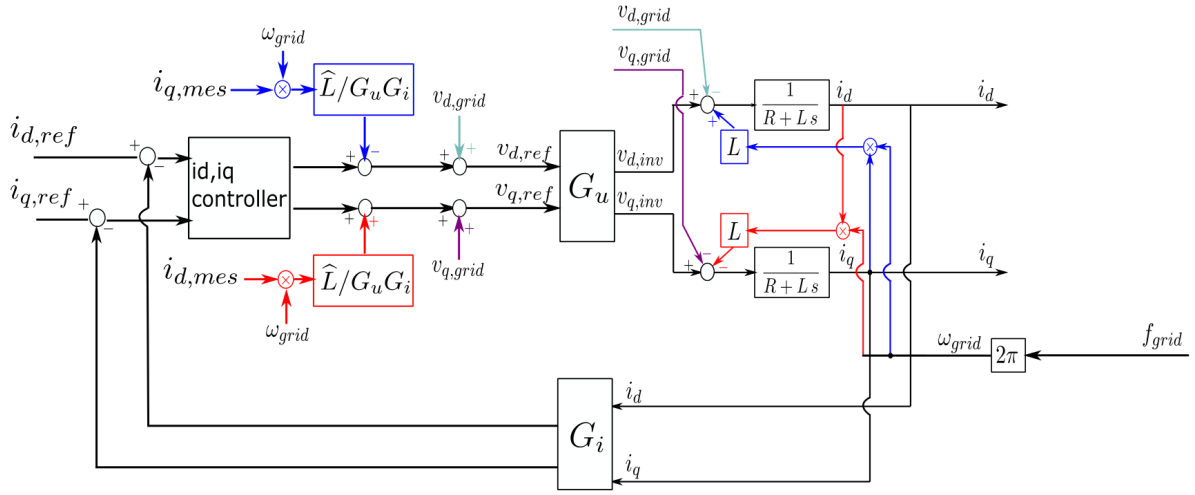

Figure 4.24: Compensation of the grid side dq coupling terms

Considering the assumptions above and that all the voltages and currents are perfectly measured, the block system reduces to figure 4.25

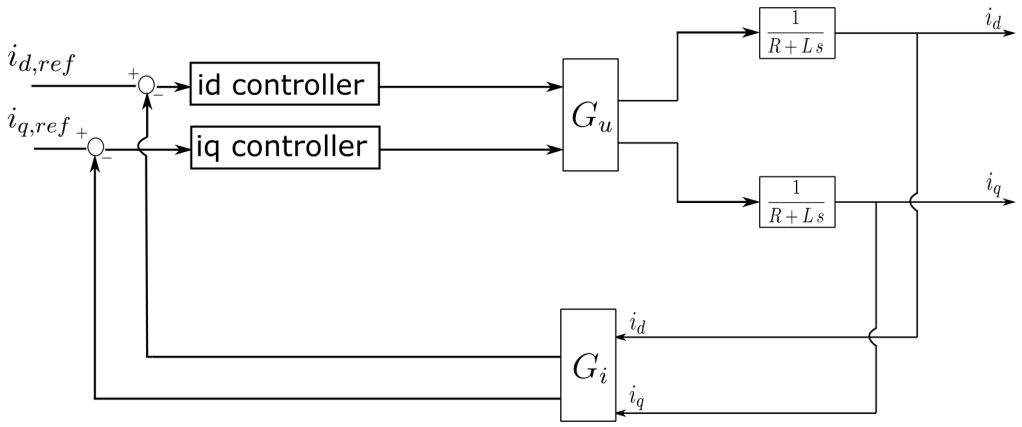

Figure 4.25: Simplified block system of the grid side control

Grid side controller model parameters

Same assumptions as for the rotor side controller are used which is that the line inductance of the grid is considered to be perfectly known and the gain representing the power converter and sensors is unitary.

Line inductance estimation	$\widehat{L_{grid}} = 0.22\ mH$
Power converter gain	$G_u = 1$
Sensor gain	$G_i = 1$

Table 4.4: Grid side controller model parameters

4.10 Tuning of the grid side controller

The grid side control loop is the exact same one obtained as for the rotor side (figure 4.26 and 4.27).

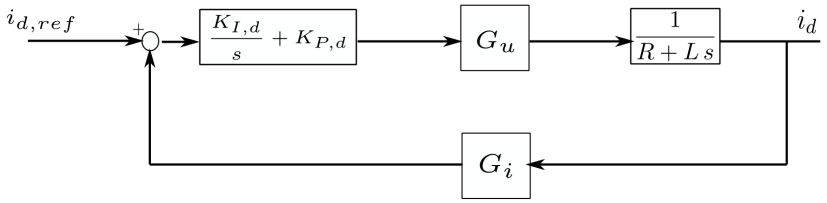

Figure 4.26: PI control of the i_d grid current

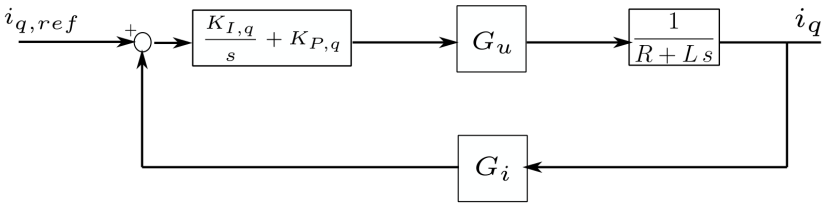

Figure 4.27: PI control of the i_q grid current

Thus, we will also use a PI controller with correctly tuned proportional and integral action K_P and K_I for each dq current loop.

dq axes control

By using the same control theory described for the rotor controller and also setting the parameters to have a critically damped control with time response of the controller 100 times faster than the natural dynamic reposne of the dq grid currents ($\zeta = 1$ and $\tau_{controller} = \frac{L}{100\,R}$), we find the correct tuning for the PI controller as :

$$K_{I,d} = K_{I,q} = \frac{(100R)^2}{LG_iG_u} \qquad\qquad K_{P,d} = K_{I,q} = \frac{199R}{G_iG_u} \tag{4.35}$$

Reference dq grid currents

For our model of the wind turbine integration, we considered the grid as a perfectly balanced three phases sinusoidal voltage source which means that voltage magnitudes are equal at phases angles $2\pi/3$ [rad] equally spaced from each other. This means that the Park Concordia transform of the grid voltage has no q component ($v_{q,grid} = 0$). Moreover, the reactive power has no influence on the frequency thus we will fixed it at zero. //

All this implies that the the reference current $i_{q,ref}$ is equal to zero (equation 4.33) and the active power transfer to the grid is controlled only with $i_{d,ref}$ (equation 4.34).

4.11 Voltage controller

Directly controlling the active power injected to the grid with the DC/AC power converter by setting the reference power of the controller at $P_{grid,ref} = P_{turbine,ref}$ is not the good strategy. Indeed, there might be a slight mismatch between the real power produced by the generator and the real power injected to the AC network by the grid side converter. This would lead to an dangerous increase or decrease of the DC voltage until the system crash. The right approach is to control the voltage of the DC link where the capacitance C would play the role of a power buffer (figure 4.28).

Besides, a minimum voltage level is required for the DC link to make the power transfer happen because the output voltage on grid side generated by the power converter is directly related to the DC voltage behind. Indeed, one branch of the three phase power converter can generate a square wave with peak to peak maximum amplitude of U_dc on the AC grid side. Which implies that the maximum phase to peak AC voltage we can produced is $U_{dc}/2$. This yields to the minimum DC link voltage:

$$U_{dc,min} \geq 2\,V_{grid,\,peak \rightarrow ground} \tag{4.36}$$

For our case study, we have $U_{min} = 940$ $[V]$. Therefore we set $U_{dc,ref}$ at 1150 $[V]$ for security margin. This is the reason why wind turbine are placed behind a step-up transformer otherwise that DC link and power electronics would have to work directly in high voltage.

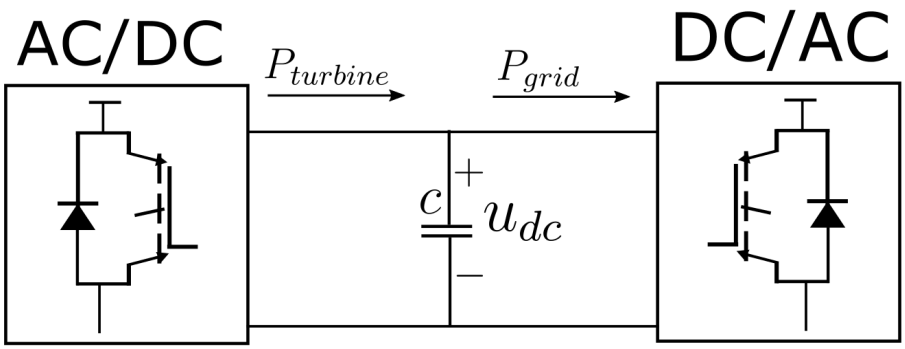

Figure 4.28: Power flow at the DC link

The active power in the DC link can be expressed as:

$$P_{dc} = P_{turbine} - P_{grid} \tag{4.37}$$

Where P_{dc} is the power stored by the capacitance C. The equation 4.37 can be re-written as:

$$C_{dc}\, u_{dc} \frac{\mathrm{d}u_{dc}}{\mathrm{d}t} = P_{turbine} - P_{grid} \tag{4.38}$$

$$\frac{\mathrm{d}u_{dc}}{\mathrm{d}t} = \frac{1}{u_{dc}\, C_{dc}} P_{turbine} - \frac{1}{u_{dc}\, C_{dc}} P_{grid} \tag{4.39}$$

By linearization around $u_{dc} = U_{dc,0}$, we can express:

$$\frac{\mathrm{d}\Delta u_{dc}}{\mathrm{d}t} = \frac{1}{U_{dc,0}\, C_{dc}} \Delta P_{turbine} - \frac{1}{U_{dc,0}\, C_{dc}} \Delta P_{grid} \tag{4.40}$$

The block diagram of the control loop for the DC voltage is shown in figure 4.29 where we represent the equation 4.40. The current control loop for i_d is considered much faster therefore it can be neglected for the voltage control loop.

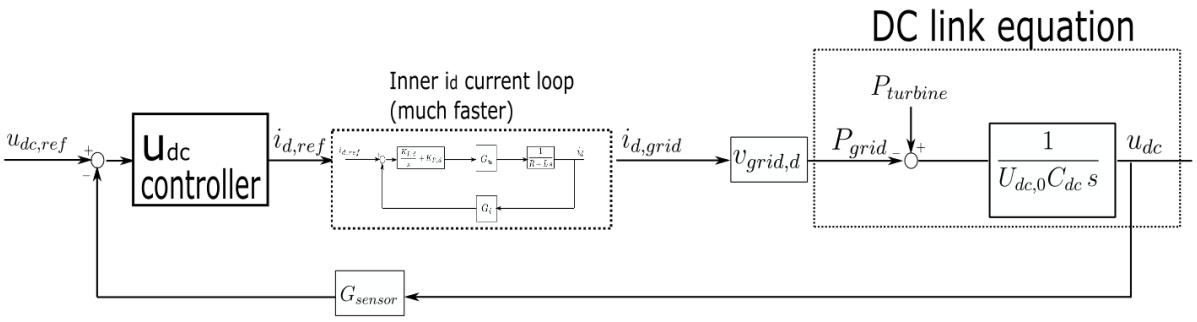

Figure 4.29: Control loop of the DC voltage link

DC link model parameters

Parameter	Value
DC link nominal voltage	$U_{dc,0} = 1150\ V$
DC link capacitance	$C = 10\ mF$

Table 4.5: DC link model parameters

4.12 Tuning of PI voltage controller

Again a proportional and integral action will be used for this controller.

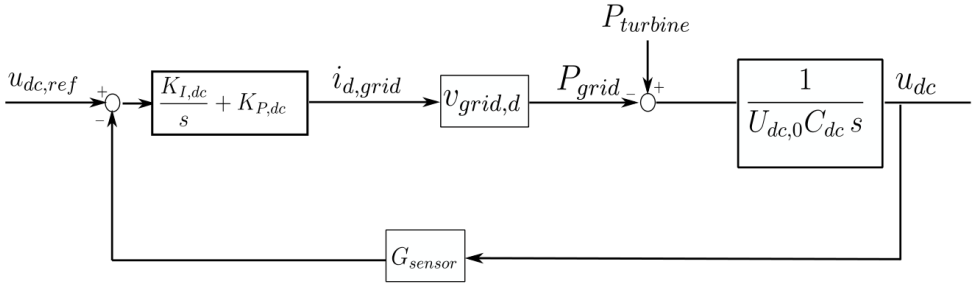

Figure 4.30: PI control of the DC voltage link

The transfer function of the voltage loop (figure 4.30) is expressed as:

$$T(s) = \frac{u_{dc,ref}(s)}{u_{dc}(s)} = \frac{(K_{P,dc} + K_{I,dc}) v_{grid,d} \frac{1}{sC_{dc}U_{dc,0}}}{1 + G_{sensor}(K_{P,dc} + K_{I,dc}) v_{grid,d} \frac{1}{sU_{dc}U_{dc,0}}} \tag{4.41}$$

Which is expressed in the standard form as:

$$T(s) = \frac{\frac{1}{C_{dc}U_{dc,0}}(K_{P,dc} + K_{I,dc}/s)}{s^2 + s\frac{G_{sensor}K_{P,dc}v_{grid,d}}{C_{dc}U_{dc,0}} + \frac{G_{sensor}K_{I,dc}v_{grid,d}}{C_{dc}U_{dc,0}}} \tag{4.42}$$

By comparison with the standard second order transfer function 4.21 we obtain:

$$2\zeta\omega_n = \frac{Gsensor\, K_{P,dc}\, v_{grid,d}}{C_{dc}\, U_{dc,0}} \qquad \omega_n^2 = \frac{G_{sensor}\, K_{I,dc}\, v_{grid,d}}{C_{dc}\, U_{dc,0}} \tag{4.43}$$

By setting a time response slower than the control of the grid current and for a critically damped control loop ($\tau_{dc,controller} = \tau_{i,controller}$) and $\zeta = 1$), we obtain:

$$K_{I,dc} = \frac{(\frac{20R}{L})^2\, C_{dc}\, U_{dc}}{G_{sensor}\, v_{grid,d}} \qquad K_{P,dc} = \frac{\frac{40R}{L}\, C_{dc}\, U_{dc}}{G_{sensor}\, v_{grid,d}} \tag{4.44}$$

4.13 Virtual inertia recovery

As explained in the preceding section, the power output of the system only depends on the wind speed. Indeed, at first the rotor side controller will impose an optimal rotational speed and a power output depending on the measured wind while the grid side controller will transfer this power into the grid. Therefore the power produced by the system is clearly independent on the grid frequency which is a big difference compared to the traditional synchronous generator.

If we want the system to participate to the frequency control through inertia and even primary response, a supplementary control at the rotor side is needed. This additional controller is shown in figure 4.31 where the lower part emulates the inertia response if the rotor was directly connected to the grid and naturally responding to the frequency deviation (for $K = J$). The upper part may be used if we desire to also have a primary control with the wind turbine.

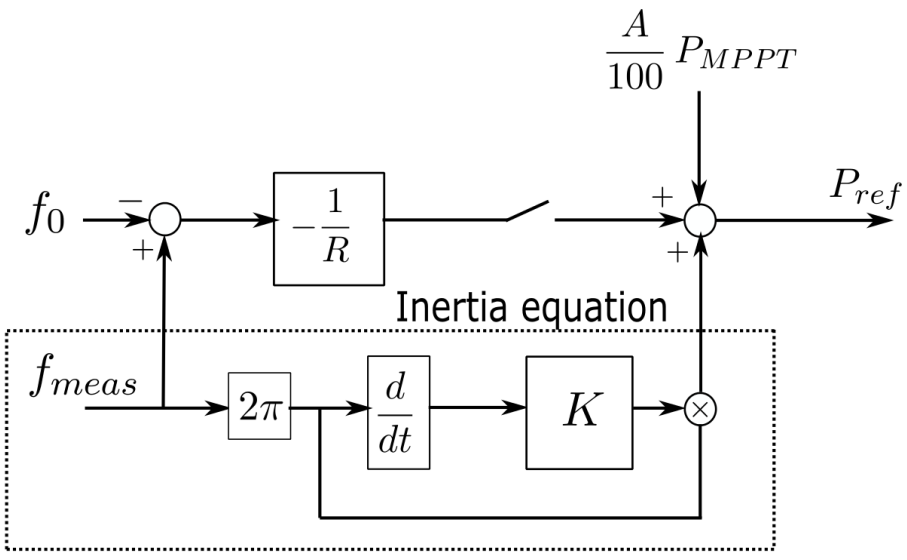

Figure 4.31: Supplementary controller for the rotor side

The different measurements needed for the grid side and rotor side controllers for the wind turbine grid integration is presented in the figure 4.32 where the new supplementary frequency measurement is shown in blue.

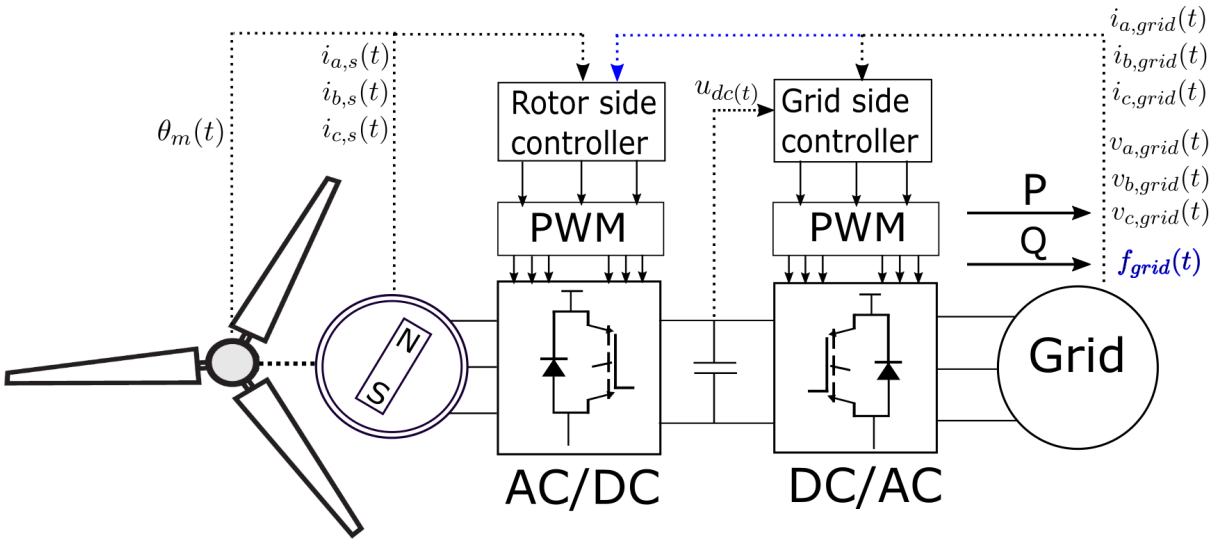

Figure 4.32: Complete wind turbine system with the different inputs for the controllers

4.14 Simulation results

In order to verify the design of the model, Matlab Simulink with the Simscape Power Systems tool is used to simulate the system. (A figure of the simulink model is shown in the Appendix A.1)

Constant wind

The model simulated is performed with an ideal constant wind of 11.5 m/s and the grid is represented as an ideal perfectly balanced three phases sinusoidal voltage sources. Therefore, the impact of the voltage quality on the wind turbine integration is not considered in the simulation.

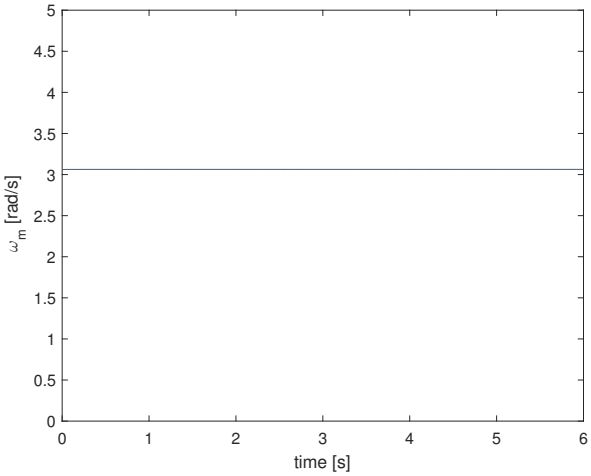

Figure 4.33: Speed of the rotor

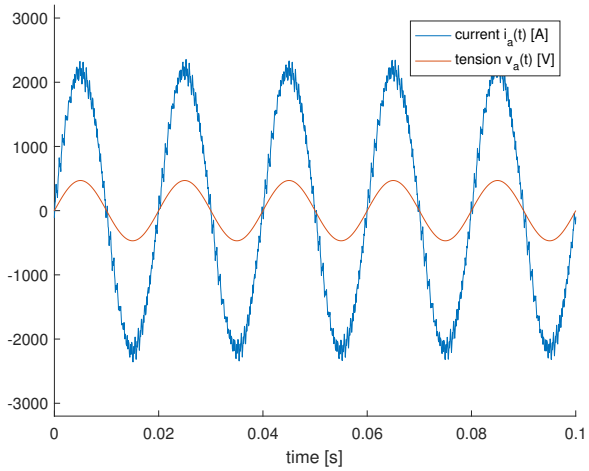

Figure 4.34: Phase voltage $v_a(t)$ with the current injected $i_a(t)$ into the grid during 0.1 second

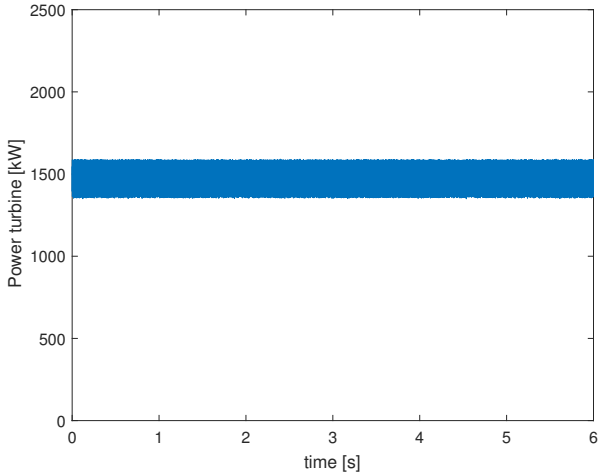

Figure 4.35: Electric active power captured at the turbine side

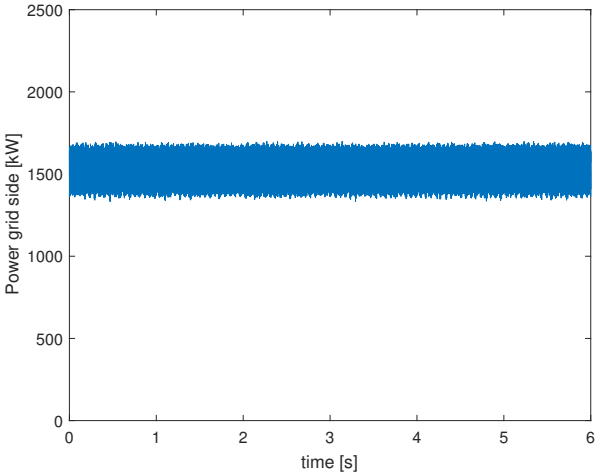

Figure 4.36: Active power injected into the grid

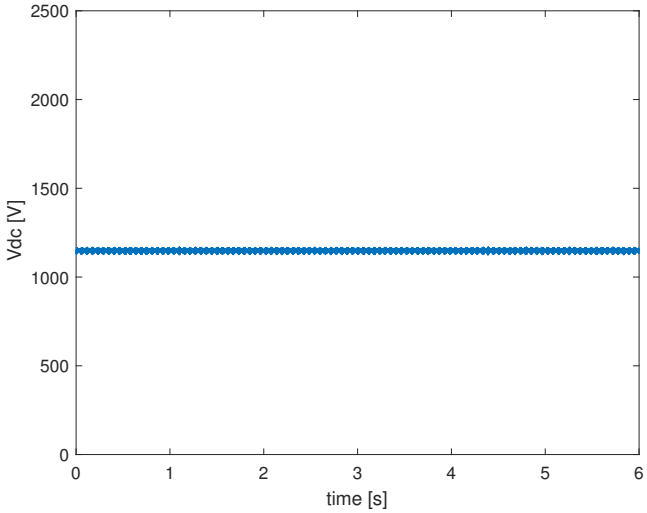

Figure 4.37: Voltage of the DC link

We can observe the phase voltage $v_a(t)$ and the phase current $i_a(t)$ describing sinusoid in phase with 50 Hz frequency in figure 4.34. There is visible non negligible undesirable current components. Harmonic currents are injected into the grid, indeed they are produced by the non linearity of the 6-pulse power converter producing harmonic of rank 5, 7, 11, 13,.. [9] Moreover, the tuning of the controller might not be optimal because we neglected the zeros of the transfer function and the time delay due to the switching time of the power electronics.

Variable wind

An other simulation is made with an "ideal variable wind" which means that turbulent effect are neglected and the flow is considered laminar. Again the same ideal voltage sources are used to represent the rest of the grid.

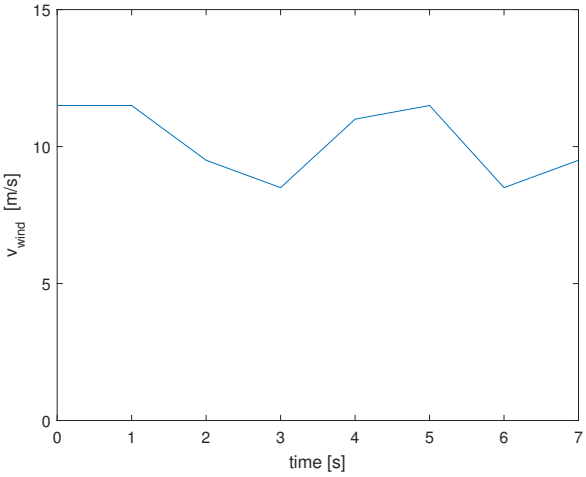

Figure 4.38: Variable wind speed

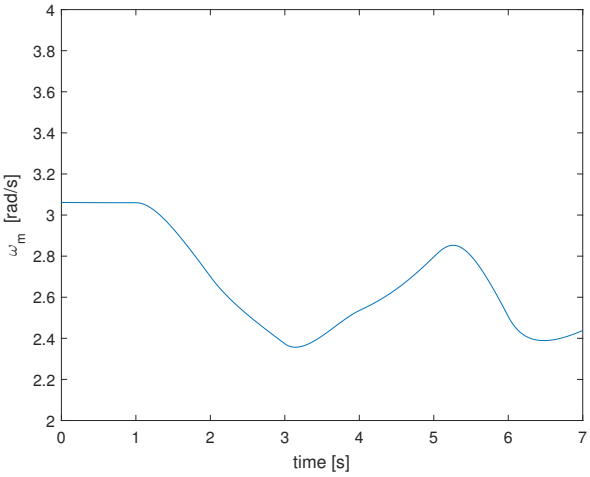

Figure 4.39: Speed of the rotor

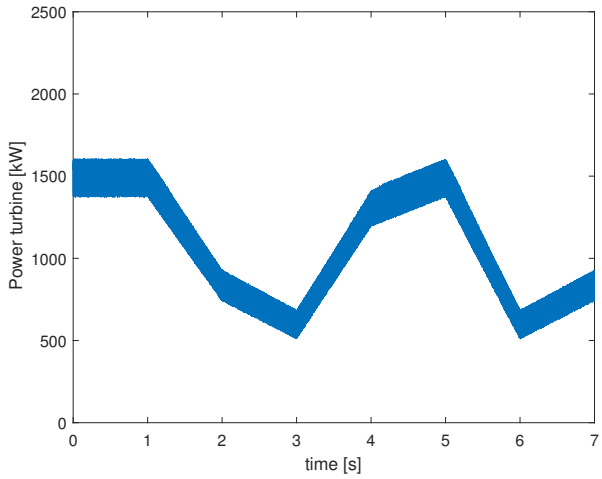

Figure 4.40: Electric active power captured at the turbine side

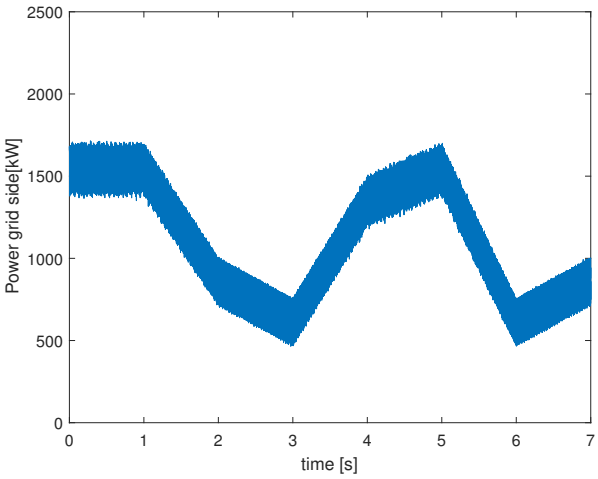

Figure 4.41: Active power injected into the grid

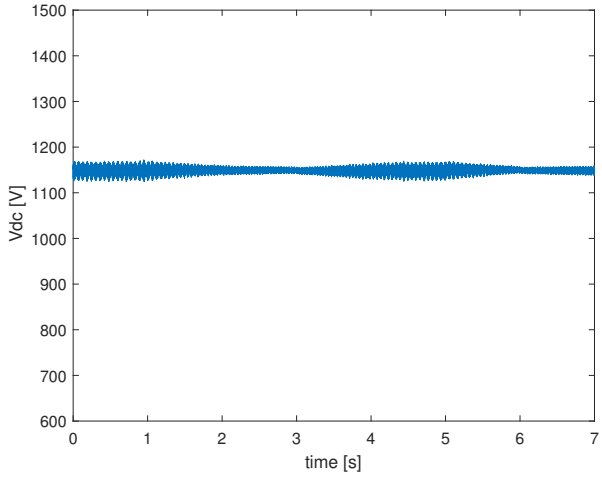

Figure 4.42: Voltage of the DC link

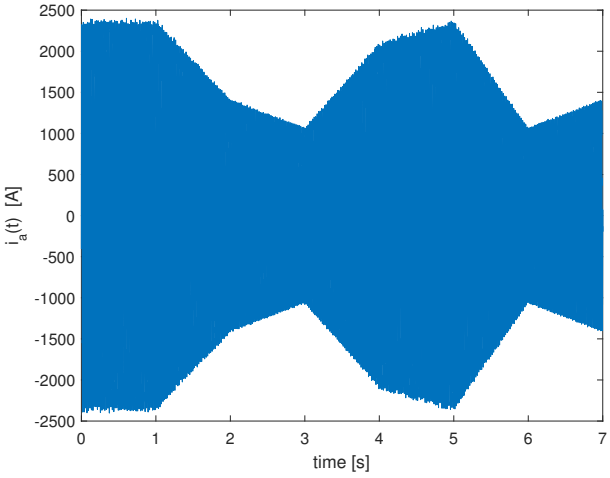

Figure 4.43: Current $i_a(t)$ injected into the grid

We can observe this time the rotational speed of the rotor changing depending on the wind speed to extract the maximum power out of it. The DC link voltage is less constant because it is subjected to more important power flow variation (figure 4.42). Instantaneous grid current $i_a(t)$ is also shown in figure 4.43, we can see that its peak value varies with time depending on the active power injected into the grid.

Maximum power point tracking is done with a pre-calculated lookup table. This technique should be taken with caution because as well as it performs in simulation, it relies on the assumptions of perfectly measuring the wind speed between every instant. Unfortunately, it is not feasible in practice and a proper MPPT tracking algorithm must be used for the wind turbine [13]. Research on the optimal algorithm still needs to be carried out and algorithms are often protected by patent in the wind turbine industry.

Virtual inertia

For the virtual inertia emulation analysis, we used the frequency data obtained the 14 March at 20:00 to modify the frequency of the balanced three phase sinusoidal ideal voltages sources representing the grid. This time, the supplementary control shown in figure 4.31 fed with the PLL frequency measurement will be used.

By doing some simulations equipped with the supplementary frequency control, one can notice that the rotor speed drops easily, leading to the crash of the simulation (Appendix). Indeed we might be tempted to think that the inertia of the wind turbine is important due to the really long radius of the rotor and its associated important moment of inertia. However, the rotational speed of the machine, decreasing with its size, leads to really slow rotor speed. This makes the total kinetic energy ($E_{kinetic} = \frac{1}{2}J\omega_m^2$) of the wind turbine really low compared to a synchronous machine with a much lower moment of inertia but rotating at the grid frequency (for $N_P = 1$).

The first simulation is made with a constant wind speed of 11.5 m/s. The supplementary control only acts on the emulation of virtual inertia while the upper part of the control acting as a primary control is deactivated. Indeed, primary control needs power reserve which is not the case if the wind turbine is working really close to the MPPT. The gain K of the rate of frequency change loop is set at $2J$. The grid frequency used is purposely chosen to be quite stable and to contain only little frequency drops.

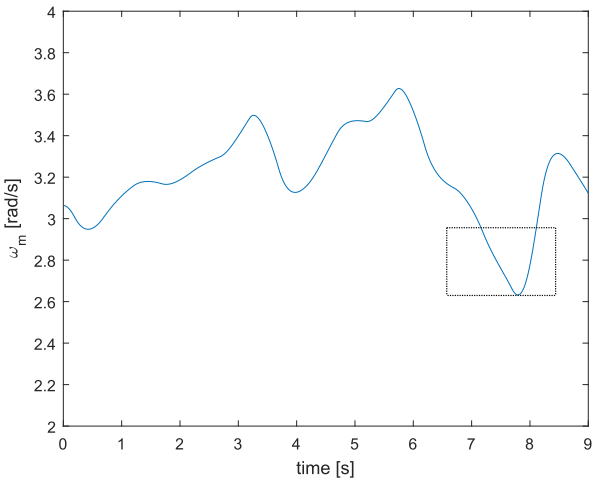

Figure 4.44: Speed of the rotor

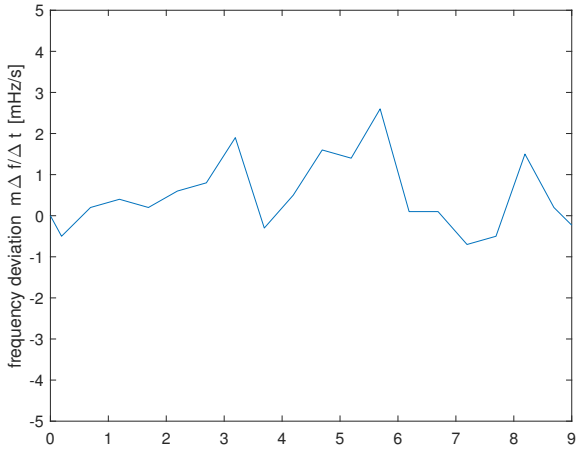

Figure 4.45: Rate of frequency change

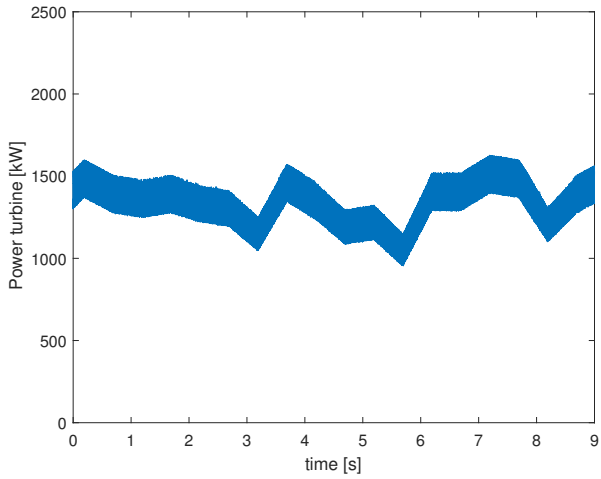

Figure 4.46: Electric active power captured at the turbine side

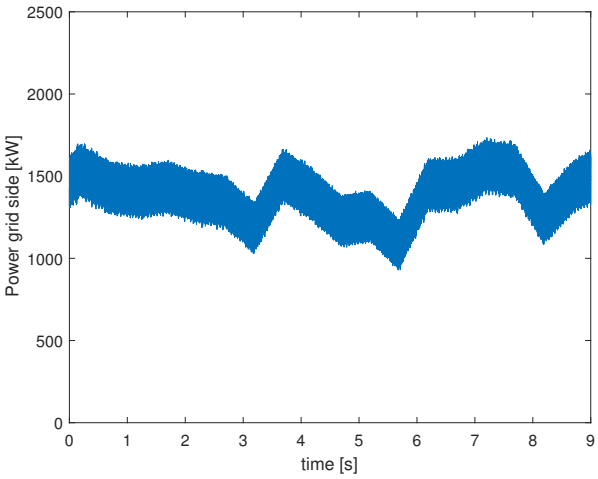

Figure 4.47: Active power injected into the grid

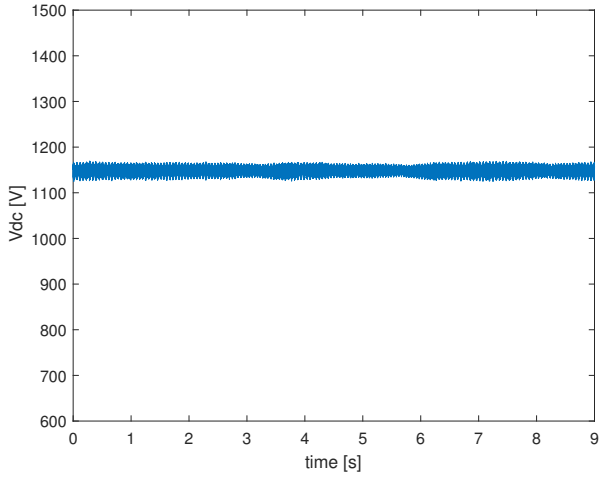

Figure 4.48: Voltage of the DC link

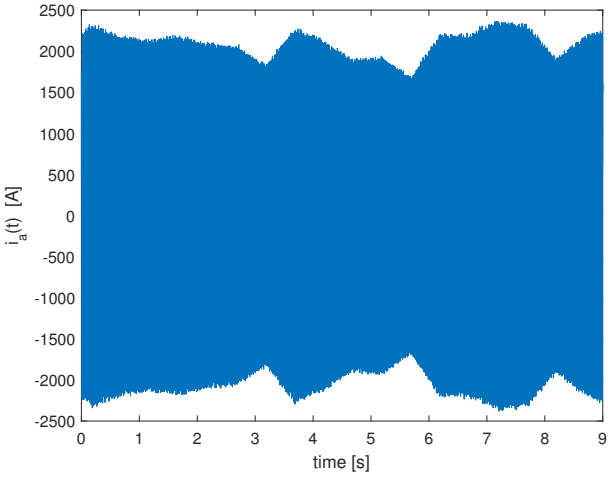

Figure 4.49: Instantaneous grid current $i_a(t)$

We can observe that the power changes depending on the rate of frequency deviation. This should help the grid to smooth the rate of frequency deviation by injecting more or less power to reduce the mismatch between the power consumed and produced (see equation 1.8). After time $7s$, the turbine power goes slightly over its MPPT and we observe the speed decreasing. The rotor is actually transferring its kinetic energy to the grid to go a little further than the power only available by the wind. This effect is shown in the doted rectangle in figure 4.44. Additionally, we chose to stop the supplementary control when the speed reaches non acceptable value (60% of the regular speed for instance) and might not be capable to regain its speed. Furthermore, the gain in power is minor compared to the dangerous drop of rotor speed. Indeed, as explained above, the total kinetic energy contained in the wind turbine is actually low. Consequently, the inertia response emulated with the wind turbine is fine when the rate of change of frequency is rising. However, in case of a frequency drop its contribution is quite low. It would need larger power reserve to actually really supply an inertia response for a grid frequency decay.

Working at 75% of the maximum power point

In this simulation we work at 75% of the maximum power point ($A = 75$ in figure 4.31) with the same ideal frequency changing voltage sources. Also, the gain K is doubled this time to greatly increase the emulated inertia response of the system.

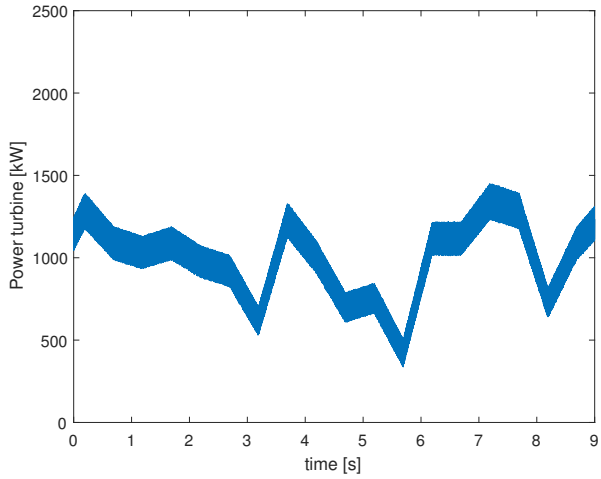

Figure 4.50: Electric active power captured at the turbine side

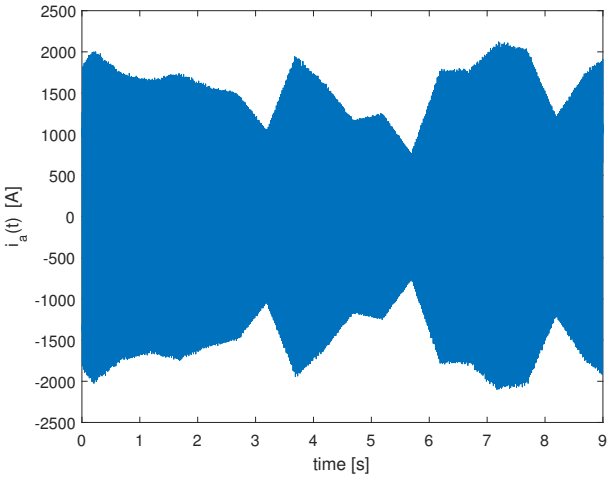

Figure 4.51: Instantaneous grid current $i_a(t)$

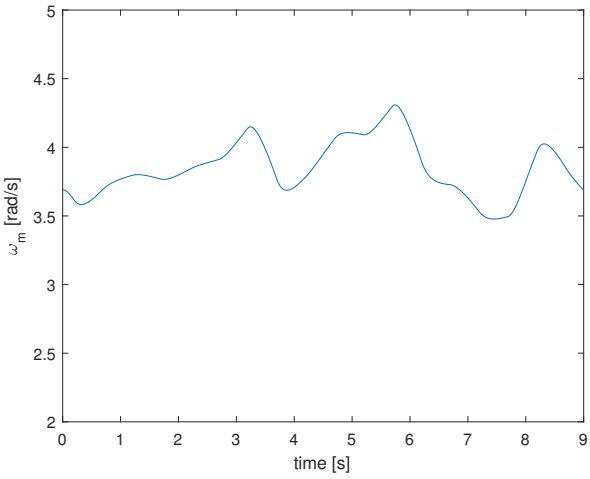

Figure 4.52: Rotor speed when working at 75% of the MPPT

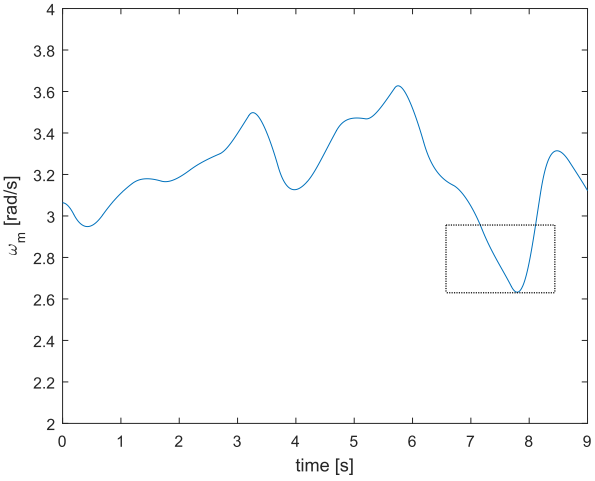

Figure 4.53: Rotor speed when working close to the MPPT

We can observe really important power variations (figure 4.50) which should support significantly the grid frequency dynamic. Here the rotor speed does not suddenly decreases between time 7 $[s]$ and time 8 $[s]$ to transfer its mechanical kinetic energy to the grid (figure 4.52 and 4.52). Indeed, the wind turbine is working with a quite large power reserve which allows the system to raise its power output when the frequency decreases. Unlike the traditional synchronous generator, the inertia response is modulable by tuning the parameter of the supplementary control at the rotor side. Theoretically, the lower we go under the maximum power point, the

more this system can participate to the grid frequency control. The primary control might be also used to participate at the first part of frequency restoration when the frequency is lower than f_0 after a disturbance.

However, those simulated results must be taken with vigilance. Indeed, running under the MPPT to keep a power reserve comes with the really questionable hypothesis that wind will be available when more power is needed. But still, this approach to support the frequency might work better than nothing if we imagine a grid fed almost exclusively by wind turbines and no other alternative means to support it. Therefore, a more reliable strategy for the wind turbine system would be to lean on actually available fast responding power reserve such as battery for instance to support the inertia response and grid frequency.

Conclusion

This master thesis goal was to study the grid frequency dynamic with emphasis on the inertia decreasing aspect due to inverter-connected renewable energy sources.

The results obtained show that stable frequency dynamic can be obtained for instance with really high renewable penetration but with with a minimum level of sufficiently fast primary control to support it. However as we are aware that the overall inertia is lowering, grid operator will have to work at frequency stability closer to the edge and to enforce the fast frequency control and the requirements to use the grid. This tendency is increasing and therefore new grid codes are being studied for the interconnected European grid in order too keep the global frequency at a stable state.

Indeed, all the evidences suggest that we will have no choice but to use more and more renewable as the fossil fuel resources is exhausting and the climate is dramatically changing, thus having to strengthen the frequency control with the right technology.

With the detailed model of the modern variable speed wind turbine studied, we can see that some tricks do exist to play on the frequency control even with power converter connected energy sources. The results are quite promising for the rapid control of an uprising frequency. However, when it come to the decaying frequency, the results obtained must be taken with caution. Indeed, forcing the transfer of the wind turbine kinetic energy to the grid with the appropriate controllers as a limited impact due to the low rotating speed of the rotor. As for the approach consisting on running at a lower maximum power point, it comes with the rather questionable hypothesis that wind will still be available when more power would be needed.

A more reliable strategy to deal with the decaying frequency would be to rely on tangible power reserve. In fact, some actual wind parks are equipped with batteries to support the grid frequency. A detailed model of a wind turbine acting on the frequency control with a battery at the DC link could be done for further research. Additionally, the study of areas interconnected with HVDC links would have been relevant as the power exchanges can be quickly adjusted and thus play on the fast frequency control.

Bibliography

[1] All island - system information. http://www.eirgridgroup.com/how-the-grid-works/system-information/. Accessed: 2017-02-07.

[2] Elia grid load. http://www.elia.be/en/grid-data/Load-and-Load-Forecasts/Elia-grid-load. Accessed: 2017-10-04.

[3] Entsoe online grid map. https://www.entsoe.eu/map/Pages/default.aspx. Accessed: 2017-02-07.

[4] La centrale d'accumulation par pompage de coo. http://www.corporate.engie-electrabel.be. Accessed: 2017-15-05.

[5] COMMISSION REGULATION (EU) 2016/631. Establishing a network code on requirements for grid connection of generators. *Official Journal of the European Union*, 2016.

[6] R.W.De Doncker A. Veltman, D.W.J. Pulle. *Fundamentals of Electrical Drives*. Springer, 2007.

[7] Siegfried Heier. Grid integration of wind energy conversion systems. 1998.

[8] James R. Bumby Jan Machowski, Janusz W. Bialek. *Power System Dynamics: Stability and Control*. John Wiley Sons,Ltd, 2008.

[9] George C. Verghese John G. Kassakian, Martin F. Schlecht. *Principle of Power Electronics*. ADDISON-WESLEY PUBLISHING COMPANY, 1991.

[10] Dimitrios Zafirakis John Kaldellis. Impact analysis of vehicle-to-grid technology and charging strategies of electric vehicles on distribution networks. *Journal of Power Sources*, 277:205–214, 2011.

[11] Dimitrios Zafirakis John Kaldellis. The wind energy (r)evolution: A short review of a long history. *Renewable Energy*, 36:1887– 1901, 2011.

[12] Arnaud Latier. Seminar on organizing energy flows in electricity networks. *LELEC2520*, 2016.

[13] Chee Wei Tan Saidur Rahman Majid A Abdullah, Abdul Halim Yatim. A review of maximum power point tracking algorithms for wind energy systems. *Renewable and Sustainable Energy Reviews*, 16:3220– 3227, 2012.

[14] H.Gualous M.S.Camara, B.Dakyo. Permanent magnet synchronous generators for offshore wind energy. *16th International Power Electronics and Motion Control Conference and Exposition*, 2014.

[15] Wach P. *Dynamics and Control of Electrical Drives*. Springer, 2011.

[16] IEEE Committee Report. Dynamics models for steam and hydro turbine sin power system dynamics studies ieee trans vol pas pas-92 pp. pages 1904–1915, November/December 1973.

[17] Barry Van Veen Simon Haykin. *Signals and Systems second edition*. John Wiley Sons, 2003.

Appendix A

Appendix

Simulink model of the permanent magnet synchronous wind turbine

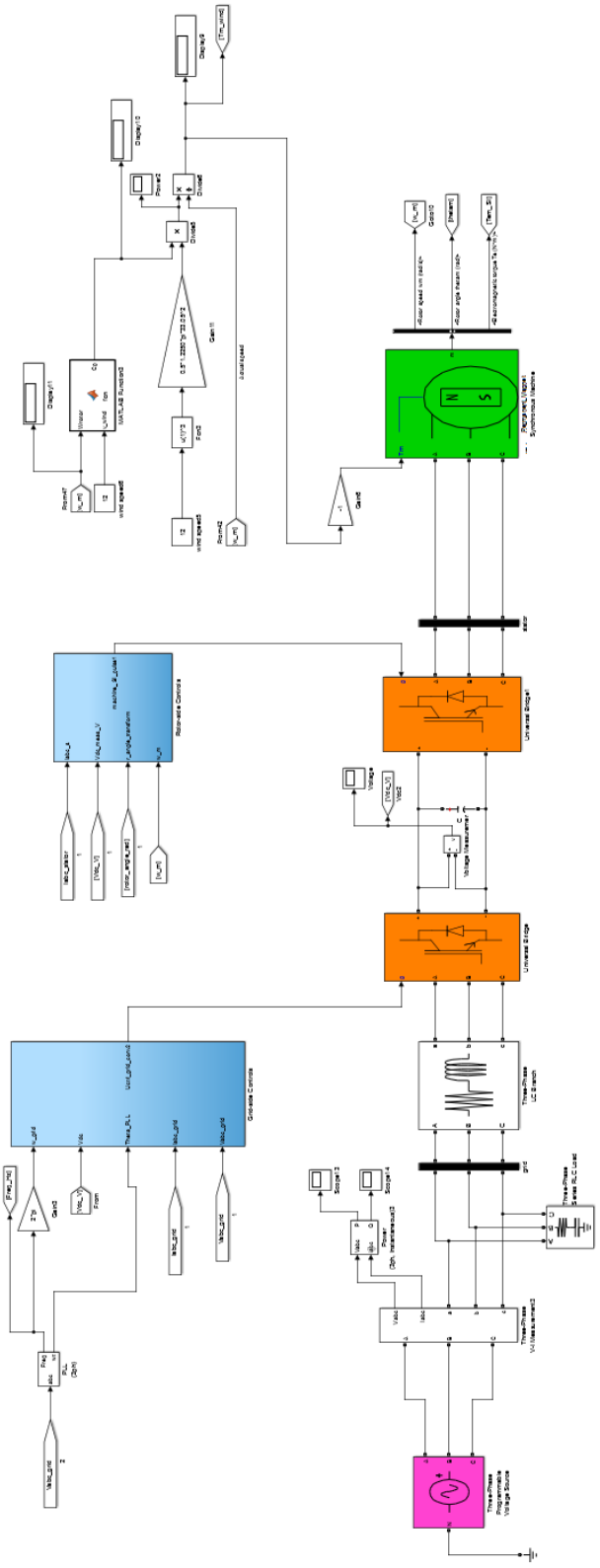

Figure A.1: Simulink model of the control of a permanent magnet wind turbine

Simplified model of turbines with their governor [16]

Block diagram model of a reheat steam turbine

Parameter	Value
Time constant main servo motor	$T_G = 0.2\ s$
Time constant of the steam chest	$T_{CH} = 0.3\ s$
Time constant of reheating	$T_{RH} = 7\ s$
Fraction of the High Pressure power	$F_{HP} = 0.3$

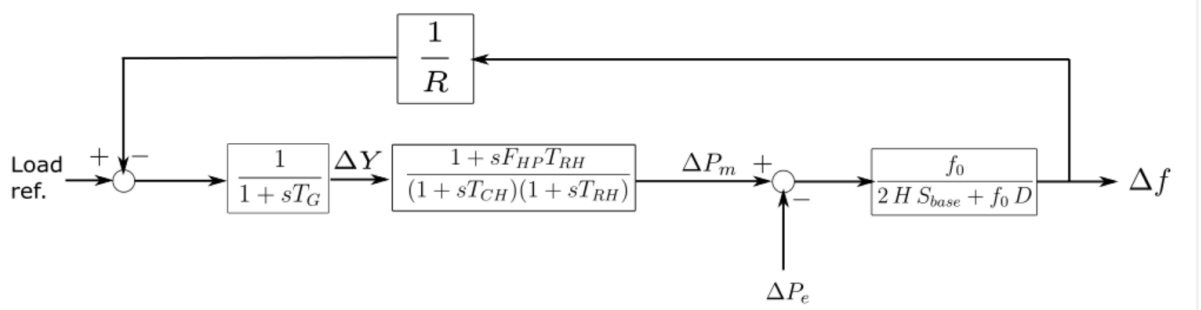

Figure A.2: Block diagram of a reheat steam turbine

Block diagram model of a non-reheat type steam turbine

Parameter	Value
Time constant main servo motor	$T_G = 0.2\ s$
Time constant of the steam chest	$T_{CH} = 0.3\ s$

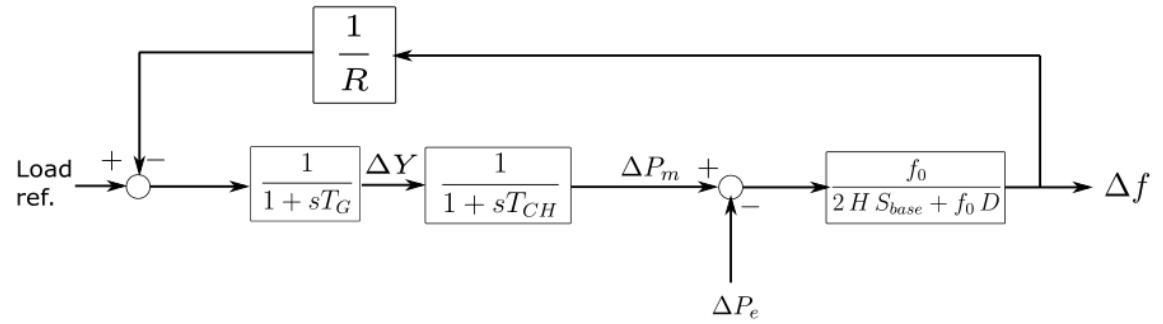

Figure A.3: Block diagram of a non-reheat type steam turbine

Block diagram model of an hydraulic turbine equipped with a transient droop

Parameter	Value
Time constant main servo motor	$T_G = 0.2\ s$
Water starting time	$T_w = 1\ s$
Reset time	$T_R = 5\ s$
Temporary droop	$R_T = 0.38$
Permanent droop	$R_P = 0.5$

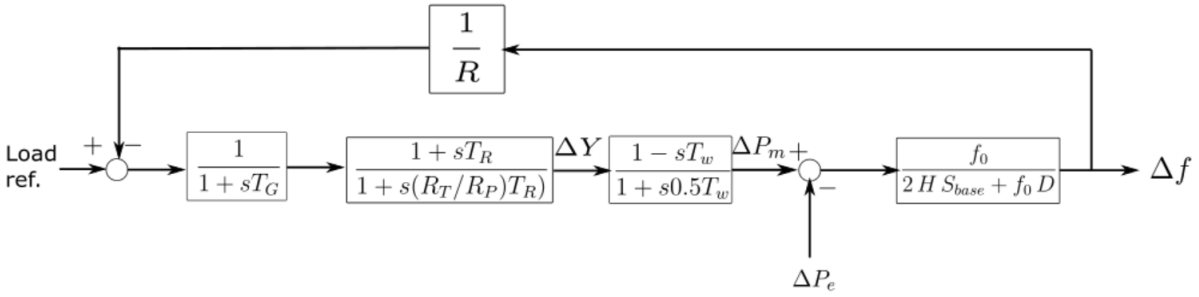

Figure A.4: Block diagram of an hydraulic turbine

Histogram frequency data

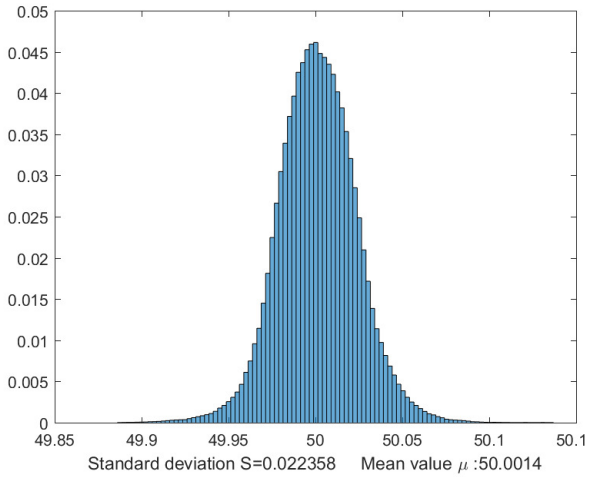

Figure A.5: Histogram of the frequency in January

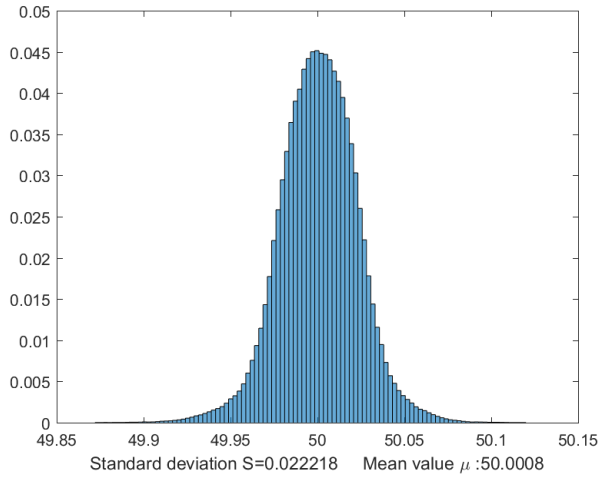

Figure A.6: Histogram of the frequency in February

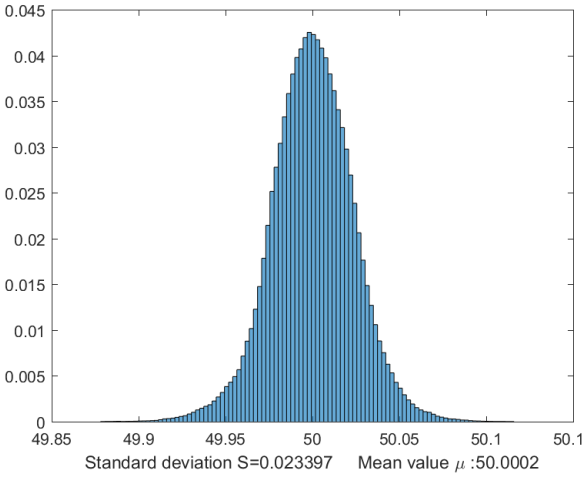

Figure A.7: Histogram of the frequency in March

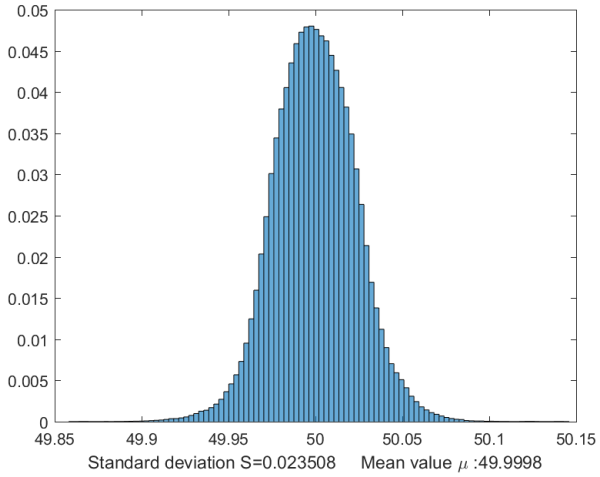

Figure A.8: Histogram of the frequency in April

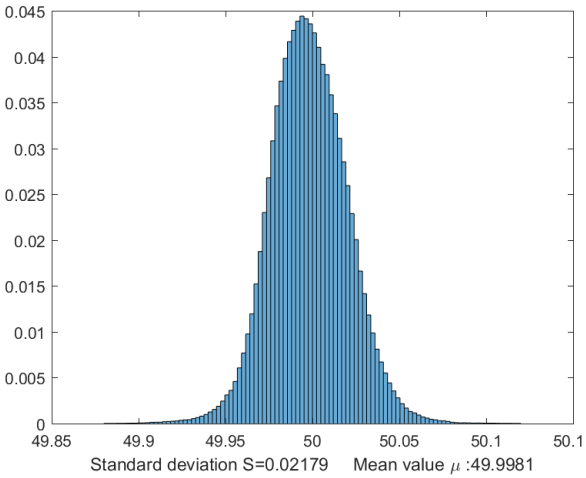

Figure A.9: Histogram of the frequency in May

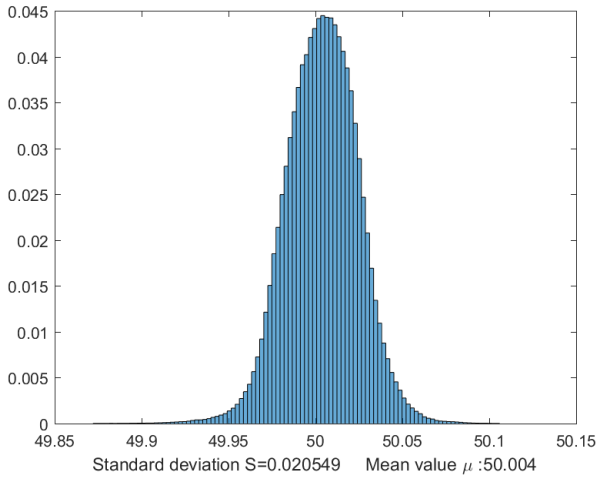

Figure A.10: Histogram of the frequency in June

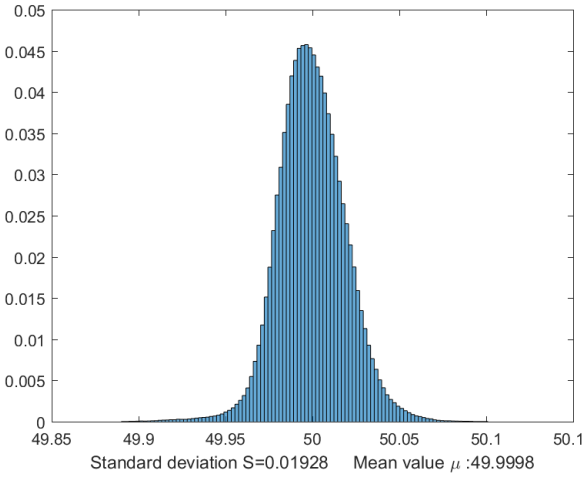

Figure A.11: Histogram of the frequency in July

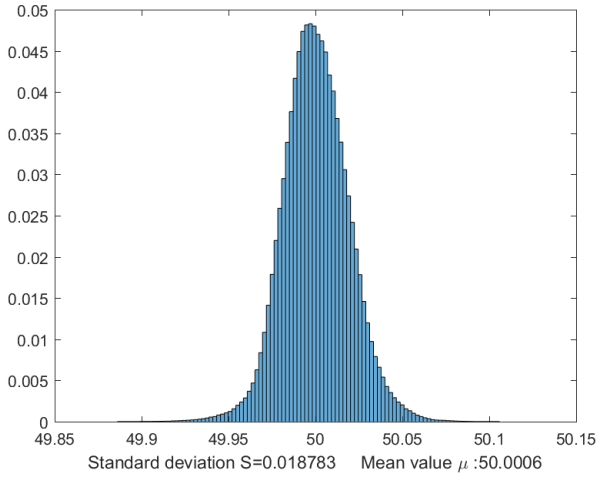

Figure A.12: Histogram of the frequency in August

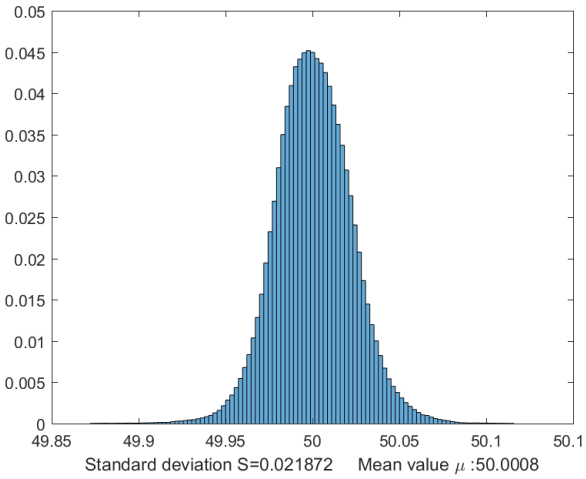

Figure A.13: Histogram of the frequency in September

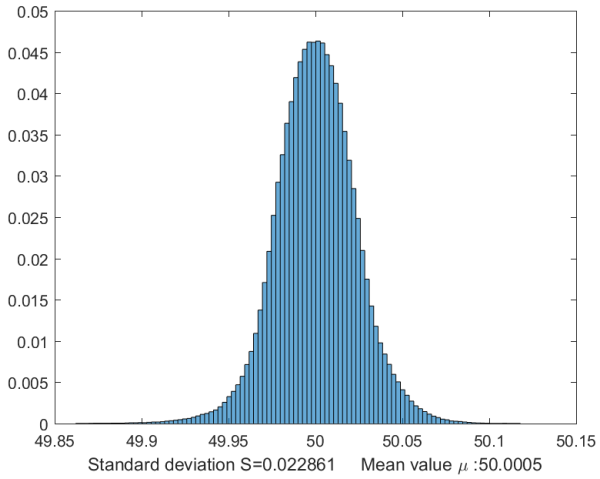

Figure A.14: Histogram of the frequency in October

Histogram rate of frequency change

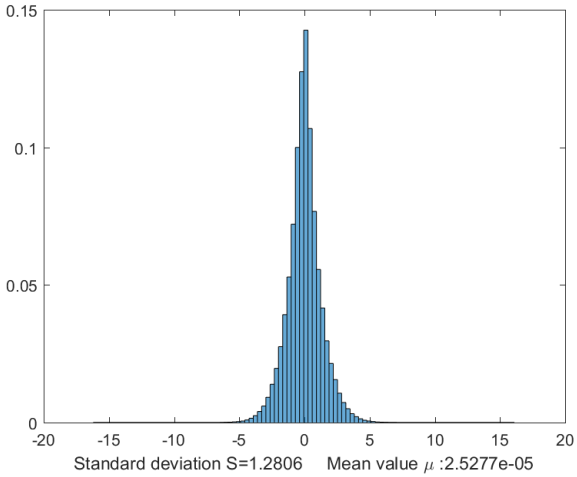

Figure A.15: Histogram of the rate of frequency deviation in January

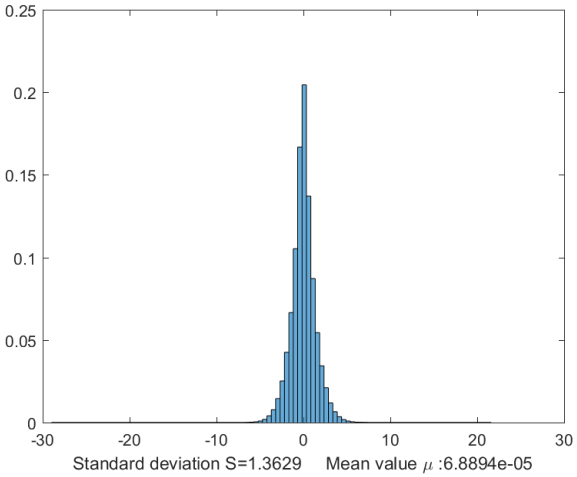

Figure A.16: Histogram of the rate of frequency deviation in February

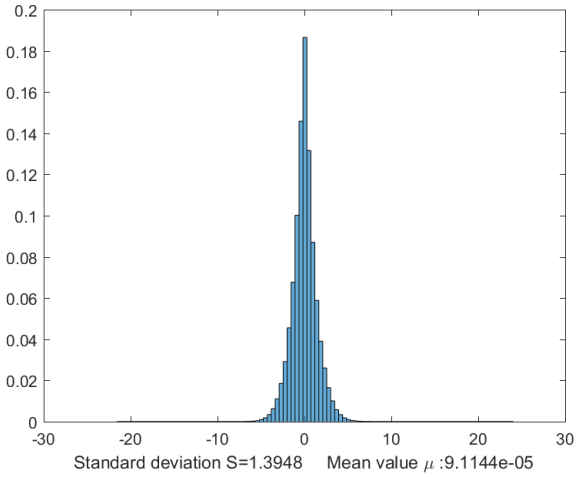

Figure A.17: Histogram of the rate of frequency deviation in March

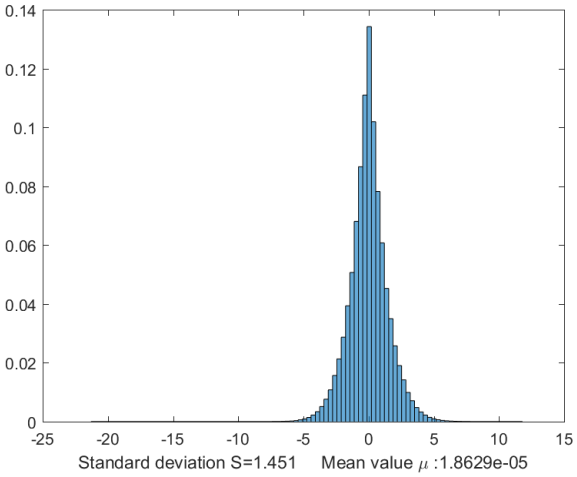

Figure A.18: Histogram of the rate of frequency deviation in April

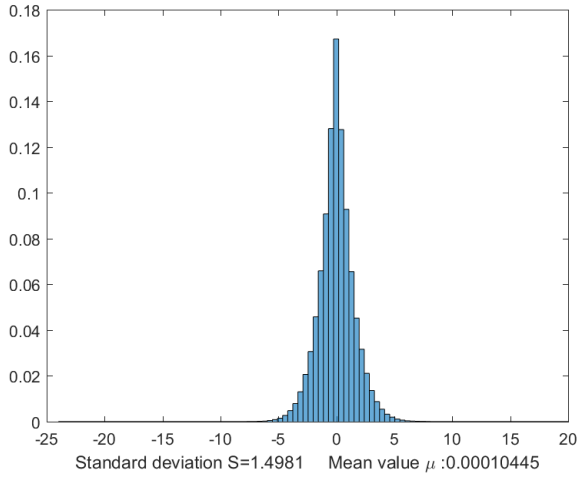

Figure A.19: Histogram of the rate of frequency deviation in May

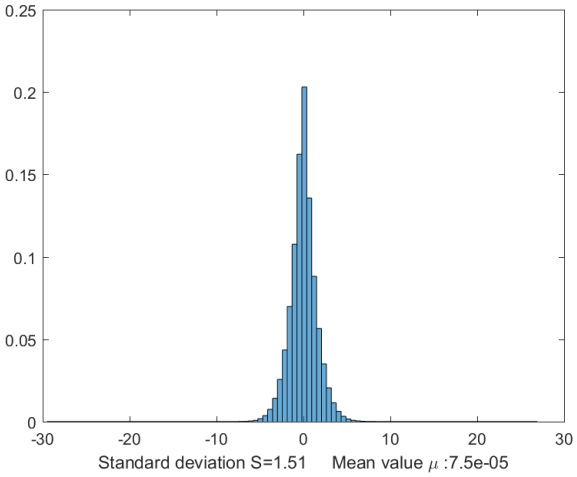

Figure A.20: Histogram of the rate of frequency deviation in June

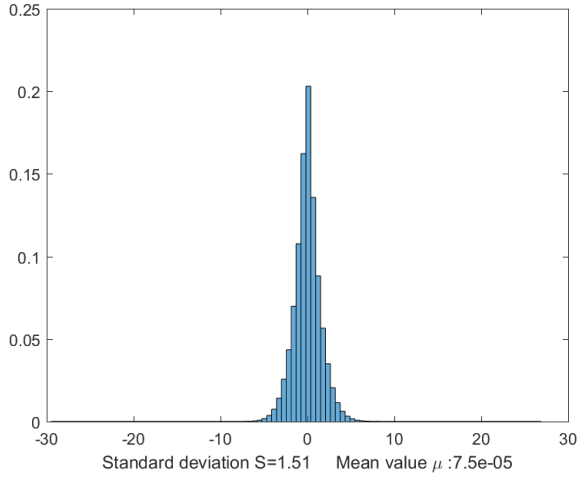

Figure A.21: Histogram of the rate of frequency deviation in July

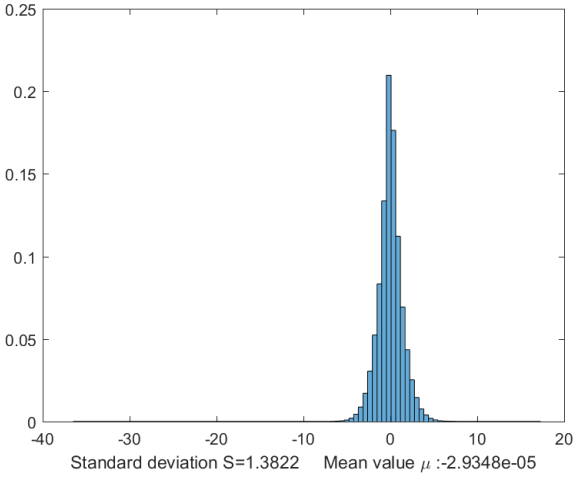

Figure A.22: Histogram of the rate of frequency deviation in August

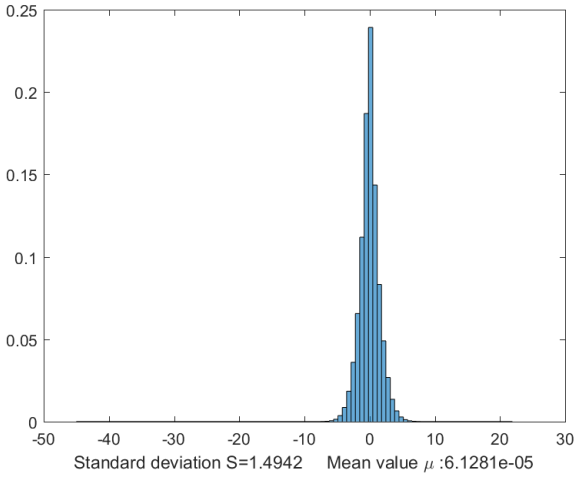

Figure A.23: Histogram of the rate of frequency deviation in September

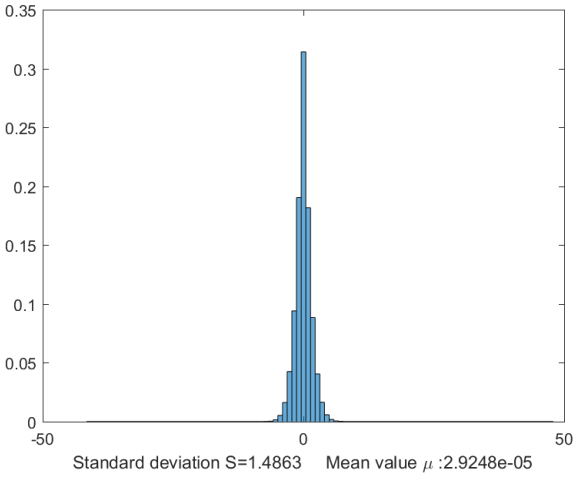

Figure A.24: Histogram of the rate of frequency deviation in October

Rue Archimède, 1 bte L6.11.01, 1348 Louvain-la-Neuve **www.uclouvain.be/epl**